ADVANCED ENERGY MATERIALS
www.advenergymat.de

Interfaces in Perovskite Solar Cells

Azhar Fakharuddin, Lukas Schmidt-Mende, Germà Garcia-Belmonte, Rajan Jose,* and Ivan Mora-Sero**

Rapid improvement in photoconversion efficiency (PCE) of solution processable organometallic hybrid halide based perovskite solar cells (PSCs) have taken the photovoltaic (PV) community with a surprise and has extended their application in other electronic devices such as light emitting diodes, photo detectors and batteries. Together with efforts to push the PCE of PSCs to record values >22% – now at par with that of crystalline silicon solar cells – origin of their PV action and underlying physical processes are also deeply investigated worldwide in diverse device configurations. A typical PSC consists of a perovskite film sandwiched between an electron and a hole selective contact thereby creating ESC/perovskite and perovskite/HSC interfaces, respectively. The selective contacts and their interfaces determine properties of perovskite layer and also control the performance, origin of PV action, open circuit voltage, device stability, and hysteresis in PSCs. Herein, we define ideal charge selective contacts, and provide an overview on how the choice of interfacing materials impacts charge accumulation, transport, transfer/recombination, band-alignment, and electrical stability in PSCs. We then discuss device related considerations such as morphology of the selective contacts (planar or mesoporous), energetics and electrical properties (insulating and conducting), and its chemical properties (organic vs inorganic). Finally, the outlook highlights key challenges and future directions for a commercially viable perovskite based PV technology.

1. Introduction

Progress in organic-inorganic hybrid perovskite solar cells (PSCs) has been remarkably impressive since its inception in 2009. The organic-inorganic hybrid perovskites have been known for applications in optical devices[1] and field-effect transistors[2] since early 1990's; however, their usefulness in a photo-energy conversion device is realized only in 2009 by Miyasaka et al.[3] They crystallized halide based hybrid perovskites ($CH_3NH_3PbI_3$ or $CH_3NH_3PbBr_3$) as light absorbers onto a 8–12 μm thick TiO_2 layer, an architecture similar to the dye-sensitized solar cells (DSCs),[4] and by making a junction with iodide/triiodide redox electrolyte as a hole transporting medium (HTM) demonstrated a photoconversion efficiency (PCE) ≈3.8%. Subsequently, Park et al.[5] demonstrated PCE up to 6.5% in a similar device but with a TiO_2 film of lower thickness (≈4 μm). However, these devices exhibited poor operational stability, typically less than an hour, due to the liquid electrolyte used. The first solid-state device based on $CH_3NH_3PbI_3$ as an absorber was reported by Kim et al.[6] that employed a mesoporous TiO_2 scaffold (≈1 μm) in conjunction with 2,2′,7,7′-tetrakis-(N,N-p-dimethoxy-phenylamino)-9,9′-spirobifluorene (Spiro-OMeTAD) as a hole conductor and reported a remarkable PCE ≈9.7%. Subsequent developments in PSCs such as enabling better charge extraction at electron and hole selective contacts (ESC and HSC), optimizing the perovskite composition, for example, incorporation of formamidinium (FA) or Caesium (Cs) or both into methyl ammonium cation (MA), and optimizing the morphology of perovskite layer brought PSCs to deliver PCE 20–22%.[7] Besides their high PCE – which is comparable to silicon and thin film solar cells – they have also shown fair stability up to few thousand hours,[7b,8] added functionalities such as possibility to be printed on flexible substrates,[9] transparency[10] and their workability in low light condition,[11] thereby marking them as a potential candidate for future solar cell technology that can offer the 'golden four' of a solar cell technology,[12] i.e., low-cost, stability, efficiency and added functionality. These achievements are partly because PSCs offer a wider variety of device designs as well as varied choice materials combinations for electron and hole selective contacts as shown in **Figure 1**, where the charge separation

Dr. A. Fakharuddin, Prof. L. Schmidt-Mende
Department of Physics
University of Konstanz
D-78457 Konstanz, Germany
E-mail: azhar-fakhar.uddin@uni-konstanz.de
Dr. A. Fakharuddin, Prof. R. Jose
Nanostructured Renewable Energy Materials Laboratory
Universiti Malaysia Pahang
Kuantan, Malaysia
E-mail: rjose@ump.edu.my
Prof. G. Garcia-Belmonte, Prof. I. Mora-Sero
Institute of Advanced Materials (INAM)
Universitat Jaume I
12006 Castelló, Spain
E-mail: sero@uji.es
Dr. A. Fakharuddin
Nanosciences and Technology Department
National Center for Physics
Quaid-i-Azam University
Islamabad, Pakistan
The ORCID identification number(s) for the author(s) of this article can be found under https://doi.org/10.1002/aenm.201700623.

DOI: 10.1002/aenm.201700623

mechanism varies from that of sensitized cell to band type. This makes it hard to generalize the working principle for all these designs, and consequently, various underlying physical processes such as charge transport mechanism, hysteresis and the origin of instability are still not fully understood.

The first all-solid PSC employs a perovskite absorber between an ESC on a conducting glass substrate (FTO) and a HSC (Figure 1a) with a metal back contact on top. The working principle of this device was initially conceived to be similar to that of DSSCs, i.e., perovskite is a light absorber and ESC (typically TiO_2) takes part in charge separation and electron transport whereas the holes are transferred to HSC although subsequent research showed the working principle is not excitonic.[13] This design holds the state-of-the-art PCE ≈20–22% with (i) a compact (pin-hole free) hole blocking layer between FTO and TiO_2 scaffold, (ii) a dense perovskite capping layer over TiO_2 scaffold with perovskite infiltrated within the pores, and (iii) optimized interfaces.[7f,14] In another design (**Figure 2**b), the semiconducting TiO_2 scaffold is replaced with an insulating Al_2O_3 or ZrO_2 layer with a reported maximum PCE ≈15.9%.[15] Herein, the charges are carried by the perovskite itself, thereby evidencing that PSCs work without an electrically conducting ESC.[16] Alternatively, devices without any mesoporous TiO_2 scaffold (planar, Figure 2c) have also shown impressive photovoltaic performance (PCE ≈19–20%, but with hysteresis)[7d,17] where a compact layer (usually compact TiO_2) is employed to prevent a direct contact of perovskite or HSC with FTO. The PSCs without an ESC[18] and also an HSC[19] (Figure 2d,e) have also been tested and shown significantly high PCE 14–16%. In addition, inverted solar cell configuration in which holes, instead of electrons, are collected at the FTO/ITO are also reported (Figure 2f) with PCE >18%.[20] In such devices, NiO and PEDOT:PSS are commonly utilized HSCs whereas a thin layer (<50 nm) of phenyl-C61-butyric acid methylester (PCBM) or other fullerene derivatives are employed as ESC.

As the PSCs are fabricated in a range of architectures, their photovoltaic performance over time and hysteresis in current – voltage characteristics largely depend on the electrical and morphological properties of the selective contacts. For example, perovskite crystals' size and morphology have shown to largely depend on the nature of ESC/HSC–$CH_3NH_3PbX_3$ interface and play a key role in the final PCE.[21] Furthermore, when it comes to the practical deployment of PSCs, it is not only their PCE but operational stability also determines the success of the technology for real-life application. In PSCs, ESC and HSC have shown significant impact on thermal, electrical, structural, UV-light and long-term operation stability thereby establishing its quintessence.[22] A notable report by Olthof and Meerholz[23] suggest that the nature of the interfacing material underneath perovskite not only determines energy levels (deviation from a common assumption of flat band conditions) but also can induce gap states and influence film formation. In the case of metal oxide, their catalytic nature induces a chemical reaction at the interface resulting in volatile byproducts, which are far lower when an organic selective contact is used.

The wide variety of PSCs' design architectures make the role of the interfaces ambiguous and raises questions such as does a mesoporous TiO_2 scaffold or compact layer (c-TiO_2) takes part in charge separation? What is the contribution of ESC/HSC

Azhar Fakharuddin holds a Ph.D. in Advanced Materials from the University Malaysia Pahang where he worked on charge transport for dye-sensitized solar cells/modules. He has also been attached to the Centre for Hybrid and Organic Solar Energy of the University of Rome Tor Vergatta to carry on his research in perovskite solar cells and modules. He is currently an Alexander von Humboldt Postdoctoral Research Fellow at the Department of Physics of the University of Konstanz, Germany, where his work mainly includes interface engineering and long term stability of perovskite solar cells.

Rajan Jose is a Professor of Materials Science & Engineering at the Faculty of Industrial Sciences & Technology, Universiti Malaysia Pahang (UMP) since 2010. He did his doctoral research at the Council of Scientific & Industrial Research (CSIR), India and received Ph.D. degree in 2002. He supervises the Nanostructured Renewable Energy Materials Laboratory in the UMP. He has worked at the Indira Gandhi Centre for Atomic Research (India), AIST (Japan), Toyota Technological Institute (Japan), and the National University of Singapore (Singapore) before joining UMP. He is a materials engineer with most of his research on the structure – property correlation in materials for a desired device functionality.

Iván Mora-Seró is Associate Professor and group leader at the Institute of Advanced Materials (INAM), University Jaume I, Castelló (Spain). His research has been focused on crystal growth, nanostructured devices, transport and recombination properties, photocatalysis, electrical characterization of photovoltaic, optoelectronic, and water splitting systems, making both experimental and theoretical work. Recent research activity is focused on new concepts for photovoltaic conversion and light emission (LEDs and optical amplifiers) based on nanoscaled devices and semiconductor materials following two mean lines: semiconductor quantum dots and lead halide perovskites, been this last line probably the current hottest topic in the development of new optoelectronic devices.

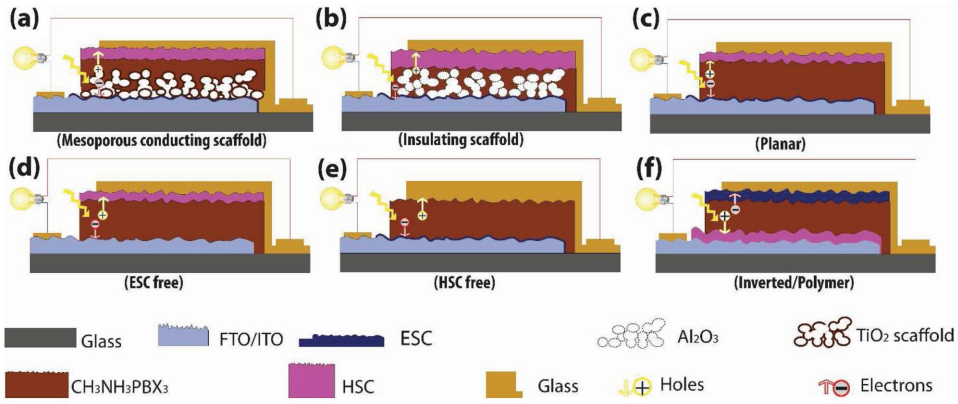

Figure 1. A schematic on various common perovskite device architectures reported with or without charge (electron/hole) transport layers. a) A metal oxide semiconductor (MOS), typically, mesoporous TiO_2 is employed as an ESC. b) MOS is replaced with an insulating scaffold (Al_2O_3 or ZrO_2), c) no scaffold is employed and instead a thin compact hole blocking layer (<100 nm) is employed on FTO, d) no hole blocking layer is employed and perovskite is deposited directly on a surface modified FTO/ITO, e) the architecture without a HTM and holes are transported via perovskite itself. The design however employs a thin n-type hole blocking layer on FTO (but often it also employs a mesoporous layer), and f) and inverted device architecture where holes are collected on the FTO using a p-type carrier layer, typically NiO, whereas electrons are collected through metal back contact. In the architectures b–d), electrons are transported to FTO via perovskite.

towards charge dynamics (transfer/recombination) and open circuit voltage (V_{OC}) in the various device designs? This is particularly intriguing after the reports where SnO_2, an MOS with a conduction band edge ≈300 mV lower than TiO_2,[24] resulted in a similar V_{OC} (≈1.1–1.2 V)[25] as of the latter, suggesting that, contrary to initial reports on the origin of the V_{OC} to be $E_F - E_{RED}$, it is rather due to splitting of the quasi-Fermi energy level of electrons and holes in perovskite itself. Questions also arise that if efficient PSCs can be made ESC- or HSC-free, as they have shown PCEs of ≈16 and 14%, respectively, why is

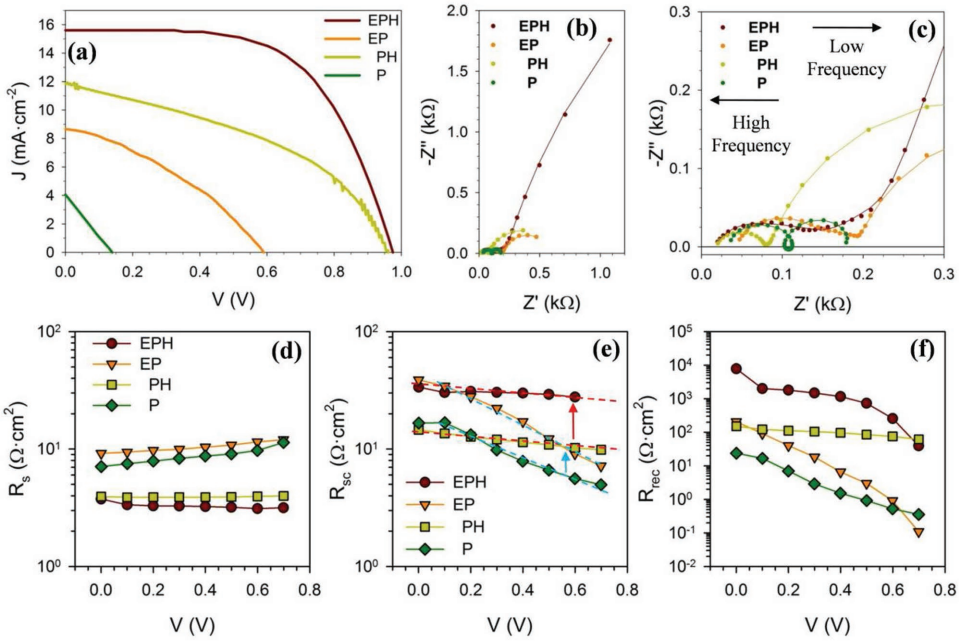

Figure 2. J-V curves and impedance spectroscopy analysis of different PSCs with a without selective contacts. Complete cell (EPH) presents: (E) compact TiO_2 electron selecting contact; (P) $MAPbI_3$ Perovskite layer and (H) spiro-OMeTAD as hole selective contact. Following this notation EP samples has no hole selecting contact while P sample does not have any of the two selective contacts and perovskite layer is directly contacted by the extracting contacts FTO and Au. a) J-V curve, reverse scan. b) Impedance spectra of the different devices under 1 sun illumination at 0.1 V applied bias. c) Zoom of high frequency region in (b), high and low frequency regions are indicated, solid lines are fitting curves obtained by the use of equivalent circuits detailed in Ref. [35,36] d) Series resistance, e) high frequency feature resistance, dashed lines are eye guides. Red and dashed lines indicate the devices with and without a hole selective contact, respectively. Red and blue arrows indicate the increase in resistance observed when electron selective contact is added to PH and P samples respectively. f) Recombination resistance.[35] Reproduced with permission.[35] Copyright 2014, American Chemical Society and reproduced with permission.[36] Copyright 2016, American Chemical Society.

that most of the device architectures still require a mesoporous layer, or at least a flat n-type layer underneath perovskite along with an HSC? Furthermore, even if high efficiency PSCs can be made without a mesoporous scaffold, such as in the case of n-i-p (PCE ≈20.7%) or p-i-n (PCE ≈18.3%) planar PSCs, how stable are such devices and can they pave road to the commercial deployment of PSCs? Similarly, if selective contacts are crucial for long term stable operation of PSCs, which particular materials and morphology must be employed? In addition, how do the interfaces help eliminating the anomalous hysteresis in PSCs? The answers to such questions remain elusive despite the rapid increase in publication trends in PSCs. Comparisons of results from different labs do not always allow conclusions for two reasons: 1) Small changes in preparation conditions can influence largely the performance, so that results are not always easily reproduced and it is not clear, whether the cells have already fully been optimized or can be further improved, and 2) efficiency measurements largely vary as the measurement protocol for PSCs is quite different in different labs and reported values are often not stabilized efficiencies. Herein, we compare the two selective contacts, i.e., ESC and HSC in PSCs to address these important questions, conclude its essentiality for a practically deployable device, and provide guidelines for future research. We visualize that selection of the selective contacts will determine, to a great extent, elimination of the anomalous hysteresis, improving the charge dynamics at ESC-HSC/perovskite interfaces, and most importantly upscaling of PSCs from a current laboratory scale to a commercially applicable level.

2. Selective Contacts and Charge Transport, Accumulation and Transfer/Recombination in Perovskite Films

The photovoltaic process requires two successive steps: photoinduced charge generation via light absorption, and charge separation as a second step in order to extract efficient electrical work from the photovoltaic device.[26] From a semiconductor point of view, the first step; i.e., light absorption excites electrons at the VB to the CB producing the splitting of Fermi level of these two bands, i.e., ($E_{Fn} - E_{Fp}$) where E_{Fn} and E_{Fp} are the electron and hole quasi-Fermi levels in the perovskite film. This splitting represents the free energy that potentially can be used as work, and also the maximum V_{OC} (obtained by dividing the Fermi level splitting by the elementary charge). However, this energy is not yet available to be employed as electrical work until the second step takes place; i.e., the charge separation, and it is where selective contacts and their corresponding interfaces with light absorbing material (perovskite) plays a fundamental role in determining the performance of a solar cell.

An ideal selective contact does not deteriorate the light absorbing layer and also does not induce degradation within the device. In addition, there are also no energy losses when photogenerated carriers are injected from the light absorbing material into the selective contact, no recombination at the interface, and the Fermi level of its corresponding carrier is maintained at the interface without any drop. As an ideal selective contact allows injection of only one kind of carriers and there are no recombination losses in the bulk of the selecting contact as just one type of carrier is present in the contact. Finally, an ideal selective contact has an infinite charge mobility, producing no transport losses. It must also be balanced with respect to perovskite layer as otherwise it would lead to charge accumulation at selective contact and interfacial charge recombination thereby. Any modification of this ideal scenario will have a deleterious effect on the cell performance so that the achievable power is less that the Fermi level splitting ($E_{Fn} - E_{Fp}$). If factors related to the reactivity and chemical stability are not taken into account, the non-ideality of a selective contact can arise from: i) interface recombination, ii) charge injection losses and iii) charge transport losses.

The density of photogenerated free-charge carriers in a PSC is expressed as:[13b,27]

$$\frac{\partial n(t)}{\partial (t)} = -k_3 n^3 - k_2 n^2 - k_1 n \quad (1)$$

Herein, k_1, k_2, k_3 are the monomolecular (trap-assisted), bimolecular (interfacial), and Auger recombination rate constants. For a perovskite device, the dominant recombination is first and second order only. Being a wide bandgap material, the Auger recombination process is negligible (the rate constant for Auger recombination at 1 sun is negligible). It is also reported that, typically, for efficient devices with highly crystalline perovskite films, the electron-hole recombination within the perovskite film is negligible.[28] The dominant bimolecular recombination in perovskite films arises from (i) morphological and structural defects within the perovskite film due to lattice mismatch and thermal vibrations,[29] (ii) the arguably imbalanced charge transport in the perovskite film arising from shorter electron diffusion length than the holes[30] (iii) the energy offset between perovskite and selective contacts,[7d,31] (iv) the sub-bandgap states and surface defects of the selective contacts such as TiO_2 or ZnO (ESC) or NiO (HSC),[32] and (v) the poor physical contact between perovskite and metal back contact[33] (in the case of HSC-free architectures).

So far, these various recombination processes are not fully understood in the case of PSCs despite their intensive research reports since 2012 and impressive PCE >22% till date. Understanding and characterization of these interfacial processes are therefore mandatory not only to further develop this photovoltaic technology but also for the development of other optoelectronic devices based on the halide perovskites. Towards this end, impedance and transient absorption spectroscopies can provide insights on the role of contacts and their respective interfaces in the performance of PSCs, and in this section, we use it to emphasize the contribution of contacts and interfaces in PSCs. Impedance spectroscopy (IS) is a characterization method in the frequency domain that allows decoupling processes associated with different characteristic time domains and has been used to characterize PSCs since very early stages of their research.[34] Despite the fact that till date there is no general model to describe the impedance spectra of PSCs in the complete frequency range and for all the different device configurations, IS can still provide useful implications about interfacial charge kinetics.

Figure 2a shows the J-V curves of PSC prepared with and without one or both selective contacts.[35] Complete PSC with an extended and standard configuration have been prepared by the successive deposition of thin film layer on top of glass/FTO transparent contact in order to form a complete device: glass/FTO/compact TiO_2/$CH_3NH_3PbI_3$ perovskite/spiro-OMeTAD/Au, denoted as EPH as it contains compact TiO_2 ESC (E), perovskite light absorbing layer (P) and spiro-OMeTAD HSC (H). In addition, devices without HSC (EP sample), without ESC (PH sample) or without both (P sample) have been also analyzed. From Figure 2a it can be clearly observed that removing of a selective contact has deleterious effect on cell performance. PSCs with high efficiency have been reported for devices without ESC or HSC, as it is reviewed in Section 5, nevertheless, the maximum reported efficiency for those configurations has always been well below compared to the devices employing both selective contacts. IS was employed to analyze the effect of selective contact.[35] Figure 2b,c show the impedance pattern of the analyzed samples under 1 sun illumination at 0.1 V applied voltage. A rich pattern can be appreciated, basically formed by two arcs at high and low frequencies. IS pattern has been fitted using equivalent circuits discussed in Ref. [35,36] (solid curves in Figure 2b,c). Three characteristic resistances can be extracted upon fitting. The diameter of the high frequency feature defines a resistance, R_{sc}, corresponding to the selective contacts, while the diameter of the low frequency feature is related to the recombination resistance, R_{rec}. In addition the real part of the impedance where high frequency feature starts indicate the series resistance, R_s, of the device due to the extracting contacts and wiring.

Figure 2d depicts R_s for the four devices analyzed in this study. High series resistance (R_S) can be noted for devices without HSC suggesting a contact resistance (R_{CON}) between perovskite and Au that disappears when spiro-OMeTAD is added and points out a first beneficial effect of including selective layer in order to couple efficiently the perovskite absorbing layer with the extracting contacts. R_{sc} is also affected significantly by the presence of extracting contacts as shown in the-Figure 2e. The slope of R_{sc} vs V depends on the presence of HSC, lower in the presence of selective contact, as displayed in the blue and the red dashed lines for devices with and without HSC in Figure 2e. This fact indicates that hole transport resistance along the HSC is contributing to R_{sc}. Moreover, electron transport resistance along ESC is also contributing to R_{sc}, as it is observed from the upwards shift of the devices containing ESC with respect to their counterparts without it (see red and blue arrows in Figure 2e). Finally, the presence of selective contacts also affects the recombination rate as can be noted from the effect on R_{rec} (Figure 2f) because recombination resistance is inversely proportional to the recombination rate.[37] Note that the highest R_{rec}, i.e., the lowest recombination rate, is observed for the complete device EPH, while removing any of the selective contacts imply an increase of recombination. The variation is significant if the interfacing material being removed is the HSC.

It is evident that the primary role of a selective contact is to reduce the interfacial recombination between perovskite light absorbing layer and the FTO and Au extracting contacts. However, their use adds a deleterious effect due to the carrier transport resistance and affects cell parameters particularly, the FF. Consequently, a good selective contact has to be as thin as possible in order to reduce the transport resistance but thick enough to avoid pinholes, hindering effectively charge recombination.

Obviously the goodness of an interfacing material for an efficient electron transport in PSC will depend on the nature and interactions of the chosen selecting contact with the light absorbing perovskite layer. We therefore analyze, in the next sections, the effect of a wide variety of selecting contacts. As an example, **Figure 3**a shows J-V curves of PSCs prepared following a similar procedure but using different ESCs.[36] The different ESCs have been prepared by ALD while the materials and deposition conditions for the rest of the layers were kept constant. This simple change results in large variation in the PV performance of the devices; from 17% for SnO_2 ESC to nearly zero (0.20%) for Nb_2O_5, passing through an intermediate value for the TiO_2. Again IS provides important clues on the origin of this difference, see Figure 3b. While for SnO_2, merely two arcs are observed in the impedance spectra, an intermediate arc is observed for Nb_2O_5 based devices, introducing an additional resistance, probably related with an interfacial process between Nb_2O_5 and perovskite. This assumption is reinforced by the observation of an inductive loop at intermediate frequencies when SnO_2 is used as ESC, see inset in Figure 3b. This loop behavior has been previously observed in solar cells and LEDs and it has been attributed to complex multistep injection processes.[39] Consequently, injection processes at the interfaces are also significantly important. However the presence of an interfacial electrostatic potential with a retarded time response, that we discus below, has probably an important role on the apparition of this feature.

The relationship of this inductive loop with interfacial process has been very recently demonstrated using unconventional scaffold forcing the photogenerated electrons to follow multistep perovskite/TiO_2 injection processes until they are extracted.[38] The use of a scaffold formed by successive thin layers of low porosity (≈5%) TiO_2 and mesoporous SiO_2 (≈40% porosity) makes that photogenerated electrons in the perovskite have two parallel paths in order to arrive to the electron extracting contact, percolating trough the perovskite present in the low porosity TiO_2 and being injected in TiO_2 and reinjected back into the perovskite. Note that injected electrons into TiO_2 cannot recombine, as there are no holes present in TiO_2. The low porosity of TiO_2 increases the weight of the second path in the transport of electrons until the extracting contact and consequently the fingerprint of the interfacial processes at Perovskite/TiO_2 is magnified. Exaggerated inductive loops are clearly observed in these samples, see Figure 3c, indicating a clear relation of this feature and interfacial processes. This loop is clearly observed even at short circuit conditions, see **Figure 4**d. The future determination of physical processes producing this loop will undoubtedly help in the characterization of interfacial processes in PSCs. At this point it is important to highlight that this feature is not linked to bad performing devices, as loops have been observed in PSCs demonstrating PCE 18%. Consequently, this feature is related to a general process on PSCs and it cannot be considered just an exotic element.

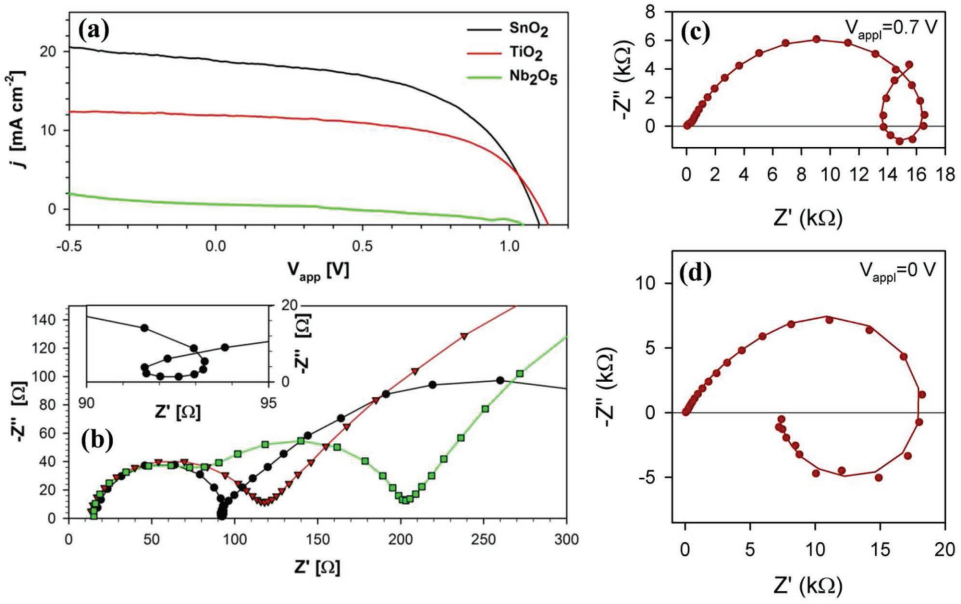

Figure 3. a) J-V curves of PSCs with different electron selective contacts, b) impedance spectra of the high frequency region for the same devices measured under 1 sun conditions and without an applied bias, inset shows an enlarged view of an inductive loop element observed in the spectra of the sample using SnO_2 as ESC. Reproduced with permission.[36] Copyright 2016, American Chemical Society. c) and d) Nyquist plots under 1 sun illumination with an applied DC bias (V_{appl}) of 0.7 and 0 V respectively. The PSC measured has an unconventional scaffold deposited on top of TiO_2 electron selecting contact formed by the sequential deposition of SiO_2 and TiO_2 mesoporous layers.[38] Concretely for the samples characterized in (c) and (d), the scaffold on top of conducting FTO is formed by sequential deposition of $TiO_2/SiO_2/$ $TiO_2/SiO_2/$ $TiO_2/SiO_2/$ TiO_2. Reproduced with permission.[38] Copyright 2017, The Royal Society of Chemistry.

Nevertheless, inductive loops is not the unique "surprise" that the analysis of impedance spectra of perovskite solar cells has provided. One of the strongest points of the IS analysis is the possibility to characterize the capacitive effects, and an accurate analysis of capacitance could allow to unambiguously link the IS features with well-determined physical processes. Probably the most surprising aspect of the IS of PSCs is the observation of 3–4 orders of magnitude increase in capacitance for the measurements in dark conditions and at 1 sun illumination(at low frequency), see Figure 4a. This enormous variation has not been observed in any other photovoltaic material, for example, crystalline silicon exhibits an increment of low frequency characterization in just a factor 2–3. Zarazua et al.[40] have explained this capacitance as an accumulation capacitance due to the accumulation of hole majority carriers at the perovskite/TiO_2 interface. They observed that at open circuit conditions this capacitance is not dependent of the perovskite thickness, pointing to an interfacial effect, while at different

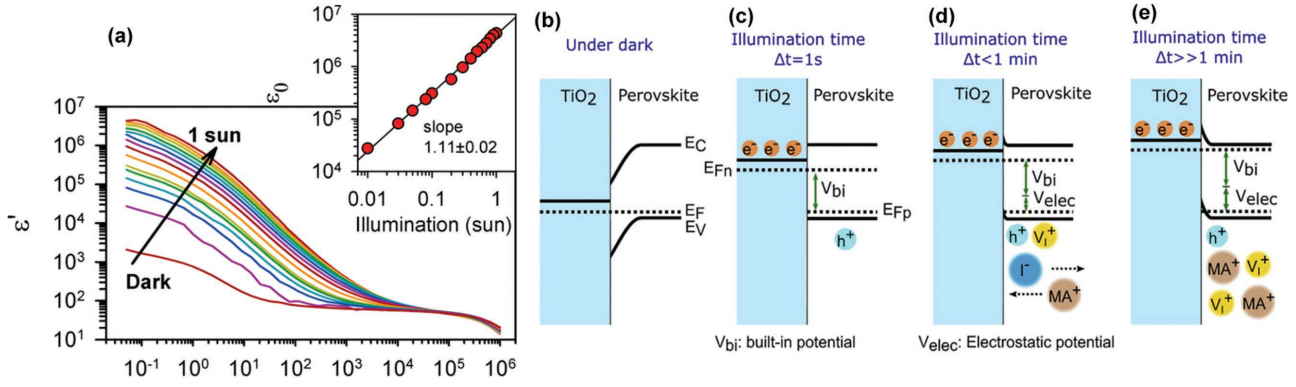

Figure 4. a) Bode plot of dielectric constant for PSCs with standard TiO_2 and spiro-OMeTAD as ESC and HSC, respectively, at different light illumination. Note that the capacitance is linearly related with the dielectric constant. Inset: Dielectric constant (capacitance) is linearly related with light intensity. Reproduced with permission.[44] Copyright 2016, American Chemical Society. b) Band diagram of perovskite and TiO_2 ESC in equilibrium under dark conditions. E_C, E_V and E_F represent the position of Conduction Band, Valence Band and equilibrium Fermi Level respectively. c) Illumination produces the Fermi level splitting producing a built-in potential, E_{Fn} and E_{Fp} represent the electron and hole quasi Fermi level respectively. d) Slow photoinduced ion migration produces an accumulation region at the interface and the apparition of an electrostatic potential. e) After long illumination time steady state is attained and V_{elec} and accumulation region fully developed. Adapted with permission.[45] Copyright 2014, Elsevier.

light intensities it follows the expected behavior for an accumulation capacitance. More recently Contreras et al.[41] observed the same behavior by impedance spectroscopy whereas, Bergmann et al.[42] detected charge accumulation at the ESC by Kelvin probe force microscopy. Furthermore, in a recent report, Chen et al.[43] observed a band bending with majority hole accumulation at perovskite interface confirming the accumulation capacitance interpretation.

This accumulation capacitance is an electronic phenomenon; however, it is strongly influenced by the presence of mobile ions in halide perovskite materials. This effect has been recently highlighted by Gottesman et al.[45] analyzing the open circuit voltage decay in perovskite solar cells and employing theoretical simulations. In equilibrium under dark condition TiO_2, perovskite and consequently their interface presents a common flat Fermi level, see Figure 4b. When light is switched on, carrier photogeneration produces rapidly a Fermi level splitting with the formation of a built-in potential, see Figure 4c. However this is not the only effect produced by light illumination. De Quilettes at al.[46] have reported a photo-induced halide redistribution in perovskite films. This is a slow process that requires relatively long times, even seconds time scales, in order to attain the steady state, see Figure 4d,e. As a consequence the hole charge accumulation at the ESC interface is ruled by the slow dynamics of ion migration. The ion redistribution at the interface produces an electrostatic potential, see Figure 4d,e. The formation of the V_{elec} has been confirmed by the analysis of the open circuit voltage decay with different pre- light soaking times. With no light soaking, a fast decay is observed. However when measurements are made after few minutes of light soaking, a slow Voc decay is observed for longer times, as in this conditions ions have had enough time to migrate and form V_{elec}, and removing this potential requires again the slow migration of these ions, producing a slower Voc decay.[45]

The presence of this accumulation capacitance mediated by ion migration has enormous implication on OSC performance. On one hand, V_{elec}, increases the Fermi level splitting which has important implications for open circuit potential as we discuss in the next section. On the other hand, majority accumulation at the interface indicates higher majority density and consequently higher recombination at the interface as recombination is directly proportional to charge density. In this sense, recombination at the interface is the dominant carrier recombination process in PSCs.[40b]

Injection, accumulation and recombination, are not the only ways in which a selective contact can affect the cell performance. As it has been discussed previously that the charge transport along the selective contacts also influences the cell performance. **Figure 5**a shows the impedance patterns of samples using SnO_2 ESC with different thickness. As the thickness of the ESC increases the diameter of high frequency pattern augment consistently with an increase in the electron transport resistance at the ESC. The highest efficiency (16.9%) has been observed for 15 nm thick ESC, probably for a thinner layer of 5 nm (13.3%) the selective contact is too thin to block completely the interfacial recombination, while in the case of a thicker layer ≈100 nm ESC (10.2%), the transport resistance at the selective contact reduces the FF (not shown here) and the final performance.[36] Unfortunately, single feature in PSCs

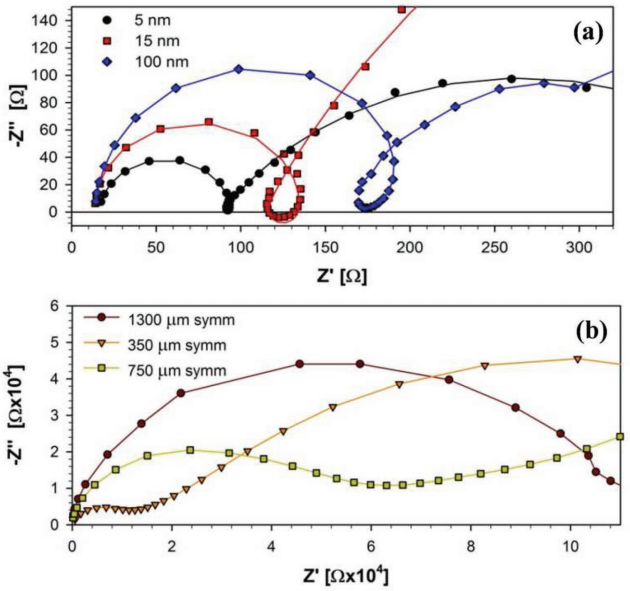

Figure 5. a) Impedance spectra of the high frequency region for samples using different thickness SnO_2 as ESC, measured under 1 sun conditions and no applied bias. b) Impedance spectra of the high frequency region for symmetric devices fabricated with perovskite pellets with different thickness and measured under dark conditions and no applied bias. Reproduced with permission.[36] Copyright 2016, American Chemical Society.

are not due to just a single process but are affected by multiple processes within similar characteristic time scale. For example, Figure 5b shows the impedance spectra of the high frequency region for symmetric devices fabricated with perovskite pellets of different thickness and measured with no applied bias under dark conditions. The high frequency impedance feature is also affected by sample bulk properties as it becomes bigger with increasing the thickness of the perovskite pellets. These findings points out the difficulty to obtain a complete PSC IS model.

Similarly, ultrafast transient optical absorption spectroscopy is employed to directly evidence the role of selective contacts towards interfacial charge dynamics.[47] The efficiency of charge injection ($A_2/\Delta A_o$ at 25 ps, with ΔA_o = 1 ps) is calculated from ratio of amplitude (A_2) with respect to the normalized amplitude (ΔA_o). This leads to $A_2/\Delta A_o$ 0.14 and 0.24 for Al_2O_3 and TiO_2 without a HSC and 0.26 and 0.34, when impregnated with HSC, respectively (**Figure 6**). In case of Al_2O_3- perovskite film (Al_2O_3 is an insulating scaffold that does not take part in charge transport) the signal completely diminishes prior to reaching a nanoscale, whereas the carriers in TiO_2-perovskite film are longer lived. Due to the absence of any HSCs, the diminishing of signal in the former is due to decay of carrier population due to recombination within the perovskite film, which upon interfacing with spiro-OMeTAD results in long living charge carriers. It also evidences electron injection from perovskite into TiO_2. The most efficient charge extraction takes place when both selective contacts, i.e., TiO_2 and spiro-OMeTAD are present. Alternatively, charge recombination dynamics, probed via nanosecond transient optical absorption spectroscopy revealed

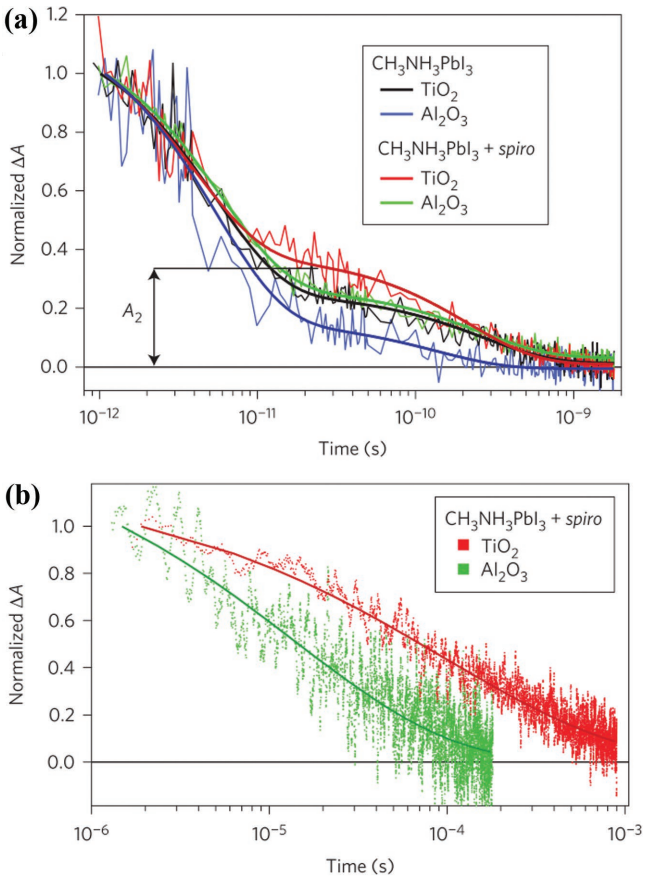

Figure 6. Transient absorption spectra to measure charge carrier dynamics in $CH_3NH_3PbI_3$ on TiO_2 (black); $CH_3NH_3PbI_3$ on Al_2O_3 (blue); $CH_3NH_3PbI_3$ and spiro-OMeTAD on TiO_2 (red); $CH_3NH_3PbI_3$ and spiro-OMeTAD on Al_2O_3 (green). The solid lines show bi-exponential fits of experimental data, b) charge recombination dynamics obtained from nanosecond-laser flash photolysis of the various systems. Thick lines are the exponential fits of the experimental data. Reproduced with permission.[47] Copyright 2014, Macmillan Publishers Ltd.

≈6–7 times faster recombination for Al_2O_3 than TiO_2 (Al_2O_3 ≈15 µs, TiO_2 ≈99 µs).

These spectroscopy experiments emphasize that although the superior charge mobility, optical absorption, density of traps, and energetics provides a platform to build high efficiency PV device, screening of rightful selective contacts (such as TiO_2, SnO_2 etc.; Al_2O_3 is only a scaffold) is ineludible. Excellent performing contacts will minimize the interfacial recombination and interfacial charge transfer resistance while not introducing significant carrier transport resistance. An appropriated balance of these characteristics will determine the most efficient contact and interfaces for PSCs.

3. Selective Contacts and Open Circuit Voltage in Perovskite Solar Cells

PSCs have surpassed the performance of other solution deposition solar cell technologies mainly due to the outstanding V_{OC} obtained which accounts for a voltage loss (EG-q V_{OC}) of <0.4 V in state-of-the-art devices (See **Table 1**). The interfacial effects are crucial in order to further push up the photovoltage. The maximum attainable photovoltage is determined by the Fermi level splitting in the perovskite layer $V_{OC,max} = (1/q)(E_{Fn} - E_{Fp})$ where E_{Fn} and E_{Fp} are the electron and hole quasi-Fermi levels in the perovskite film. As we have described in the previous section charge accumulation at interfaces produces an interfacial electrostatic potential that contributes to the Fermi level splitting and eventually increases the V_{OC}, see Figure 4d,e.[45] Herein, the unique accumulation properties of halide perovskite due to the ion migration are reflected in the high V_{OC} of PSCs. Note that $V_{OC,max}$ already takes into account the bulk recombination in the perovskite layer affecting the Fermi level splitting. Considering an almost negligible non-radiative recombination, $V_{OC,max}$ is calculated to be ≈1.33 V for $MAPbI_3$.[48] Although in a first analysis it could be considered that interfaces do not influence the bulk recombination, it is not the case in PSCs as the substrate and its interface plays an important role on the growth process of perovskite layer affecting the microstructure and defect states in bulk perovskite, and eventually the V_{OC}.[49] Climent-Pascual et al.[50] have shown that the substrate influences not only the grain size or preferential orientation of the perovskite layer but the lattice parameters, emission properties and degradation pathways, probably as different substrates induce different majority defects in the layers. After this first consideration, if an ideal selective contacts were used, $V_{OC,max}$ would be the final PSCs photovoltage. However, in a device under operation, there are multiple ways in which selective contacts produces a reduction of V_{OC} with respect to its maximum possible value (see **Figure 7**). Table 1 compares various state-of-the-art V_{OC} reports for PSCs. Although, $MAPbBr_3$ demonstrated higher V_{OC} 1.3–1.6 V (owing to its bandgap, E_g ≈2.3 eV) than $MAPbI_3$ based PSCs (V_{OC} up to 1.2 V, E_g ≈1.6 eV), the goodness of a PV device requires an account of the voltage loss and not just the obtained V_{OC}. The EG-q V_{OC} is ≈0.7 eV for the former and ≈0.4 eV for the latter (a lower EG-q V_{OC} is preferred). This leads to an excellent V_{OC}/E_g ≈0.75 in the case of $MAPbI_3$ despite the polycrystalline nature of perovskite films which is comparable to silicon (0.8), and much higher than organic solar cells (0.55).[51]

Selective contacts can directly influence the V_{OC} by the presence of surface defects/traps producing an interfacial recombination. This explains the large deviancy in the V_{OC} values for TiO_2 (from 0.6–1.1 V, see Table 1 and 3), a material well known for mid-bandgap traps. Furthermore, appropriate ESC and HSC significantly reduce interfacial recombination.[35] For example, in a comparative study of $MAPBI_3$ perovskite films deposited on top of TiO_2 with and without a HSC (spiro-OMeTD), the former showed 0.25 V higher V_{OC} than the latter.[48]

Energetics of the selective contacts also influence the V_{OC}. For example, regarding the dependency of V_{OC} on HSC HOMO level (or LUMO of the ESC), it showed ≈0.45 V increment (from 1.05 to 1.51 V) when P3HT (E_{HUMO} = –5.0 eV) is replaced with PIF8-TAA (E_{HUMO} = –5.51 eV).[52] However, band alignment is not the most determinant factor limiting the V_{OC}. This is the reason of higher V_{OC} in SnO_2 than TiO_2,[25b] a material with ≈300 meV lower CB edge than TiO_2, yet with higher electron mobility and lesser surface defects than TiO_2,[24b] making the V_{OC} of the former overcome that of the latter despite a priori

Table 1. A comparison of state-of-the-art open circuit voltage obtained using various halide perovskites in conjunction with a diverse range of electron and hole selective contacts. The CB and VB edges for $MAPbI_3$ and $MAPbBr_3$ are (–3.9/–5.4) eV and (–3.4/–5.6) eV, respectively.

V_{OC} [V]	J_{SC} [mA cm^{-2}]	FF	PCE [%]	ESC	Device architecture	HSC	Band edges (CB/HUMO)	Electron/Hole mobility [cm^2 V^{-1} s^{-1}]	Device	q V_{OC}/ EG [%]	EG-q V_{OC} [eV]	Reference
1.21	22.5	0.77	20.7	c-SnO_2	Triple cation (Cs, MA, FA) and mixed Halide(I, Br) based	Spiro-OMETAD	–	~150 (SnO_2)[60]	Planar	76	0.38	[25b]
1.13	22.5	–	19.4	PCBM/ C_{60}/BCP	$MAPbI_3$	PTAA*[a)]	–3.9■	10^{-3}(PCBM)	planar	71	0.47	[53a]
1.11	21.00	0.76	17.9	c,m-TiO_2	$Cs_x(MA_{0.17}\ FA_{0.83})_{(100x)}$ $Pb(I_{0.83}Br_{0.17})_3$	Spiro-OMETAD	–4.4■/–5.11▲	10^{-3}– 10^{-4}(HSC),[61]	Mesoporous PSC	72	0.44	[7f]
1.13	22.7	0.75	19.3	Y-TiO_2*[b)]	CH_3NH_3 $PbI_{3-x}Cl_x$	Spiro-OMETAD	–5.11▲	10^{-3}– 10^{-4}(HSC),[61]	n-i-p planar	61	0.72	[7d]
1.29	6.60	0.70	5.9	TiO_2	$MAPbBr_3$	P-TAA	–5.14▲	>0.1 (HSC),[62]	Mesoporous PSC	56	1.01	[63]
1.36	6.30	0.70	6.0	TiO_2	$MAPbBr_3$	PF8-TAA*[c)]	–5.44▲	4×10^{-3}(HSC)		59	0.94	
1.40	6.10	0.79	6.7	TiO_2	$MAPbBr_3$	PIF8-TAA*[c)]	–5.51▲	4×10^{-2}(HSC)		61	0.90	
1.04	21.3	0.73	16.2	TiO_2	$MAPbI_3$	P-TAA	–5.14▲	>0.1,[62](HSC)		67	0.51	
0.92	8.90	0.56	4.6	TiO_2	$MAPbI_3$	PF8-TAA	–5.44▲	4×10^{-3}(HSC)		59	0.63	
1.04	19.0	0.46	9.1	TiO_2	$MAPbI_3$	PIF8-TAA	–5.51▲	4×10^{-2}(HSC)		67	0.51	
1.50	4.00	0.47	2.7	Al_2O_3	$MAPbBr_{3-x}Cl_x$	CBP*[d)]	6–6.2▲[64]		MSSC	70	0.73	[56]
1.38	5.2	0.78	5.6	PCBM*[e)]	$MAPbBr_3$	PEDOT:PSS	–3.9■/–5.3▲		p-i-n inverted	60	0.92	[65]
1.61	6.04	0.77	7.5	ICBA*[f)]	$MAPbBr_3$	PEDOT:PSS	–3.7■/–5.3▲			70	0.69	

*[a)]**P-TAA**: Poly[bis(4-phenyl)(2,4,6-trimethylphenyl)amine]; *[b)]**Y-TiO2**: Yitrium doped TiO_2; *[c)]**PIF8-TAA**: poly-indenofl uoren-8-triarylamine; *[d)]**CPB**: 4,4′-bis(N-carbazolyl)-1,1′-biphenyl; *[e)]**PCBM**: Phenyl-C61-butyric acid methyl ester; *[f)]**ICBA**: 1′,1″,4′,4″-tetrahydro-di[1,4]methanonaphthaleno[1,2:2′,3′,56,60:2″,3″][5,6] fullerene-C60; ■for CB/ conduction band edge of ESC and ▲for HUMO of HSC.

worst level alignment. Similarly, the V_{OC} is also influenced by the selectivity of contacts[53] which is largely determined by the energetics of the contacts, including band alignment and surface dipoles.

Furthermore, transport properties of selecting contacts can also affect V_{OC} as high transport resistance at the selective contacts produce a voltage drop. For example, PCBTDPP showed 0.66 V higher V_{OC} than a reference P3HT based device[54] which could be attributed in part to its deeper E_{HOMO}, which is only 0.2 eV deeper than P3HT, and thereby would not account for the complete gain in V_{OC}. PCBTDPP presents ≈70 times higher hole mobility of than P3HT (0.02 cm^2 V^{-1} s^{-1}).[55] Again, one must consider that a deeper E_{HUMO} does not always guarantee a higher V_{OC}. For example, in a comparative study,[56] PSCs made using PCBM (HOMO = –6.1 eV) showed 0.24 V lesser V_{OC} than PDI (HOMO = –5.8 eV). This is because of the two orders of magnitude lower mobility of PCBM (10^{-2}–10^{-3} cm^2 V^{-1} s^{-1}) than PDI (≈2.1 cm^2 V^{-1} s^{-1}). Therefore, to obtain high V_{OC} a high charge mobility as well as suitable energy level alignment and low surface recombination are equally crucial. The same would be applicable for ESC too where selectivity of ESC and its energetics would contribute to the V_{OC}. For example, ICBA demonstrated higher V_{OC} (1.50 V) than PCBM (1.33 V) despite its lower electron mobility (0.0069 cm^2 V^{-1} s^{-1}) than the latter (0.061 cm^2 V^{-1} s^{-1}). Here, the higher lying LUMO level of ICBA facilitated better balancing of the electron quasi-Fermi level during device operation under illumination which might have created a higher built in potential across the device.[57]

An intriguing aspect regarding the V_{OC} is the role of the interfaces in radiative/non-radiative recombination ratio. Although, for a given device, it is hard to strictly quantify the V_{OC} limits from each, some initial important reports[48,53a,57,58]

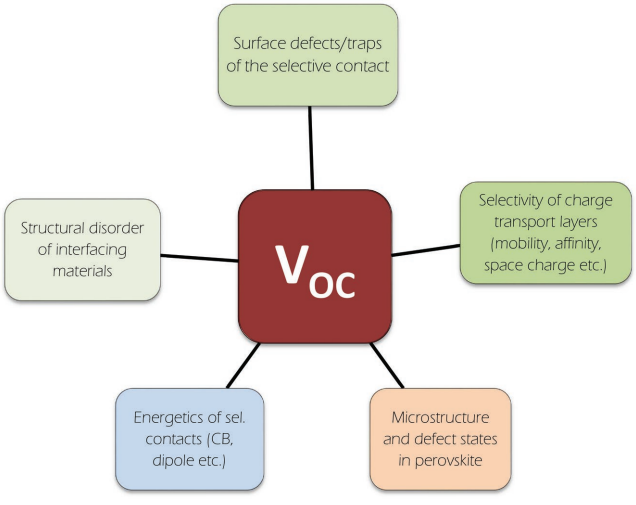

Figure 7. The various limiting factor of the open-circuit voltage in perovskite solar cells. For a details description of each, please refer to text.

suggest that the nature of interfacing materials contribute significantly to it. Two key experiments are: (i) a comparison of NiO and PEDOT:PSS as a selective contact in a planar configuration,[58] and (ii) and a comparison[48] of TiO_2 and Al_2O_3. It is noteworthy that that the non-radiative losses (arising from defects in the perovskite bulk and /or interfacial traps/defects) equal to the difference radiative losses and the V_{OC}, and are experimentally obtained as[59]

$$(\Delta V_{OC}) = V_{OC,rad} - V_{OC} = -\frac{kT}{q} ln\left(EQE_{EL}\right) \quad (2)$$

From this equation, and from electroluminescence efficiency (EQE_{EL}) Hou et al.[58] and Tress et al.[48] calculated the contribution from non-radiative losses primarily originating from the selective contact. The former reported ΔV_{OC} ≈0.39 V for PEDOT:PSS-perovskite (V_{OC} 0.92 V), and ≈0.22 V for NiO-perovskite (V_{OC} 1.08 V) whereas the $V_{OC,rad}$ was ≈1.30–1.31 V, respectively, for the both configurations. For a detailed overview on the origin of the V_{OC}, we refer to the work of Tress W.[59]

4. Hysteresis in PSCs - Role of Interfaces

The hybrid perovskites show exceptional optoelectronic properties so as to be incorporated in new kind of devices with efficient architectures. However, the observations of particular phenomena as *J–V* curve hysteresis, and switchable response by voltage pretreatment,[7c,66] point to the fact that mechanism÷nderlying PSCs performance are still only partially understood. Particularly intriguing is the scan-rate dependent hysteresis in the *J–V* curves that result in an overestimation of the photovoltaic performance when current is measured from forward-to-reverse bias sweep direction. If voltage is swept oppositely one finds lower performances, mainly through reduction in the FF as shown in **Figure 8**. Hysteresis has been related to a number of different explanations, as ferroelectric properties of the perovskite materials,[67] delayed electronic trapping processes,[68] slow ion migration,[34a,66d,69] or interfacial capacitive effect.[70] The ions/vacancies are reported to dope perovskite, make it p-/n-doped, respectively, and eventually create a built-in potential within the film and create p-i-n or n-i-p junction in the device.[66a,71] The temperature dependent poling phenomena[72] is reported to initiate once the device is exposed to illumination (a low built-in potential and the charges remain at equilibrium); however, the effect of a bias breaks the equilibrium and the ions/vacancies experience a drift towards back contact. Such a behavior often results in increase in V_{OC} under illumination that saturates after some initial light-soaking time (due to a balance between drift and diffusion of ions/vacancies).[71] Because the performance of PSCs is heavily affected by voltage scan rate and preconditioning procedures[44,68,73] concerns about device stability and reliability have appeared. As a consequence recommendations were also provided so as to show photovoltaic behavior without masking the detrimental hysteresis effect.[74]

It is widely observed that hysteresis is more apparent in planar architectures of regular deposition sequence (ITO/c-TiO_2/perovskite/*spiro*-OMeTAD/Au),[7c] in opposition to devices comprising a mesoscopic TiO_2 layer which exhibit reduced hysteretic effect.[75] The degree of hysteresis is however highly dependent on the perovskite preparation route, type and deposition method of interfaces, and specific testing conditions.[76] It is widely recognized that operation modes of PSCs greatly depend on the structure and composition of the cathode contact. Several researchers have shown a significant hysteresis reduction in planar PSCs when MOS ESCs at cathode contacts are modified. The incorporation of a self-assembled monolayer (SAM) of C_{60} on the planar TiO_2 film acting as electron collector was demonstrated to change dramatically the operation characteristic of $CH_3NH3PbI_{3-x}Cl_x$PSCs, and reduces hysteresis effects.[32c] It is believed that the fullerene derivative-SAM inhibits the formation of trap states at the TiO_2/perovskite interface, blocking as a consequence recombination paths. Modifying TiO_2 interface by fullerene post treatment has improved solar cell operation.[77] An alternative way aimed at reducing the hysteresis effect is the treatment of TiO_2 layer with Li.[78] Li-treated TiO_2 matrix is formed by spin Bis(trifluoromethane)sulfonimide lithium salt (Li-TFSI)/acetonitrile solution on the untreated mesoscopic TiO_2. It is shown that *J–V* hysteresis is further reduced by suppression of surface traps in comparison to bare mesoporous TiO_2-based PSCs.

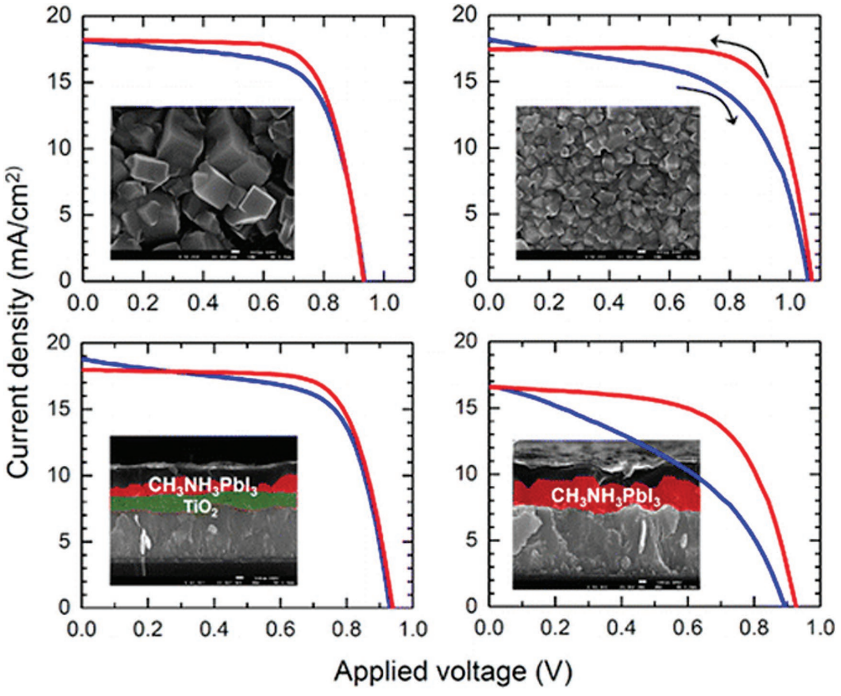

Figure 8. Some examples of the variation of the hysteretic response as a function of the $CH_3NH_3PbI_3$ crystal size and solar cell structure. Reproduced with permission.[76] Copyright 2014, American Chemical Society.

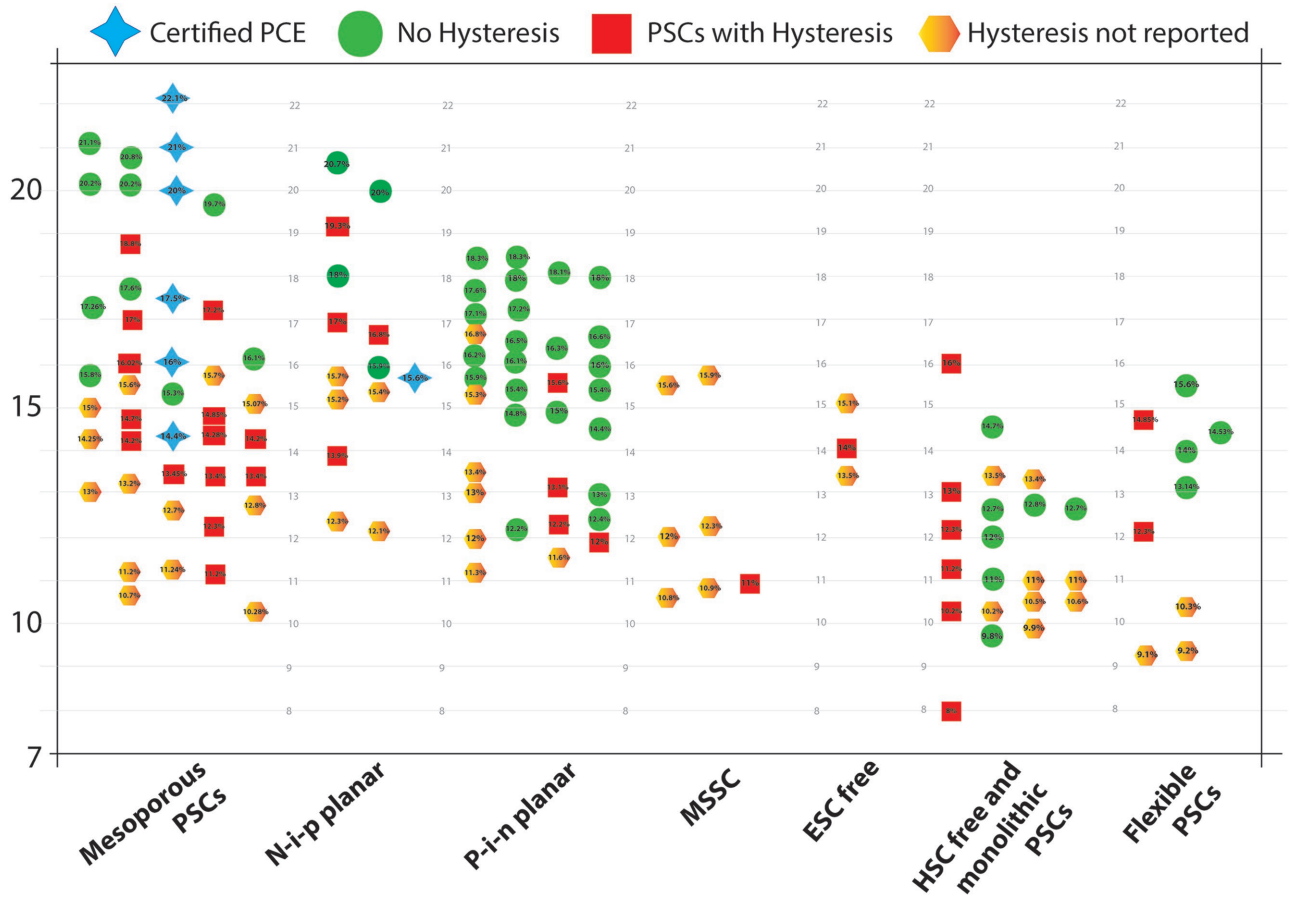

Figure 9. PCE and hysteresis measured for most successful PSCs in all six architectures and also the flexible PSCs (a total of 132). A device with relative variation ≤5% in PCE is only considered to be hysteresis-free. Detail PVs parameters (including J_{SC}, V_{OC}, FF), details on material components (ESC, HSC, perovskite), and reference of each corresponding PSC will be explained in Table 2 of the manuscript.

Similarly, incorporation of Zr into TiO_2 also demonstrated reduced hysteresis compared to a bare analogue due to interface modification and passivation of defect sites.[79]

Inverted planar architectures in which the cathode contact is deposited on top of the layer stack, replicating the OPVs, have exhibited significant or total hysteresis suppression (**Figure 9**), pointing to the important role of interfaces in this effect. For instance, devices comprising poly(3,4-ethylenedioxythiophene) poly(styrenesulfonate) (PEDOT:PSS) as anode contact and thin PCBM (20 nm)/C_{60} (20 nm) films as ESC showed improved operating characteristics.[68] Again, the reduction in hysteresis was connected to the PCBM-induced passivation of $CH_3NH_3PbI_3$ interfacial traps. Incorporation of LiF on PCBM also produced beneficial outcomes in terms of hysteresis reduction and photocurrent increment.[80] Very recently it has been observed that a reduction in hysteresis occurs not only by cathode layer engineering but also by deposition of hybrid PCBM/perovskite absorbers between planar TiO_2 and *spiro*-OMeTAD transporting layers.[22c] This would suggest that hysteresis is largely related to the characteristics of selective contacts, as also depicted in Figure 9, which compares hysteresis profile of various best performing devices from all six device architectures of PSCs and also those built on flexible substrates. Suppression of the *J–V* hysteresis observed with inverted structures comprising fullerene molecules as cathode interlayers at varying scan rates is usually checked at room temperature. This opens the question of the kinetic origin for the hysteresis reduction. If the time scale underlying the hysteresis is greater than the time window defined by the scan rate, *J–V* distortion is expected to be invisible. By cooling $CH_3NH_3PbI_3$ solar cells with top cathode containing fullerenes below room temperature significant hysteresis does appear where the thermally activated kinetic processes have been slowed down.[81] Slower relaxation of hysteretic processes seems to be behind *J–V* curve insensitivity on scan direction at higher temperatures/rates.[82] Recently a distinction between capacitive and non-capacitive hysteretic currents has been made.[83] The former being related to the charge, both ionic and electronic, accumulation ability of the TiO2/perovskite interface without any influence on the steady-state operation.

Non-capacitive hysteresis is observable in all kind of architectures being more prominent in inverted architectures, including organic compounds as bottom hole selective layers and fullerene materials as top contact, with larger distortions caused by the inherent reactivity of contact materials and absorber perovskites.[83] While capacitive hysteresis gives rise to reversible variations of the *J–V* curves that enlarge with the scan rate, non-capacitive hysteresis yields pronounced distortions of

the operation currents at slow time scale.[84] Importantly, noncapacitive hysteresis behaves in the opposite way (positive current contributions for reverse sweep directions) in comparison to capacitive contributions.[83] Irreversible chemical interactions at the perovskite/contact interfaces in relation to aging processes have been proposed to account for noncapacitive hysteresis,[85] along with strong electrical field enhancement by dipole layers in the vicinity of the contacts.[86] Recent reports reinforce the previously discussed explanation of hysteretic phenomena in terms of mechanisms occurring at the outer interfaces of the perovskite solar cells.[87]

5. Interface Engineering and Device Designs in PSCs

Research in interface engineering can be classified into two categories: (i) interface engineering via screening alternative selective contact materials or their various morphologies, and (ii) surface modification of selective contact (mostly TiO_2 and ZnO) to alter the charge carrier dynamics – both to influence stability, working mechanism, improving charge kinetics and hysteresis in PSCs. Owing to the crucial role the interfaces (or the interfacing materials) play for PSCs, a rise in dedicated research activities can also be observed for them (see **Figure 10**) in a similar fashion to that of the PSCs. For example, the conventionally employed TiO_2 or ZnO, well-known for their inferior electronic transport and surface defects, respectively, are replaced with high mobility SnO_2 or their doped counterparts and various binary oxides such as $BaSnO_2$, Zn_2SnO_4, and $SrTiO_3$. Similar, high performance (PCE 18–19%) and stability of few hundreds of hours in planar architectures of PSCs, which often demonstrates reduced trap-assisted non-radiative recombination, is also noticed owing to the judicious selection of interfacing materials. For example, inverted PSCs (p-i-n) are known for unstable performance due to the presence of organic selective contacts (PEDOT:PSS and PCBM). Replacement of organic HSC (PEDOT:PSS) by an inorganic counterpart (NiO) and PCBM by inorganic TiO_2 or ZnO has shown that the device could retain >90% of initial PCE after 60 days of testing at ambient.[88] Similarly, surface modification of ESC (TiO_2) has also improved UV-photo stability of the devices[22b] and also restricted degradation of perovskite at the ESC-perovskite interface,[22a,39,89,126] as will be discussed in the stability section of this article.

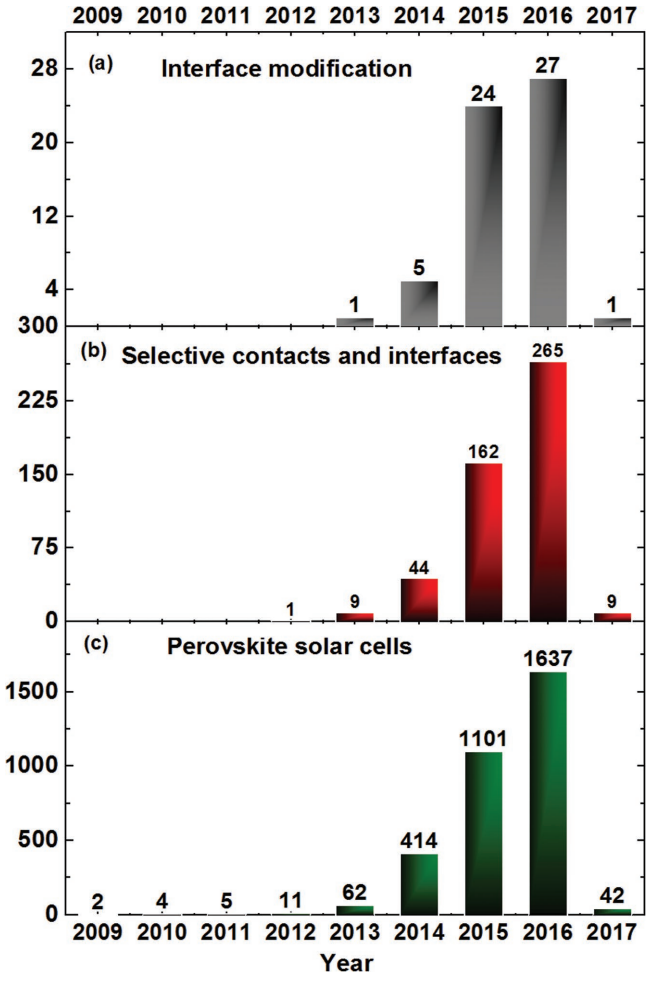

Figure 10. A trend of research publications showing a comparison between total articles on perovskite solar cells, selective contacts and interfaces, and interface engineering/modification in PSCs since their inception in 2009 till date (14 December 2016). The data is obtained from Scopus using key words "*perovskite solar cells*", *perovskite solar cells and interface*" and "*perovskite solar cells* AND *interface modification/engineering*", respectively.

5.1. Nanostructured Scaffolds for Perovskite Solar Cells

Typically, the state-of-the-art efficiency (20–22%) is obtained for devices with TiO_2 scaffold (see Table 3 and **Figure 11**), although recently a first planar PSC with PCE >20% is also demonstrated.[17] Despite the fact that the origin of this effect is not fully understood, Anaya et al.[38] suggested that the mesoporous scaffold could hinder ion migration producing lower majority carrier accumulation at the interface and consequently a lower recombination thereby. A more clear interpretation of the advantageous effects of the scaffold can be understood in the case of lead-free perovskites. Given the diffusion length (L_D) of perovskite is shorter for such perovskites than the light absorption length, scaffold helps in the photocarrier collection. For example, no photocurrent is measured in planar $ASnX_3$ PSCs whereas the mesoporous rivals showed high J_{SC} (15–21 mA cm^{-2}).[90]

Ever since the first report on PSCs, TiO_2 nanoparticles (NPs) scaffold has been a successful material of choice and the highest PCE ≈20–22.2% in PSCs is achieved using the them in conjunction with optimized perovskite, i.e., combining formamidinium (FA) and methyl ammonium (MA) as inorganic cations[14a] and I and Br as anions, and using molecularly engineered HSC.[14b] For example, a high PCE ≈20.8% is obtained using mixed perovskite containing MA and FA and also I and Br over TiO_2 scaffold whereas the device reporting PCE 21.1% utilized a perovskite with triple cation (MA/FA/Cs) (Table 3). They key reason behind the success of TiO_2 NPs is the intensive research being carried out to develop high quality pastes

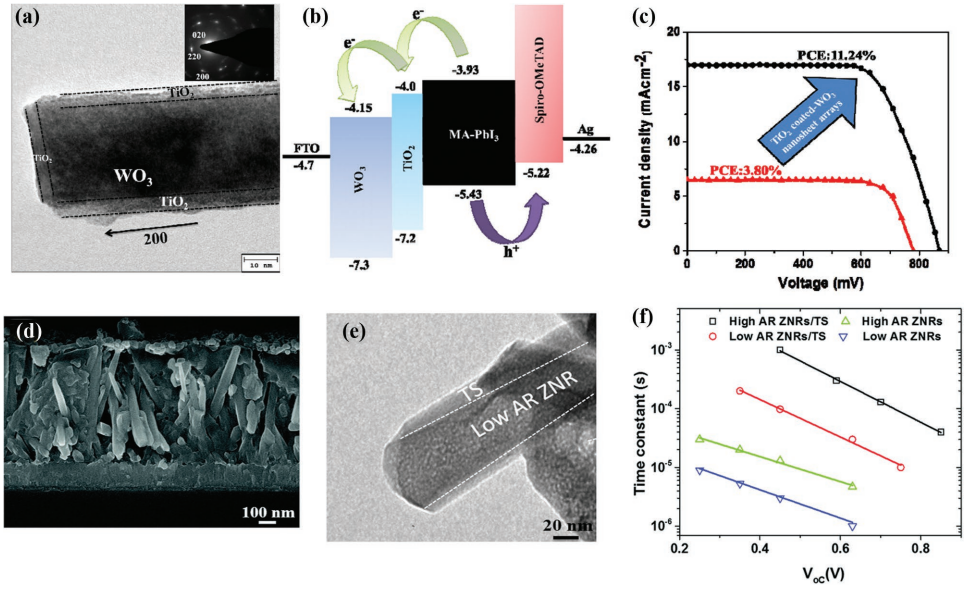

Figure 11. a) TEM image of WO_3-TiO_2 core-shell nanorod, b) energy level diagram of the $WO_3/CH_3NH_3PbI_3$/HTM/Ag device exhibiting a favored electron injection and hole extraction, c) a characteristic current-voltage curve of a pure WO_3 and a WO_3-TiO_2 core-shell analogue. Redroduced with permission.[119] Copyright 2015, The Royal Society of Chemistry. d) Cross-sectional view of device employing ZnO nanorods coated with TiO_2 (ZNRs), e) TEM image of a ZNR with TiO_2 shell (TS), and f) charge recombination lifetime of four different ESC-based PSCs, employing various ratio of ZNR and TS. Reproduced with permission.[118] Copyright 2015, The Royal Society of Chemistry.

that provide a porous architecture ultimately providing a desired scaffold for perovskite crystals.

Despite the fact that the TiO_2 NPs are the champion material, they offer various challenges for a commercial deployment of PSCs that would require efficient, stable and cost-effective material constituents. The key problems associated with TiO_2 NPs are their susceptibility to UV light,[40] its low electron mobility (μ_e<0.1 cm^{-2} v^{-1} s^{-1})[60,91] their sub-bandgap trap states that hinders charge collection, and their surface defects that are reported to act as a humidity trap and also known to form a reactive interface to perovskite making it vulnerable to degradation.[22a,89] Also, TiO_2 layer require sintering at high temperature (≈450 °C)[9d,92] which is not compatible with roll-to-roll production. This brings into account the UV-stable SnO_2[24b,93] and low-temperature processable ZnO nanostructures[94]; materials that offer higher electron mobility than TiO_2. However, ZnO nanoparticles have not been a very successful choice in PSCs, particularly when employed as a mesoporous scaffold, resulting in a typical PCE 9–10.5%.[95] Despite the fact that ZnO films can be processed at temperature as low as ≈70 °C,[95b] they typically experience interfacial charge recombination, primarily due to presence of defect states in ZnO and a lower PCE thereby. The reasons for lower performance in ZnO based PSCs is also understood to be the decomposition of perovskite crystals when deposited on ZnO-NPs surface. An investigation of the $CH_3NH_3PbI_3$ crystal growth on bare ZnO-NPs film shows that the presence of hydroxide groups and residual acetate ligands on the surface of ZnO lead to deprotonation of perovskite crystals,[96] an issue which can partly be overcome via suitable doping[97] or via sintering the films at higher temperature[98] to remove defect states. Another remedy is to add a buffer layer such as $PC_{61}BM$ between ZnO and perovskite which has shown to effectively reduce charge recombination at ZnO-perovskite interface and improved PCE from ≈6.4% to ≈10.2%,[96] however the best performance of ZnO/buffer-layer PSCs is still reported in planar device architectures (PCE 15.9%)[99] that will be discussed in a subsequent section of planar PSCs. Nevertheless, the performance in ZnO based PSCs is improved by either employing pure (PCE ≈10–11%)[100] or doped one-dimensional nanorods (PCE ≈14.35%),[101] and their planar (PCE up to 15.7%)[102] or inverted planar device architectures (PCE ≈16.1%).[88]

PSCs based on SnO_2, unlike its ZnO counterparts, have shown great success with an average PCE as high as ≈16% (photocurrent density (J_{SC}) ≈22.8 mA cm^{-2}, open circuit voltage (V_{OC}) ≈1.11 V and fill factor (FF) ≈0.64) owing to their high electronic mobility.[25a] The highest performance using SnO_2 nanocrystals, till date, is achieved in inverted PSCs in conjunction with NiO as HSC (PCE 18.8%) which also showed remarkably stable performance for 30 days at high humidity conditions.[103]

CdS quantum dots and Nb_2O_5 are two other ESC materials employed in PSCs owing to their higher electronic conductivity and significantly higher CB and demonstrated PCE ≈11.2%[104] and 8.8%, respectively.[105] In addition, binary oxides such as $SrTiO_3$,[106] $BaSnO_3$ and Zn_2SnO_4 have been reported in PSCs.[106b] It is important to note that $SrTiO_3$ has nearly similar conduction band edge (CB) as that of $CH_3NH_3PbI_3$, i.e., −3.9 eV (vs vacuum) where electron injection might be an issue; and therefore, $CH_3NH_3PbI_{3-x}Cl_x$ with CB at ≈−3.8 eV (vs vacuum) is more favored for electron injection. Similarly, $BaSnO_3$ having a similar crystal structure as that of $MAPbI_3$ is employed in PSCs that demonstrated PCE 12.3%, higher than that of a reference device made using TiO_2 (PCE ≈11.1%).[107] However, the PSCs employing $BaSnO_3$ showed higher charge recombination at high bias voltage and also a very high hysteresis.

Another successful material that offers high electron mobility (10–30 $cm^2\ V^{-1}\ s^{-1}$)[108] is Zn_2SO_4. Till date, the best performance in Zn_2SO_4 PSCs is reported when a thin flat layer is deposited over flexible substrates (PET/ITO) via low temperature processing resulting in PCE ≈14.85%.[109] This high performance is achieved by developing a pin-hole free flat perovskite layer over a Zn_2SO_4 flat film via spin coating at a temperature ≈100 °C which also makes it compatible with roll-to-roll processing.

5.1.1. Doped and Composite ESC Materials

Doping have been known as an effective method to modify electronic bands structure of MOS in organic solar cells[110] which routinely resulted in improved PV parameters, particularly, the V_{OC}.[111] In mesoscopic PSCs, doping has shown to improve charge transport properties eventually overcoming the interfacial recombination and hysteresis and also have demonstrated an increase in the V_{OC} in these device.[112] In such cases, the CB is tuned by suitably doping a metal ion, such as Y^{3+}, Al^{3+}, Nb^{5+}, and Mg^{2+} etc., into crystal lattice of MOS ESC (typically TiO_2, ZnO or SnO_2).[112a,b,113]

A crucial aspect during doping is to optimize the dopant concentration because addition of impurities induces strains in the TiO_2 crystal, which increases grain boundaries within the TiO_2. Nb doping by Kim et al.[112d] showed that while 0.5% Nb doping in TiO_2 resulted in improved optical properties, a further increase in dopant concentration to 1 and 5% lowered the device performance. The 0.5% doping resulted in V_{OC} as high as 990 mV, ≈40 mV higher than pure TiO_2 analogues, higher J_{SC} and FF and demonstrated a final PCE ≈13.4% notably higher than pure TiO_2 (≈12.9%).

Doping has also shown to reduce charge recombination at MOS/perovskite interface by reducing the surface defects of the ESC and also played a role in improving perovskite crystallization behavior. In a report by Qin et al,[114] 0.5% Y^{3+} doped TiO_2 although resulted in 15% improved J_{SC}, surprisingly no change in the V_{OC} is observed. Other possibilities to modify the ESC crystal structures are through incorporation of Nb^{5+} and Ga^{3+} or coating with a thin layer of an insulating oxide such as ZrO_2 or $CaCO_3$, strategies that have demonstrated potential to alter electron injection dynamics by modifying the interface properties in DSCs.[115]

The ESC–$CH_3NH_3PbX_3$ interface is a possible recombination center which not only suppresses the FF in PSCs but often also results in inferior V_{OC}. Herein, surface coating of scaffold layer is a remedy to avoid charge recombination.[116] For example, Han et al.[117] reported modification TiO_2 ESC in PSCs using an ultrathin MgO layer (1–2 nm) on TiO_2 NPs that extended carrier lifetime (τ_n). The V_{OC} increased from ≈840 mV (PCE 11.4%) to ≈1000 mV (PCE 12.7%) when the MgO layer thickness is systematically increased. Despite the improvement in V_{OC} the J_{SC} decreased while increasing the insulating over-layer thickness beyond a critical threshold due to reduced electron injection owing to large bandgap of MgO monolayer (7.8 eV) compared to TiO_2 (3.2 eV). Similar strategy adopted in ZnO MOS, a material known for its surface defects[94a] and to decompose perovskite crystals during thermal annealing,[96] resulted in PCE ≈4.3% and ≈15.4% in ZnO/CdS NPs[164] and ZnO-NRs/TiO_2-NP[118] core-shell architectures, respectively. The ZnO surface modification not only resulted in performance improvement due to improved light absorption, passivation of the notorious defect states, and improved charge injection efficiency from $CH_3NH_3PbI_3$ to ESC, but also, more importantly, eliminated the perovskite degradation on its surface and reduced the anomalous hysteresis significantly. A similar progress is also shown in WO_3-TiO_2 core-shell architectures resulted in ≈11.2% PCE where a highly porous WO_3 ESC is post-treated with a thin TiO_2 NP layer (Figure 11).[119]

5.1.2. One-Dimensional and Three-Dimensional Electron Selective Contacts

The electron transport through a material strongly depends on its morphology; the transport is anisotropic for one- and three-dimensional nano-architectures such as wires, flowers and hierarchical structures. Available evidences suggest that charge separation and transport in PSCs take place within perovskite, perovskite-ESC and perovskite-HSC interfaces; therefore, morphology of the selective contacts are detrimental for the interfacial recombination and hence the PCE.[120] The diffusion lengths of electron and hole in hybrid perovskites are over ≈1 μm[121] with orders of magnitude higher electron mobility than materials used for ESC and HSC (Table 1), which makes the charge recombination significant at the interfaces. This put stringent conditions, particularly on ESC, to be a material of high charge mobility and defect-free. Besides the inferior electronic mobility of the typically employed TiO_2 NPs, another crucial issue is their poor pore-filling due to labyrinthine mesoporous morphology which could be resolved by employing one-dimensional materials with more porous morphology such as nanotubes (NTs), nanowires (NWs), nanorods (NRs) or hierarchical structures (HS).

Alternative morphologies to NPs, which are known for inferior electronic transport and large grain boundary density, have been widely adopted to improve charge kinetics at the interfaces. Such morphologies improved charge collection in PSCs, particularly those made using ZnO. The state-of-the-art PCE of TiO_2 NP and 1D nanostructures is 21.2% (although 22.1% is published in NREL efficiency chart, the details of the device are not given) and 14%, respectively, whereas in ZnO these values are 15.7% and 16.1%, respectively (Table 3), clearly demonstrating the beneficial effects in the latter in removing surface defect when employing 1D nanostructures. A detailed account of such various key-reports is listed in Table 3. The first report on TiO_2 NRs PSCs was by Kim et al.[127] who employed highly crystalline NRs, a material that offers two orders of magnitude higher electron mobility than their NP counterparts, and reported a PCE ≈9.4% (J_{SC} ≈15.6 mA cm^{-2}). Surface passivation of the ESC interface (TiO_2 nanorods) by a thin TiO_2 layer grown via atomic layer deposition resulted in further improvement in PCE (13.45%),[128] which is also, to the best of our knowledge, the best PCE by a pure TiO_2 NR PSC. In addition to the pristine TiO_2 NRs, their doped analogues such as Mg-, Sn- and Nb-doped are also employed in PSCs resulting in PCE ≈4.17%,[112a] 7.5%,[112b] and 6.3%,[112c] respectively. In addition to TiO_2 NRs,

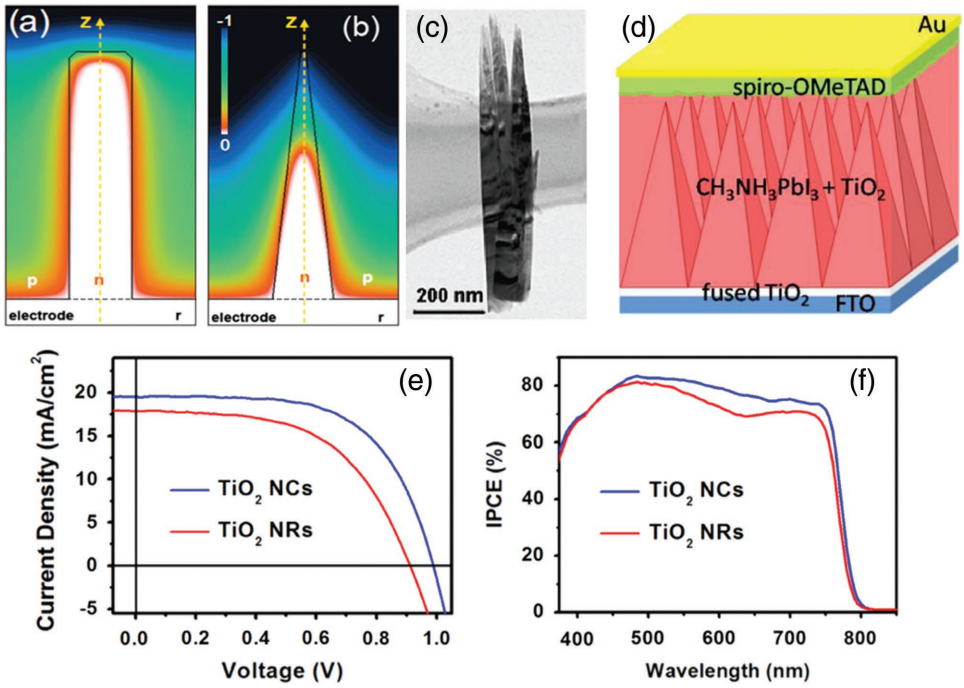

Figure 12. a,b) Electric potential contours of n-type nanorod and nanocone in a p-type matrix. Herein, for the electric potential created due to the p-n junction. For nanocones the electrostatic potential varies in both axial and radial directions whereas it remains constant for nanorods in axial direction. This potential variation creates an electric field in nanocones along the axial direction which acts as a driving force for electrons in nanocones eventually resulting in improved electronic transport.[131,133] c) is a TEM image of a nanocone employed in PSCs whereas d) is a schematic of a full PSC fabricated using NCs, e,f) are I-V and IPCE spectra of two PSCs fabricated using NCs and NRs.[131] Reproduced with permission.[131] Copyright 2015 Elsevier Inc.

ZnO NRs ESC (thickness ≈600 nm) have also demonstrated a PCE ≈14.35%, achieved in their surface modified architectures by over coating a thin TiO_2 layer (<10 nm). The efficiency is slightly lower in pure ZnO NRs (13.4%) prepared by magnetron sputtering (thickness <200 nm),[129] which is the best PCE in pure ZnO NRs. However, the best performance (≈16.1%) of ZnO NRs based PSCs is achieved in their nitrogen-doped nanostructures and also by optimizing its aspect ratio, enhancing electron density, and substantially reducing their work function than conventional ZnO NRs.[94b] The results showed that surface modification to overcome intrinsic defects sites on ZnO and their suitable doping have the potential to further improvement. These examples demonstrate that for an efficient selective contact, surface properties and energy level alignment with perovskite should also be taken into account besides its electrical properties.

The nanorods are typically grown via a highly acidic synthesis route making is challenging for large scale fabrication. An acid free synthesis of TiO_2 NRs is also reported resulting in PCE ≈11.1%.[130] Furthermore, other morphologies such as nanocones (NCs)[131] synthesized using a green-method have also been employed as ESC resulting in PCE ≈11.9% (thickness >1 µm). These NCs provided additional advantages of superior charge collection and enhanced absorbance owing to the greater perovskite loading in their relatively wider voids than NRs (Figure 11).[132] The superior charge collection can be attributed to the fact that NCs provide larger surface to volume ratio compared to other 1D morphologies and thereby improve charge separation or the presence of electrostatic force that acts as a driving force for electrons collection within NCs with enhanced carrier lifetime (**Figure 12**).[133]

Nanowires (NWs) as an ESC material have also shown remarkable performance in PSCs leading to a maximum PCE ≈14.2% using a dendritic morphology (thickness ≈250 nm),[134] an improvement from initial ≈4.9% and ≈12.8%, using ≈1.5 µm thick TiO_2 NWs[135] and <500 nm thick TiO_2 NWs.[136] TiO_2 Nanotubes (NTs) have also been an ESC material of choice in PSCs owing to their directed electron transport and hollow morphology.[137] The state-of-the-art PCE 14.8% is reported by Qin et al.[137d] via efficient pore-filling of NTs. Future route to improve performance of NT based PSCs could be to employ SnO_2 NTs which offer high electronic mobility.[24a]

Another strategy to engineer the ESC interface with 1D materials is to employ composite nanostructures which typically resulted in high PCE >14%. A surface treatment of low mobility MOS such as TiO_2 with a high mobility SnO_2 or an insulator such as MgO to remove surface traps or alternatively, reduction in surface defects of ZnO by TiO_2 thin layer has already been established with few successful architectures such as ZnO/CdS NR (≈4.3%),[138] SnO_2 NWs/TiO_2 shell (≈14.2%),[139] WO_3/TiO_2 (≈11.2%),[119] MgO coated TiO_2(≈15.3%) and core-shell ZnO-TiO_2 (≈15.3%).[118] Three dimensional (3D) nanostructures are employed to simultaneously offer high surface area, improved light harvesting and also superior electron transport,[140] as evidenced by their inception in PSCs (PCE ≈9%).[141,192] In a such report involving in inverse-opal like multifunction TiO_2 scaffold (≈200 nm) synthesized via a simple solution processing a PCE ≈13.1% is reported which is higher than a TiO_2NP analogue

Table 2. An account of electronic properties of various common perovskites, electron and hole transport materials. Values are taken from ref. [90c] if not stated otherwise.

Material/Morphology	Diffusion Length [μm]	Diffusion coefficient [$cm^2\ s^{-1}$]	Charge mobility [$cm^2\ V^{-1}\ s^{-1}$]
$CH_3NH_3PbI_3$	14.0 ± 5.1	1.59–2.41	56.4 to 93.9[90c,122]
$CH_3NH_3PbBr_3$	6.0 ± 1.6	0.50 to 1.44	19.4–56.1
$CH_3NH_3PbI_xCl_{3-x}$	≈8 times higher than $CH_3NH_3PbI_3$[168]	≈2.5 times higher than $CH_3NH_3PbI_3$[121]	≈2.5 times higher than $CH_3NH_3PbI_3$
TiO_2 (spherical)	10–90[123]	$\approx 10^{-5}$–10^{-4}[124]	1×10^{-7},[91]
TiO_2 (1-D)		2 order of magnitude higher than NPs[124]	2 order of magnitude higher than NPs
Spiro-OMeTAD	–	–	4×10^{-5},[125]
P3HT			$\approx 10^{-4}$–10^{-3},[126]

(≈11%).[142] These novel structures alleviated the deposition of a compact layer that is typically required to block holes reaching the FTO and thereby made the device fabrication easier. Other unconventional 3D morphologies employed are branched shaped M13-virus enabled ESC (PCE ≈7.5%)[140b] and 3D TiO_2 nanodendrites (PCE ≈13.2%).[140a]

5.1.3. Bi-Layered Mesoporous Scaffolds

So far, the two important factors, such as low interfacial recombination at ESC/perovskite or FTO/ESC, have been achieved in separate materials or via cumbersome surface modification of MOS. ZnO although provide high electron mobility its energy offset with perovskite and its poor hole blocking characteristics hinder its further progress in PSCs. Similarly, TiO_2, which has shown to effectively block holes reaching FTO and thereby achieving a remarkable progress in its mesoporous or planar architectures, still suffers from intrinsic lower electron mobility (**Table 2**). To overcome this issue and to develop an easy to fabricate ESC combining the two crucial parameters, Xu et al.[143] proposed a simple TiO_2/ZnO bilayer architecture thereby combining good blocking behavior and electrical conductivity in a single ESC. The bilayer ESC resulted in PCE ≈17.2% with negligible hysteresis which is a significant improvement when compared to corresponding PSCs employing a single ESC (TiO_2 ≈10.2% and ZnO ≈13.2%). The bilayer not only demonstrated efficient charge extraction but also no dark current thereby establishing an efficient hole blocking behavior. A similar performance enhancement is also observed in inverted PSCs where a ZnO/PCBM bilayer ESC has shown remarkable PCE ≈14.2%, significantly higher than a pristine ZnO or PCBM counterpart.[144]

5.1.4. Compact Layer to Avoid Interfacial Recombination

High performance PSCs typically employ a thin compact hole blocking layer (CL, <50 nm) underneath the mesoporous scaffold (200–300 nm) on conducting substrates to avoid a direct contact between HSC and transparent conductive oxide which may otherwise induce short circuit in the device eventually resulting in a low FF. The interfacial charge recombination may become even intense as perovskite layer itself act as a hole transporter[145] and a physical barrier between FTO and $CH_3NH_3PbX_3$ is important. The function of CL is conceived to be hole blocking only, although there are arguments that it can also act as an ESC.[7a,146] Nevertheless, the compact layer has shown to significantly improve the performance of PSCs by minimizing charge recombination, particularly, in cases when the mesoporous TiO_2 layer or perovskite layer is characterized by nano size pinholes.[16,147]

A crucial aspect while preparing CL is optimizing its thickness as demonstrated by Hong et al.[148] and Wang et al.[149] Although it is reported that performance of PSCs increases with increasing CL thickness (from 0 to 90 nm)[149] because a thicker layer has lesser pinholes which suppress interfacial recombination, it increases transport resistance within the film. Nevertheless, an optimized selective contact thickness is crucial to efficient block shunting within the device and also not to increase electron transport resistance.

5.2. Planar Selective Contacts and Improved Charge Extraction at Interfaces

Planar heterojunction architecture of PSCs resembles thin film solar cells or polymer solar cells (OPVs) where an absorber layer is employed between flat electron and hole selective contacts, making it a planar heterojunction cell unlike mesoporous scaffolds based PSCs which are more like a bulk heterojunction device.[7a] The elimination of mesoporous TiO_2 scaffold is beneficial when commercial scale production is concerned as planar architecture eliminates two-step processing of the mesoporous layer, i.e., coating and subsequent high temperature sintering. This marks them as a preferred device design in PSCs, particularly after their high PCE report (19–20%, **Table 3**)[7d,17] which is closer to the state-of-the-art mesoporous architecture counterpart (22.1%). Although from a production related cost viewpoint the planar architecture seems to be adopted as the ultimate device design, it is rather challenging (at least at the moment) when the stability (next important parameter to efficiency) is taken into account. Whereas the mesoporous architecture delivered a certified efficiency 22%, the value, for a planar rival, is only 15.6% (certified).[51] However uncertified PCE >20% is recently reported.[17] Nonetheless, in the high efficiency planar *vs* mesoporous PSCs, a distinction is hard to draw, not only because the planar layers often resemble a

Table 3. Photovoltaic parameters of perovskite solar cells employing various types of MOS as electron transport layer. Only the key reports are included in the table for comparison. The table is categorized according to the device architectures and within each category according to the type of ESC employed.

Device architecture	ESC/Morphology	ESC Thickness [nm]	Method of deposition (perovskite)	Substrate	Perovskite	HSC	J_{SC} [mA cm^{-2}]	V_{OC} [V]	FF	PCE [%]	Ref.
Mesoporous or Mesoscopic (Include mono and binary MOS and their various morphologies, composite and bilayer structures)	c-TiO_2/m-TiO_2 NPs	150 nm	Single step	FTO	$Cs_x(MA_{0.17}FA_{0.83})_{(100-x)}Pb(I_{0.83}Br_{0.17})_3$	Li- and Co doped Spiro	23.5	1.15	0.78	21.2	Saliba et al.[7f]
	c-TiO_2/m-TiO_2 NPs	≈200 nm	Single step	FTO	PbI/FAI_2, MABr/$PbBr_2$	Spiro-OMeTAD	24.6	1.16	0.73	20.8	Bi et al.[14c]
	c-TiO_2/m-TiO_2 NPs	≈200 nm	VASP	FTO	FA0.81MA0.15 PbI2.51Br0.45	Spiro-OMeTAD	23.4	1.14	0.76	20.5 (19.5) cert*	Li et al.[14c]
	c-TiO_2/m-TiO_2 NPs	–/≈300 nm	Sequential deposition	FTO	$FAPbI_3$	PTAA	24.7	1.06	0.77	20.2	Yang et al.[14a]
	c-TiO_2/m-TiO_2 NPs	30 nm/200 nm	Sequential deposition	FTO	$CH_3NH_3PbI_3$ And $CH_3NH_3PbBr_3$	FDT[a)]	22.7	1.15	0.76	20.2	Saliba et al.[14b]
	c-TiO_2/m-TiO_2 NPs	40 nm/230 nm	Sequential deposition	FTO	$MAPbI_3$.DMSO	Spiro-OMeTAD	23.83	1.09	0.76	19.7	Ahn et al.[173]
	c-TiO_2/m-TiO_2 NPs	≈150 nm	Single step	FTO	$((FAPbI_3)_{0.85}(MAPbBr_3)_{0.15})$	Spiro-OMeTAD	22.3	1.1	0.70	18.8	Aitola et al.[174]
	c-TiO_2/m-TiO_2 NPs	70 nm/300 nm	2-step spin coating	FTO	$CH_3NH_3Pb(I_{1-x}Br_x)_3$	PTAA	19.6	1.1	0.76	16.5	Jeon et al.[7c]
	TiO_2 (0D + 1D + 2D)	30 nm/150 nm	Single step	FTO	$CH_3NH_3PbI_3$	Spiro-OMeTAD	22.6	1.05	0.70	16%	Wu et al.[175]
	TiO_2 Nanotubes	420 nm	Two step spin coating	FTO	$CH_3NH_3PbI_3$	Spiro-OMeTAD	22.6	1.0	0.64	14.8	Qin et al.[137d]
	TiO_2 Nanowires	220 nm	One step spin coating	FTO	$CH_3NH_3PbI_3$	Spiro-OMeTAD	20.3	0.99	0.70	14.2	Wu et al.[134]
	TiO_2 NRs	≈1.5 μm	Two-step spin coating	FTO	$CH_3NH_3PbI_3$	Spiro-OMeTAD	19.8 ± 0.7	0.97 ± 0.01	0.72 ±	13.45 ± 0.35	Mali et al.[128]
	TiO_2 Nanowires	430 nm	Sequential deposition	FTO	$CH_3NH_3PbI_3$	Spiro-OMeTAD	18.2	1.05	0.67	12.8	Tao et al.[136]
	TiO_2 NRs	≈1.8 μm	Single step	FTO	$CH_3NH_3PbI_{3-x}Cl_x$	Spiro-OMeTAD	21.8	0.8	0.68	11.8	Li et al.[176]
	TiO_2Nanocones	150 nm	Two step spin coating	FTO	$CH_3NH_3PbI_3$	Spiro-OMeTAD	18.2	0.94	0.67	11.4	Peng et al.[132]
	Nb-doped TiO_2 NRs	≈600 nm	Single step	FTO	$CH_3NH_3PbI_xBr_{3-x}$	Spiro-OMeTAD	16.6	0.89	≈0.52	7.5	Yang et al.[112b]
	Sn-doped TiO_2 NRs	>600 nm	Sequential deposition	FTO	$CH_3NH_3PbI_3$	Spiro-OMeTAD	14.9	0.74	0.52	6.3	Zhang et al.[112c]
	3D TiO_2	400 nm	Sequential deposition	FTO	$CH_3NH_3PbI_3$	Spiro-OMeTAD	22.9	0.92	0.62	13.2	Lin et al.[140a]
	TiO_2/ZnO bi layer	–	Spin coating	FTO	$CH_3NH_3PbI_3$	Spiro-OMeTAD	20.8	1.08	0.71	16.1	Xu et al.[143]
	ZnO NPs	≈25 nm	Sequential deposition	ITO	$CH_3NH_3PbI_3$	Spiro-OMeTAD	20.4	1.03	0.75	15.7	Liu et al.[9f]
	ZnO NRs	40–160 nm	Sequential deposition	FTO	$CH_3NH_3PbI_3$	Spiro-OMeTAD	22.4	1.04	0.57	13.4	Liang et al.[129]
	N:ZnO NRs	0.6–1.1 μm	Sequential deposition	ITO	$CH_3NH_3PbI_3$	Spiro-OMeTAD	21.5	0.96	0.70	16.1	Mahmood et al.[94b]
	Al-doped ZnO NRs	≈600 nm	–	FTO	$CH_3NH_3PbI_3$	Spiro-OMeTAD	≈20	≈0.91	≈0.58	10.7	Dong et al.[113d]
	ZnO-NR/TiO_2 core-shell	600–700 nm	Sequential deposition	FTO	$CH_3NH_3PbI_3$	Spiro-OMeTAD	22	1	0.7	15.4	Mahmood et al.[118]
	ZnO NRs-TiO_2NPs	≈600 nm	Two step spin coating	FTO	$CH_3NH_3PbI_3$	Spiro-OMeTAD	19.4	1.05	0.70	14.35%	Son et al.[177]
	SnO_2 NPs	60 nm	Sequential deposition	FTO	$CH_3NH_3PbI_3$	Spiro-OMeTAD	22.83	1.11	0.64	16	Ke et al.[25a]

Table 3. Continued.

Device architecture	ESC/Morphology	ESC Thickness [nm]	Method of deposition (perovskite)	Substrate	Perovskite	HSC	J_{SC} [mA cm^{-2}]	V_{OC} [V]	FF	PCE [%]	Ref.
	SnO_2 NWs	300 nm	Sequential deposition	FTO	$CH_3NH_3PbI_3$	Spiro-OMeTAD	21.2	1.02	0.65	14.2	Han et al.[139]
	CdS	30 nm	Sequential deposition	FTO	$CH_3NH_3PbI_3$	Spiro-OMeTAD	16.1	1.05	0.66	11.2%	Liu et al.[104]
	$SrTiO_3$	–	Sequential deposition	FTO	$CH_3NH_3PbI_3$	Spiro-OMeTAD	18.08	0.97	0.57	10%	Wang et al.[106b]
	$BaSnO_3$	≈300 nm	Sequential deposition	FTO	$CH_3NH_3PbI_3$	Spiro-OMeTAD	16.8	1.03	0.71	12.3	Zhu et al.[107]
	Zn_2SO_4	≈100 nm/ ≈300 nm	Sequential deposition	FTO	$CH_3NH_3PbI_3$	Spiro-OMeTAD	13.78	0.83	0.61	7.02	Oh et al.[178]
	Zn_2SO_4 NFs (C-L + m-L)	≈700 nm	Sequential deposition	FTO	$CH_3NH_3PbI_3$	Spiro-OMeTAD	12.68	0.99	0.59	7.38	Mali et al.[179]
	Zn_2SO_4 NPs	–/≈200 nm	2-step spin coating	PET/ITO	$CH_3NH_3PbI_3$	PTAA	21.4	1.05	0.66	14.85	Shin et al.[109]
	WO_3-TiO_2 core-shell	≈700 nm	Sequential deposition	FTO	$CH_3NH_3PbI_3$	Spiro-OMeTAD	17	0.87	0.76	11.24	Mahmood et al.[119]
Device architecture	ESC/Morphology	CL Thickness [nm]	Method of deposition (ESC/perovskite)	Substrate	Perovskite	HSC	J_{SC} [mA cm^{-2}]	V_{OC} [V]	FF	PCE [%]	Ref.
Planar (n-i-p) on glass substrates	c-TiO_2	<50 nm	Vapor deposition	FTO	$CH_3NH_3PbI_{3-x}Cl_x$	Spiro-OMeTAD	21.5	1.07	0.67	15.4	Liu et al.[151]
	c-TiO_2	<50 nm	Sol. processing	FTO	$CH_3NH_3PbI_{3-x}Cl_x$	Spiro-OMeTAD	17.6	0.84	0.58	8.6	Liu et al.[151]
	c-TiO_2	–	Sol. processing	FTO	$CH_3NH_3PbI_{3-x}Cl_x$	Spiro-OMeTAD	20.3	0.89	0.64	11.4	Eperon et al.[150]
	c-TiO_2	<50 nm	LP-VASP[b,c]	FTO	$CH_3NH_3PbI_{3-x}Cl_x$	Spiro-OMeTAD	21.7	1.04	0.75	16.8	Li et al.[153]
	Y-TiO_2[d]	<50 nm	Sol. processing	PEIE-ITO[e]	$CH_3NH_3PbI_{3-x}Cl_x$	Li-,Co-doped Spiro-OMeTAD	22.7	1.13	0.75	19.3	Zhou et al.[7d]
	c-ZnO	≈25 nm	Sol. processing	ITO	$CH_3NH_3PbI_3$	Spiro-OMeTAD	20.4	1.03	0.75	15.7	Liu et al.[9f]
	c-ZnO	40 nm	Sputtering/Sol. processing	ITO	$CH_3NH_3PbI_3$	Spiro-OMeTAD	21.8	1.00	0.73	15.9	Tseng et al.[158]
	c-SnO_2	<40 nm	Sol. Processing/ ALD	FTO	$Cs_x(MA_{0.17}FA_{0.83})_{(100-x)}Pb(I_{0.83}Br_{0.17})_3$	Li- and Co doped Spiro	22.6	1.17	0.76	20.7	Anaraki et al.[25b]
	c-SnO_2	–	Sol. processing	FTO	$CH_3NH_3PbI_3$	Spiro-OMeTAD	19.9	1.06	0.58	12.1	Song et al.[157]
	c-SnO2	≈30 nm	ALD/ Sol. processing	FTO	$(FAPbI_3)_{0.85}(MAPbBr_3)_{0.15}$	Spiro-OMeTAD	21.3	1.19	0.74	18.1	Baena et al.[156]
	c-SnO_2 (T 70 °C)		sequential deposition	ITO	$CH_3NH_3PbI_3$	Spiro-OMeTAD	19.5	1.08	0.62	13	Song et al.[180]
	TiO_2–ZnO bi layer	≈30 nm each	Sol-gel/Sol. processing	FTO	$CH_3NH_3PbI_3$	Spiro-OMeTAD	20.8	≈1.08	0.75	17.2	Xu et al.[143]
	ZnO-SnO_2 composite	–	Sol. processing	FTO	$CH_3NH_3PbI_3$	Spiro-OMeTAD	19.5	1.07	0.73	15.2	Song et al.[157]
	C60/phlm	10/40 nm	Vacuum processing	ITO	$CH_3NH_3PbI_3$	TaTm/F_6: TCNNQ	22.1	1.14	0.80	20.3	Momblona et al.[17]
Planar (n-i-p) on flexible substrates	c-TiO_2	≈100 nm	Sol. processing	IZO-PET[f]	$CH_3NH_3PbI_3$	Spiro-OMeTAD	17.6	≈1	0.7	12.3	Dkhissi et al.[181]
	c-TiO_2	≈60 nm	e-beam/Sol. processing	PET/ ITO	$CH_3NH_3PbI_{3-x}Cl_x$	poly(triaryl amine) doped PTAA	20.5	0.89	0.73	13.4	Qiu et al.[159]
	c-ZnO	40 nm	Spin coating	PEN/ ITO	$CH_3NH_3PbI_3$	PTAA	18.7	1.1	0.76	15.6	Heo et al.[160]
	c-ZnO	–	Sputtering/sol. Processing	W. glass,[f] flexible	$CH_3NH_3PbI_3$	Spiro-OMeTAD	19.3	0.98	0.69	11.7	Tavakoli et al.[182]

Table 3. Continued.

Device architecture	ESC/Morphology	CL Thickness [nm]	Method of deposition (ESC/perovskite)	Substrate	Perovskite	HSC	J_{SC} [mA cm^{-2}]	V_{OC} [V]	FF	PCE [%]	Ref.
	c-ZnO	≤50 nm	Sol. processing	PET/ ITO	$CH_3NH_3PbI_3$	Spiro-OMeTAD	13.4	1.03	0.74	10.2	Liu et al.[9f]
	c-TiO_2-Al_2O_3	50/350 nm	Spin coating	Ti foil	$CH_3NH_3PbI_{3-x}Cl_x$	Spiro-OMeTAD + PEDOT:PSS	17	0.98	0.61	10.3	Troughton et al.[183]
Device architecture	ESC		Method of CL	Substrate	Perovskite	HSC	J_{SC} [mA cm^{-2}]	V_{OC} [V]	FF	PCE [%]	Ref.
ESC Free	NO ESC	–	Sol. Processing (DS)	ITO	$CH_3NH_3PbI_3$	Spiro-OMeTAD	≈17.5	1.01	≈0.66	13.5	Liu et al.[18]
	NO ESC	–	Sol. Processing (DS)	Cs_2CO_3-ITO	$CH_3NH_3PbI_3$	Spiro-OMeTAD	19.9	1.07	0.71	15.1	Hu et al.[184]
Meso-superstructures solar cells (employing insulating scaffolds) MSSC-PSCs	c-TiO_2/Al2O3 (T > 400 °C)	≈50/≈200 nm	Sol. processing	FTO	$CH_3NH_3PbI_{3-x}Cl_x$	Spiro-OMeTAD	17.8	0.98	0.63	10.9	Lee et al.[7a]
	c-TiO_2/Al_2O_3 (T~150 °C)	<50/≈20 nm	Sol. processing	FTO	$CH_3NH_3PbI_{3-x}Cl_x$	Spiro-OMeTAD	18	1.02	0.67	12.3	Ball et al.[16]
	TiO_2-GRO/ Al_2O_3 bi-layer	≈100/≈400 nm	Sol. processing	FTO	$CH_3NH_3PbI_{3-x}Cl_x$	Spiro-OMeTAD	21.9	1.04	0.73	15.6	Wang et al.[185]
	c-TiO_2/Al_2O_3	–/>300 nm	Sol. processing	FTO	$CH_3NH_3PbI_{3-x}Cl_x$	PDI	1.08	1.3	0.4	0.56	Edri et al.[62]
	c-TiO_2/Al_2O_3	–	Sol. processing	FTO	$CH_3NH_3PbBr_{3-x}Cl_x$	p-doped CBP	4.0	1.5	0.46	2.7	Edri et al.[56]
	c-TiO_2/ZrO_2	–/>300 nm	Sol. Processing (DS)	FTO	$CH_3NH_3PbI_3$	Spiro-OMeTAD	17.3	1.07	0.59	10.8	Bi et al.[186]
	c-TiO_2/m-Al_2O_3	–/≈200 nm	Spin coating	FTO	$CH_3NH_3PbI_{3-x}Cl_x$	Spiro-OMeTAD	21.5	≈1.07	0.71	15.9	Wojciechowski et al.[15]
Device architecture	Device Architecture	Thickness (active layers)	Method of ESC/perovskite	Substrate	Perovskite	HSC	J_{SC} [mA cm^{-2}]	V_{OC} [V]	FF	PCE [%]	Ref.
HSC-free PSCs	c-ZnO/P/C	55 nm	Spin coating/sequential deposition	FTO	$CH_3NH_3PbI_3$	HTM free	20	0.81	0.54	8.7	Zhou et al.[187]
	c-TiO_2/TiO_2/P/MWCNTs	–	Spin coat/drop cast	FTO	$CH_3NH_3PbI_3$	HTM free	18	0.88	0.8	12.7	Wei et al.[188]
	c-TiO_2/TiO_2/ZrO_2/P/C	100 nm, 1/2/10 µm	Spray pyr., sc. Print./ drop cast.	FTO	$(FA)_{0.6}(MA)_{0.4}PbI_3$	HTM free	20.9	0.92	0.67	12.9	Hu et al.[164b]
	c-TiO_2/TiO_2/P/Graphene (MW)	–/200/400 nm, >10 µm	Spin coating/–	FTO	$CH_3NH_3PbI_3$	HTM free	16.7	0.94	0.73	11.5	Yan et al.[189]
	c-TiO_2/TiO_2/ZrO_2/P/C	100 nm, 1/2/10 µm	Spray coating, screen pr../ drop casting	FTO	$(5\text{-AVA})_x(MA)_{1-x}PbI_3$	HTM free	22.8	0.86	0.66	12.8	Mei et al.[8b]
	c-TiO_2/TiO_2/ZrO_2/P/C	100 nm, 1/2/10 µm	Spray coating, screen pr../ drop casting	FTO	$(5\text{-AVA})_x(MA)_{1-x}PbI_3$	HTM free	22.9	0.87	0.67	13.4%	Yang et al.[190]
Inverted Perovskite solar cells (p-i-n)	PTAA doped with F4-TCNQ[g)]	<100 nm	spin coat./double step	ITO	$CH_3NH_3PbI_3$	PCBM + C_{60} + BCP	~22	1.07	0.77	18.3	Bi et al.[166b]
	PEDOT:PSS	<50 nm	Spin coating	ITO	$CH_3NH_3PbI_3$	PCBM	20.9	1.1	0.78	18.1	Heo et al.[20a]
	PEDOT:PSS		Spin coating/ single step	FTO	$CH_3NH_3PbI_{3-x}Cl_x$	PCBM	22.4	0.92	0.82	18	Nie et al.[166a]
	PEDOT:PSS	–	Spin coating	ITO	$CH_3NH_3PbI_3$	PCBM/PFN	20.3	1.05	0.8	17.1	You et al.[168]

Table 3. Continued.

Device architecture	Device Architecture	Thickness (active layers)	Method of ESC/perovskite	Substrate	Perovskite	HSC	J_{SC} [mA cm^{-2}]	V_{OC} [V]	FF	PCE [%]	Ref.
	PEDOT:PSS	20 nm	Spin coating	ITO	$CH_3NH_3PbI_{3-x}Cl_x$	PCBM/ZnO	22	1.02	0.74	16.8	Zhang et al.[171]
	PEDOT:PSS	~20 nm	Spin coating	ITO	$CH_3NH_3PbI_3$	$PC_{61}BM$	10.8	0.91	0.76	7.4	Sun et al.[162]
	PEDOT:PSS	<50 nm	Spin coating	ITO	$CH_3NH_3PbI_3$	C_{60}/BCP	10.3	0.60	0.63	3.9	Jeng et al.[165]
	PEDOT:PSS	<50 nm	Spin coating/ALD	ITO	$CH_3NH_3PbI_3$	ZnO NWs	≈21	1.02	≈77	≈16.5	Chang et al.[191]
	PEDOT:PSS	<50 nm	Spin coating	ITO	$CH_3NH_3PbI_3$	PCBM/ZnO NC	20.5	0.97	0.80	15.9	Bai et al.[99]
	NiO_x	20 nm	Spin coating	ITO	$CH_3NH_3PbI_3$	C_{60}-Bis-C_{60}	21.8	1.03	0.78	17.6	Zhang et al.[167a]
	NiO_x	<50 nm	–	ITO	$CH_3NH_3PbI_3$	$PC_{61}BM$/LiF	20.2	1.06	0.81	17.3	Park et al.[167b]
	NiO	<50 nm	60–100 nm	FTO	$CH_3NH_3PbI_3$	SnO_2/C_{60}	21.8	1.12	0.77	18.8	Zhu et al.[103]
	NiO_x	80 nm	Spin coating	ITO	$CH_3NH_3PbI_3$	ZnO	21	1.01	0.76	16.1	You et al.[88]
	CuI	–	Spin coating	ITO	$CH_3NH_3PbI_3$	PCBM	21.1	1.04	0.62	13.3	Chen et al.[192]
	CuSCN	57 nm	Spin coating	ITO	$CH_3NH_3PbI_3$	C_{60}/BCP	21.9	1.00	0.76	16.6	Ye et al.[20b]
Device architecture	ESC	Thickness (CL/scaffold) nm	Method of CL	Substrate	Perovskite	HSC	J_{SC} [mA cm^{-2}]	V_{OC} [V]	FF	PCE [%]	Ref.
Fiber or wire shaped PSCs	TiO_2	≈50/>500 nm	Dip coating	Stainless steel	$CH_3NH_3PbI_3$	Spiro-OMeTAD	10.2	0.66	0.49	3.3	Qiu et al.[193]
	TiO_2	–	Electrochemical anodization	Ti foil	$CH_3NH_3PbI_3$	Spiro-OMeTAD	11.97	0.73	0.44	3.85	Lee et al.[194]
	ZnO	–	Dip coating	Stainless steel	$CH_3NH_3PbI_3$	Spiro-OMeTAD	15.3	0.66	–	3.8	He et al.[195]

[a]**FDT**: 2′,7′-bis(4-methoxyphenyl)amino)spiro[cyclopenta[2,1-b:3,4-b′]dithiophene-4,9′-fluorene; [b]**VASP**: Vapor assisted solution process; [c]**LP-VASP**: Low pressure-vapor assisted solution process; [d]**Y-TiO_2**: Yttrium doped TiO_2; [e]**PEIE-ITO**: poly-ethyleneimineethoxylated (PEIE) doped ITO; [f]**IZO-PET**: Indium doped zinc oxide coated polyethylene terephthalate; [g]**F4-TCNQ**:tetrafluoro-tetracyanoquinodimethane (F4-TCNQ); [h]**DCIP**: direct contact and intercalation process.

thin nanoporous layer, but also, almost all high performing PSCs with mesoporous ESC also employ a compact (flat) thin layer underneath and a ≈200 nm thick capping layer on top of mesoporous-perovskite junction (a mixture of bulk heterojunction and planar configuration).[8a]

The pre-requisites for high efficiency planar PSCs are (i) pin-hole free thin selective contacts and (ii) high quality perovskite films to maximize light absorption,[150] minimize charge recombination and reduce defect densities at the ESC-perovskite interface. The fact that perovskite itself is characterized by ambipolar charge transport puts more stringent conditions on the selective contacts to block opposite charges (holes and electrons) reaching the substrate or metal contact, respectively. It would otherwise results in significant deterioration of device performance as shown by Liu et al.[151] Whereas an inhomogeneous perovskite layer (50–400 nm) with voids demonstrated inferior PCE (8.6%), a uniform, even, and pin-hole free perovskite layer by dual source evaporation demonstrated nearly doubled PCE (15.4%). The dual source evaporation process is not compatible with mass production as it is both time and energy consuming. This brings into account simple vapor assisted perovskite deposition (VASP) method to produce high quality perovskite films as shown by Chen et al.[152] (PCE 12.1%) and Li et al.[153] (PCE 16.8%). The latter also manifested remarkably low *J-V*-hysteresis, an anomalous typical behavior[66b,154] in planar PSCs. A further improvement in device performance is made by Zhou et al.[7d] where optimized selective contacts enabled efficient charge injection and extraction in addition to light absorption and carrier generation in perovskite layer. They employed a surface modified ITO with lower work function, Yttrium doped TiO_2 (Y-TiO_2) for efficient charge extraction and transport, and Co- and Li- co-doped spiro-OMeTAD and reported PCE ≈19.3% at 1 sun condition with nearly unity external quantum efficiency owing to extreme transparency offered by modified ESC and FTO interface. However, this particular device showed *J-V*-hysteresis.

The best performance in planar PSCs (PCE ≥ 20%) is recently reported by Momblona et al.[17] in a fully vacuum processed PSC and Anaraki et al.[25b] using SnO_2 as a selective contact (Table 3). Herein, the perovskite layer was employed between fully organic ESC and HSCs, all prepared via vacuum processing, resulting in high quality films, as shown in Figure 14. This important report highlights two key findings: Firstly, contrary to the general perception, that larger perovskite crystals favor high PCE, this reports employs small perovskite grains and yet demonstrate high PCE 18% (average, 20% in a champion device), suggesting that the nature of grain boundaries and defects within the perovskite layer are the primary performance determining factors. This affirms a previous report that the benign grain boundaries in perovskite films do not create sub-bandgap states.[155] Secondly, it compares p-i-n and n-i-p architecture, where exactly same materials (except metal back contact) shows large difference in performance (**Figure 13**). This is because, in p-i-n architecture, HTM (employed in this study) forms poor contact at the front contact (ITO), whereas in n-i-p architecture, a good contact is formed as metal contact is thermally evaporated over HTM. Similarly, the PSCs made using SnO_2 (PCE 20.7%)[25b] as a selective contact resulted in one of the highest V_{OC} 1.21 V (for $CH_3NH_3PbI_3$), close to its thermodynamic limit[48,53b] of 1.32 V.

Alternatives to TiO_2 such as ZnO,[9f] SnO_2[156] and ZnO-SnO_2 composites[157] are also employed that resulted in remarkable PCE ≈15.7%, 18% and 15.2%, respectively. The efficiency of ZnO planar PSCs is further improved to 15.9% via modifying ZnO energy levels by introducing oxygen vacancies in which it resulted in improved electron extraction.[158] A similar performance rise is witnessed when suitable conduction band alignment to SnO_2 compact layer resulted in a remarkable PCE >18% with almost no I-V hysteresis.[156] Additionally, a bi-layer design where ZnO CL over TiO_2 suppressed interfacial recombination at ESC/perovskite interface and resulted in over 17% PCE.[143] Similarly, progress in flexible planar PSCs is also remarkable.[9e] PCE 13.5% is reported in high quality TiO_2 compact layer prepared via e-beam at T < 80 °C.[159] The highest performance (PCE 15.6%) in flexible planar PSCs is however achieved using a thin ZnO layer.[160]

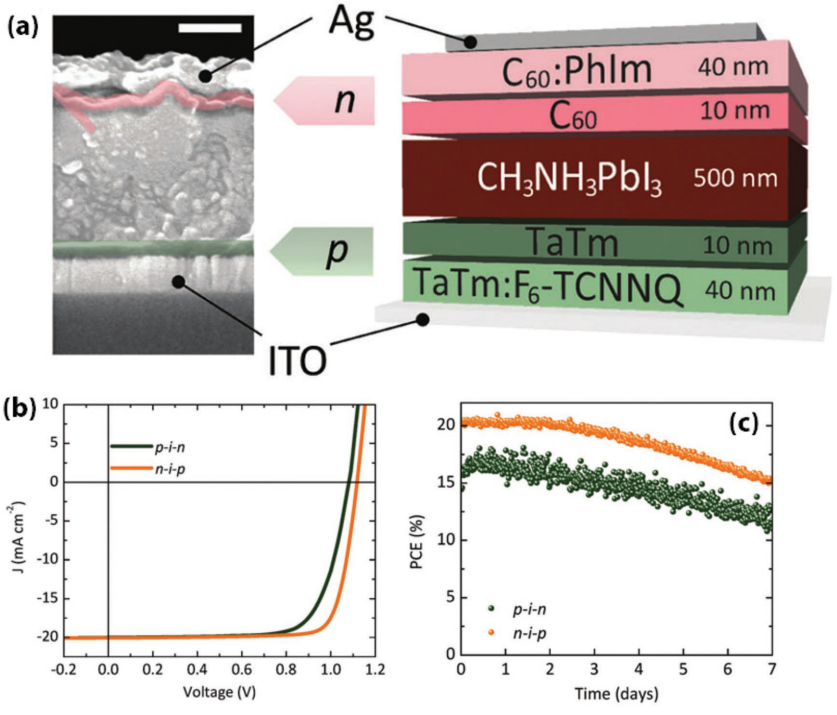

Figure 13. a) A cross-section view and schematics of a completed p-i-n solar cell (scale bar 200 nm), b) J–V curves for the n-i-p and p-i-n solar cells under standard test conditions (both device employ the same materials, just the order the changed), and c) PV performance as a function of time under ≈100 mW cm^{-2} illumination. Reproduced with permission.[17] Copyright 2016, The Royal Society of Chemistry.

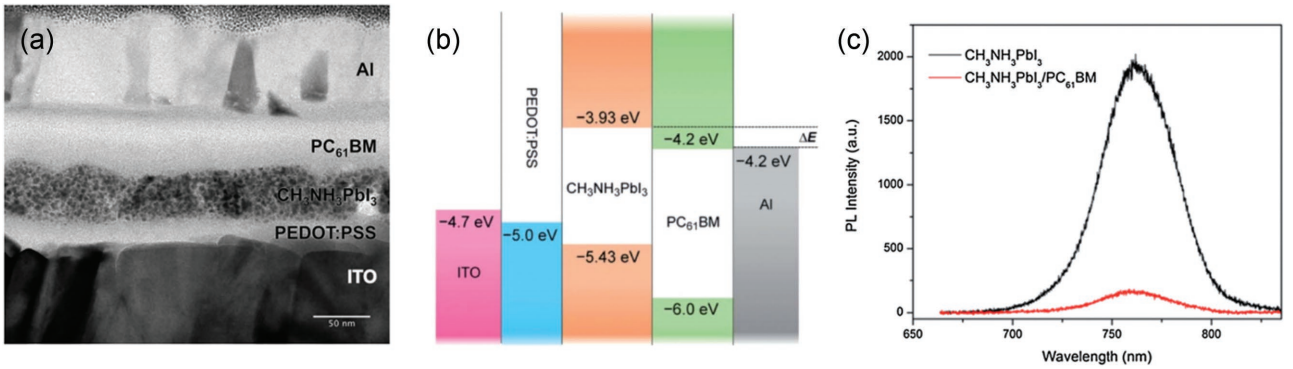

Figure 14. a) A cross-section TEM of a typical inverted PSC (p-i-n) employing PEDOT:PSS and $PC_{61}BM$ as HSC and ESC, respectively, b) schematic showing energy level diagram of ITO, PEDOT:PSS, $CH_3NH_3PbI_3$, $PC_{61}BM$ and Al. c) Steady-state PL spectra for $CH_3NH_3PbI_3$ and $CH_3NH_3PbI_3/PC_{61}BM$ (λ_{ex} = 600 nm) showing efficient charge separation when a $PC_{61}BM$ layer is employed. Reproduced with permission.[162] Copyright 2014, The Royal Society of Chemistry.

5.2.1. Inverted Perovskite Solar Cells: Case for Organic and Inorganic Interfaces

Inverted PSCs, also called p-i-n type PSCs, employ a p-type organic or inorganic layer on conducting substrates to collect holes whereas electrons are collected from the back contact (Figure 1).[161] These designs are particularly interesting as, contrary to their n-i-p rival, high quality selective contacts can be fabricated at low temperature and also they often do not show *JV*-hysteresis (Figure 9).

The charge separation in these devices is conceived to be due to the presence of internal electric field at the perovskite and HSC or ESC interface, and the electrons are injected to the LUMO of ESC, viz $PC_{61}BM$ whereas the holes are transferred to conducting substrate via HSC, i.e., PEDOT:PSS (donor-acceptor mechanism). This is validated by the steady state photoluminescence (PL) measurements by Sun et al.[162] who compared PL quenching of $CH_3NH_3PbI_3$, $CH_3NH_3PbI_3$/PEDOT:PSS and $CH_3NH_3PbI_3/PC_{61}BM$ bilayers. The bilayers showed 3 and 4 times higher PL quenching respectively, compared to a perovskite layer itself validating the improved charged separation at bilayer interface. Surprisingly, unlike the ambipolar charge transport properties of perovskite,[163] and the reports that it can work with a single interface only,[18,164] the devices in this report did not work with single interface probably due to the less efficacious perovskite/PEDOT:PSS interface compared to perovskite/spiro-OMeTAD analogue and also due to energy mismatch between perovskite and back contact (Al) as shown in **Figure 14**b which hinders efficient exciton dissociation in the absence of $PC_{61}BM$. This can also be confirmed from a plot of PL intensity versus temperature that the exciton binding energy is ≈20 meV, indicating that an electric field is still required for efficient exciton dissociation. The energy level difference between perovskite and ESC is ≈0.27 eV which is ≈10 times higher than the required energy for charge separation (Figure 14c).

From an initial PCE ≈3.9% in their first report,[165] the p-i-n planar device now demonstrate a state-of-the-art PCE ≈18.8% (V_{OC} ≈1.12 V, J_{SC} ≈21.8 mA cm^{-2}, FF ≈77%) as shown in Table 3.[103] The best performing device (FTO/NiO/$MAPbI_3$/C_{60}/SnO_2/Ag) also showed a stable power output of 18.5%. Various reports employing PEDOT:PSS[166] or NiO_x[88,167] as HTL (see **Figure 15** and Table 3) reported PCE >17% in PSCs with minor or no hysteresis making them one of the successful device designs so far, although there are concerns on their stability. The remarkable improvement in these devices has been due to improvement dense and pinhole free perovskite layers that enable complete light absorption as well as selection of charge selective contacts which are mostly adapted from

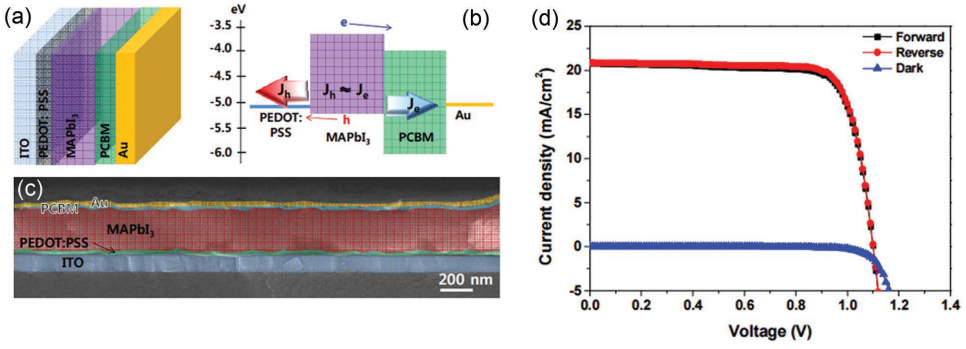

Figure 15. A schematic showing device architecture and band energy diagram of an inverted planar $MAPbI_3$ PSC a,b), c) the SEM cross-sectional image of representative device showing a perovskite layer of thickness ≈300 nm, d) J-V curves of a representative inverted PSC with respect to forward and reverse scan direction demonstrating no hysteresis. Reproduced with permission.[20a] Copyright 2015, The Royal Society of Chemistry.

polymer solar cells such as PEDOT:PSS and fullerene derivatives, i.e., PCBM.

5.2.2. Buffer Layers to Improve Interfacial Charge Collection

A typical problem in these devices is the poor contact formed between fullerene derivatives when conjugated directly with metal back contact. This brings into account additional buffer layers such as PFN (polyelectrolyte poly[(9,9-bis(3′-(N,N-dimethylamino) propyl)-2,7-fluorene)-alt-2,7-(9,9-dioctylfluorene)]), BCP (bathocuproine), and LiF to improve Ohmic contact and eventually the charge transfer at the interface.[80,165,168] In such a report, You et al.[168] reported a moisture assisted perovskite growth to synthesize a thick absorber layer and showed a remarkable PCE ≈17.1%. A buffer layer of PFN is employed to support efficient charge extraction to back contact which enabled a FF as high as 0.80.[168] Other such works include a thin layer of MoO_3 in conjunction with PEDOT:PSS that resulted in PCE ≈15% by improving hole collection efficiency[169] and C in conjunction with CuSCN with C_{60}+ BCP as ESC that resulted in PCE >16.8%.[20b] The buffer layers are also employed at the ESC/perovskite or ESC/TCO interface. For example, fullerene derivatives ($IC_{60}BA$, $PC_{61}BM$, C_{60}) have also shown to enhance performance of PSCs when employed in conjunction with ESC (Bis-C_{60}),[170] a thin ZnO layer in conjunction with PCBM resulted in PCE ≈16.8% and also enhanced the stability of the device significantly.[171] In addition, thin buffer layers of MOS such as ZnO and TiO_x are also employed in order to improve device operational stability.[172]

5.3. Engineering of Selective Contacts: Manipulating Defects and Charge Dynamics

A major challenge to achieving high PV parameters in PSCs is the interfacial recombination, particularly, at the ESC-perovskite interface, primarily due to low mobility materials such as TiO_2 and ZnO and their surface defects. Thanks to the ambipolar charge transport in perovskite films which opened possibility of insulating oxide scaffolds such as Al_2O_3 and ZrO_2 to be employed in PSCs (also called Meso-superstructured solar cells, MSSCs) and resulted in high PV parameters, especially, higher V_{OC}.[7a,15,22b] Not only the insulating scaffolds helped in perovskite crystallization but also had dually advantageous effect on charge transport properties of the PSCs. In a comparative study of TiO_2 vs Al_2O_3 based PSCs (TiO_2 ESC PCE ≈7.6%, V_{OC} ≈0.8 V); Al_2O_3 PSCs, PCE ≈10.9%, V_{OC} ≈1.13 V)[7a] the latter showed effective charge transfer and longer carrier lifetime, as confirmed via photoinduced absorption (PIA) spectroscopy and small-perturbation transient photocurrent decay measurements (**Figure 16**) resulting in higher J_{SC} and nearly 200 mV increased V_{OC} in a similar device configuration. The ≈10 times faster lifetime in Al_2O_3 based PSCs is due to the fact that electrons are carried by the perovskite layer itself, a material with several orders of higher electron mobility than TiO_2, whereas the ≈200 mV higher V_{OC} is due to the removal of sub-band gap states when TiO_2 is replaced with Al_2O_3. The higher V_{OC} is due to the fact that, in TiO_2, the structural disorderly induced sub-bandgap states that bring its Fermi level (E_F) much lower than its conduction band create charge storing capability. The TiO_2 ESC under illumination thereby acts store charges in it likewise a capacitor (which is called chemical potential) and limits the V_{OC}.

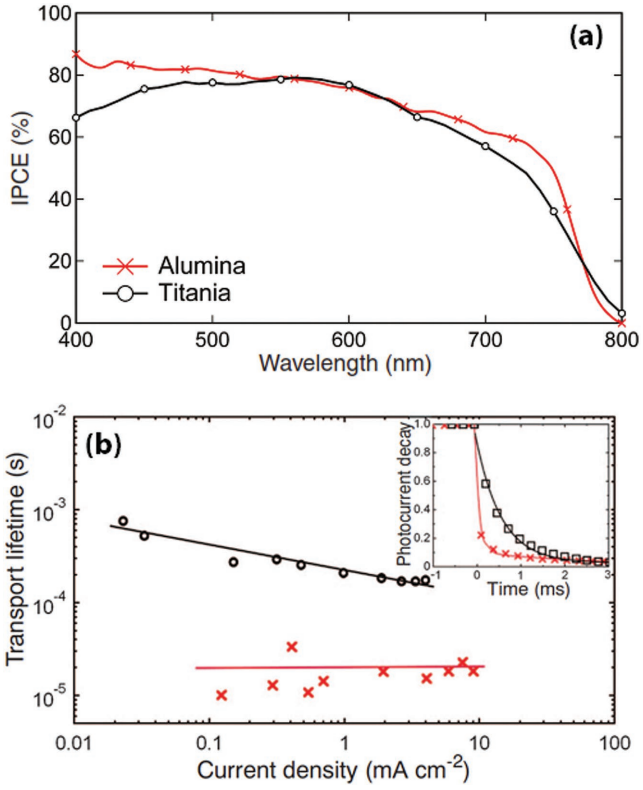

Figure 16. a) IPCE action spectrum of an Al_2O_3 and TiO_2 based and perovskite-sensitized solar cell, and b) charge transport lifetime determined by small-perturbation transient photocurrent decay measurement of TiO_2 PSCs (black circles) and Al_2O_3 PSCs (red crosses). Inset shows normalized photocurrent transients for Al_2O_3 cells and TiO_2 cells. Reproduced with permission.[7a] Copyright 2012, American Association for the Advancement of Science.

The working mechanism of a MSSC is similar to that of a planar PSC where charges are transported via perovskite itself. This is because a perovskite layer is considered as an intrinsic semiconductor with sub-bandgap trap states (predominantly the positive under-coordinated Pb^+ or Pb^{2+} species), the distribution and occupancy of which is largely influenced by the selective contact (or scaffold material) and its polarity. The negative charge on the Al_2O_3 layer due to presence of aluminol groups fills up these trap states and brings the Fermi level closer to the conduction band. Hutter et al.[196] observed an order of magnitude higher trap density (6×10^{16} cm^{-3}) for planar $CH_3NH_3PbI_3$ films than $CH_3NH_3PbI_3/Al_2O_3$ rivals (10^{15} cm^{-3}), despite the much smaller crystal size of the latter. This evidences that the presence of insulating scaffold not only influence the crystal morphology but also, the electronic properties of the resultant film. However, one must note that (i) the MSSCs only demonstrate high performance when a capping layer of perovskite exists above $CH_3NH_3PbI_3/Al_2O_3$, which makes a preferred gradient for electron collection, and (ii) the $CH_3NH_3PbI_3/Al_2O_3$

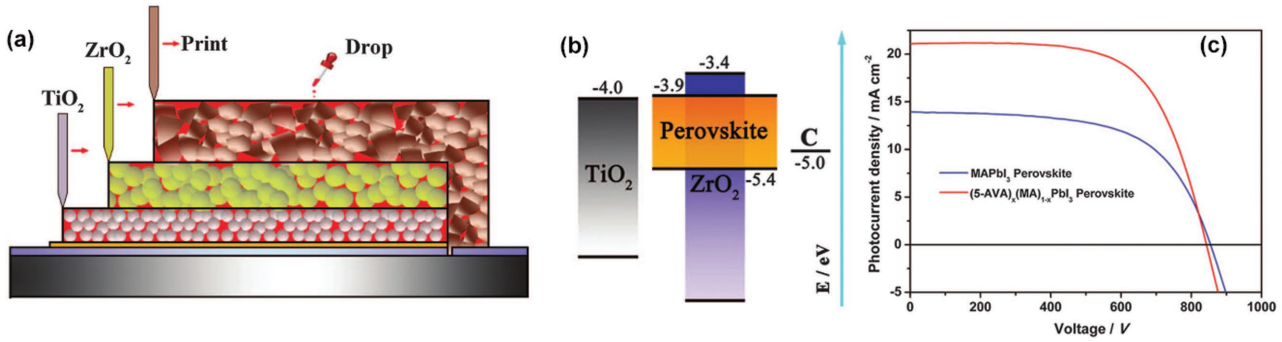

Figure 17. A typical architecture of monolithic PSCs also called HSC-free PSCs. It utilizes an insulating spacer (typically ZrO_2) between ESC and back contact (typically carbon, also conceived to be hole selective contact here) as shown in A). B,C) shows energy level diagram and also a *J-V* curve of a PSCs shown in (A). Reproduced with permission.[8b] Copyright 2014, American Association for the Advancement of Science.

films demonstrate significantly lower charge carrier mobility and PL quantum efficiency (PLQE).[197]

ZrO_2 as a scaffold layer has achieved PCE > 10%.[186] However, notable PCE (>12%) is typically reported in a bi-layer architecture (**Figure 17**) where an insulating layer of ZrO_2 is employed on top of mesoporous TiO_2 (Table 3).[8b] Such architecture offers additional advantage as it does not employ an organic HTM and instead use thick mesoporous hydrophobic carbon layer thereby yielding a stable device,[8b] as will be discussed in stability section of this article. The best performing MSSC architecture, reported so far, is 15.9% efficient employing a low temperature (<150 °C) processed scaffold.[15] Another notable performance from same group for MSSC demonstrated PCE ≈15.6% in a bi-layer design employing TiO_2-RGO/Al_2O_3 bi-layer where the inclusion of graphene flake facilitated superior charge extractions and lowered R_S.[185]

5.4. Single Interfacial Perovskite Solar Cells

5.4.1. Electron Selective Contact Free PSCs

The PSCs, likewise many common organic solar cells, also initially employed a tri-layer architecture for charge extraction where an absorber is sandwiched between two selective contacts (Figure 1) which facilitate efficient charge extraction, modify work function of TCO, and reduce interfacial recombination. However, the subsequent research that showed that pristine $CH_3NH_3PbI_3$ or $CH_3NH_3PbI_3/Al_2O_3$ has higher electron mobility than $CH_3NH_3PbI_3/TiO_2$ indicated that an efficient device can, in principal, be made without an ESC.[7a,30a] It is important to note that the low exciton binding energy (2–5 meV)[198] of perovskite enables thermal dissociation of >98% of the photogenerated excitons at room temperature which can be extracted if only one of the selective contacts is present. This is also supported by the fact that PSCs work as a n-i-p junction device with two key serially connected interfaces; i.e., perovskite/ESC and perovskite/HSC, where the device might work with presence of only one junction.[199]

This led to unconventional single interface architectures of PSCs: (i) ESC-free, where a perovskite layer is directly deposited on bare TCO or surface modified TCO, and (ii) HSC-free where a back contact is directly deposited on perovskite absorber layer without a HTM layer. For the ESC-free PSCs, Liu et al.[18] first reported PCE 13.5% when a dense ≈300 nm thick $CH_3NH_3PBI_3$ is deposited on a bare ITO. Important is to note the energy level mismatch (≈0.8 eV) between perovskite and ITO which restricted the performance. Towards this, Hu et al.[184] successively reduced this energy mismatch by ≈0.4 eV (**Figure 18**) via surface modification of ITO with Cs_2CO_3 and demonstrated PCE ≈15.1% (PV parameters are in Table 3). In a similar attempt to reduce energy mismatch at FTO-perovskite interface Ryu et al.[200] modified FTO surface with PEI (polyethyleneimine), which is widely employed in polymer solar cells to modify work function of FTO by introducing self-assembled dipoles,[201] and reported PCE >15% in a device configuration FTO/PEI/PCBM/$CH_3NH_3PbI_3$/PTAA/Au. Although the device is not ESC free rather it is a metal oxide-free architecture, it is still advantageous over their mesoporous analogues as n-type organic thin films can be prepared at much lower temperature. The use of just a self-assembled monolayer of fullerene derivatives deposited directly on FTO reduces significantly efficiency and avoids the photocurrent decrease observed when ESC is removed.[87a]

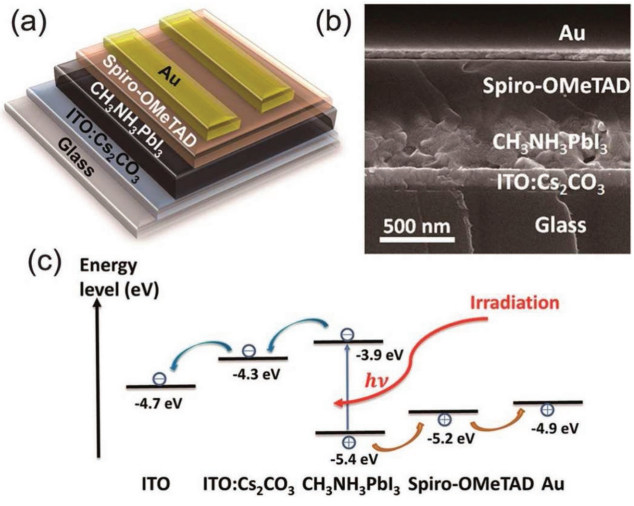

Figure 18. Device architecture of an ESC free PSC where perovskite is deposited on top of a surface modified ITO. a) Schematic of the device structure. b) SEM cross-sectional image of a perovskite solar cell based on Cs_2CO_3-modified ITO substrate, and c) schematic showing energy level diagram of various device components. Reproduced with permission.[184] Copyright 2014, American Chemical Society.

5.4.2. Hole Selective Layer Free Device Architectures

A conventional PSCs offers numerous challenges prior to its commercial deployment; it employs expensive HSC (Spiro-OMeTAD, ≈500 $) and back contact (Au).[9e,202] Furthermore, the organic HSCs are humidity sensitive and the metal back contacts typically require vacuum based deposition incompatible with roll-to-roll (R2R) production. The market acceptance of PSCs will require their mass production compatible ambient processing, cost-effectiveness so as to reach grid parity (<$0.05 kW h)[203] and a stable operational lifetime of devices (>20 years).

HSC-free PSCs offer remedy to these various challenges as they eliminate both the HSC and back contact. The first PSC (architecture: c-TiO_2/m-TiO_2/ZrO_2/perovskite/C) replacing both the HSC and the metal back contact, likewise monolithic DSCs,[204] and fabricated via mass production compatible protocols reported PCE ≈6.6%.[205] The ZrO_2 layer blocks electrons reaching the carbon back contact as also evidenced in a report by Mei et al which demonstrated a remarkable PCE ≈12.8% and a stable performance under 1000 h of light soaking in a fully-printable PSC.[8b] The same group further improved the performance in monolithic PSCs to 13.4% by optimizing the size of TiO_2 and thereby the pore size and pore volume which allowed a greater perovskite infiltration in the scaffold.[190] Similarly, performance enhancement from 11.4% to 12.9% is also reported by optimizing perovskite composition from pure $MAPbI_3$ to $FA_{1-x}MX_xPBI_3$ (FA–and MA::3:2) which resulted in a broader absorption up to ≈840 nm.[164b]

The monolithic or HSC-free PSCs typically result in a low FF (typically <0.7) owing to a poor perovskite/C interface due to the fact that carbon film has a higher sheet resistance compared to an Au (Table 3).[206] To overcome this, Yan et al.[189] employed single and multi-layered graphene (SG and MG) as HSC resulting in PCE ≈6.7 and ≈11.5%, respectively. While the SG formed an Ohmic contact, the MG formed a Schottky junction resulting in superior hole extraction rate ≈5.1 ns^{-1} than the former (3.7 ns^{-1} for SG). A further increase in performance, particularly the FF, is reported by employing multi-wall carbon nanotubes (MWCNTs, PCE ≈12.7% and FF≈0.8) (**Figure 19**).[188] Notably, the devices showed a hysteresis free performance compared to a carbon black and graphite based analogues. An optimized perovskite/C interface is also reported by directly hot-pressing free-standing thermoplastic carbon which resulted in a remarkable PCE ≈13.5%, one of the highest till date for HSC-free PSCs.[207]

Interestingly, the HSC-free PSCs may or may not employ an intermediate insulating layer between ESC and carbon/perovskite (Figure 19a–c). This is because the typically employed carbon (carbon black or graphite) has lower conductivity and inferior electronic transport compared to carbon nanotubes, the former's hole extraction rate is lower. Absence of an insulating layer in such case will further increase the interfacial charge recombination, as demonstrated by Mei et al.[8b] The performance dropped from 12.8% to 4.2% when ZrO_2 layer is not employed compared. However, as SWCNTs and MWCNTs are characterized by a superior hole extraction,[189] directional charge transport and also has shown improved perovskite/C interface,[188] it may not require an insulating layer for high performance. This is perhaps the reason that the HSC-free or monolithic PSCs with CNT derivatives as back contact do not employ an insulating scaffold layer. It is important to note that the only report (to the best of our knowledge) containing conducting carbon without an insulating spacer (ZrO_2) is by Zhou et al.[187] with a PCE ≈8.7% on rigid substrates and ≈4% for flexible polymer analogues.

Also, CNTs are a p-type material at ambient conditions and the energy level difference between HOMO of CNTs and VB of perovskite (Figure 19b) acts as a driving force for hole injection.[206] This can also be validated from the fact that a perovskite/CNT film showed 44 times enhanced charge transfer compared to a bare perovskite film when investigated using PL quenching experiment. The working of monolithic or HSC-free PSCs is conceived be similar to heterojunction solar cells.[164c] The balanced electron and hole transport in perovskite crystals[163,208] explains the charge transport in perovskite film prior to separation at the selective contact/s. There are also arguments that the diffusion length in perovskite is not solely responsible for charge collection in HSC-free PSCs. Instead the charge transport may take place due to drift owing to the built-in electric field ca. 0.9 V[187]–1.2 V,[209] provided charge generation/separation takes place near the depletion layer.[210]

5.4.3. Monolithic PSCs With a Hole Selective Contact

There are PSCs in monolithic configuration that employ alternative HSC to spiro-OMeTAD such as CuPc,[211] PTAA,[212]

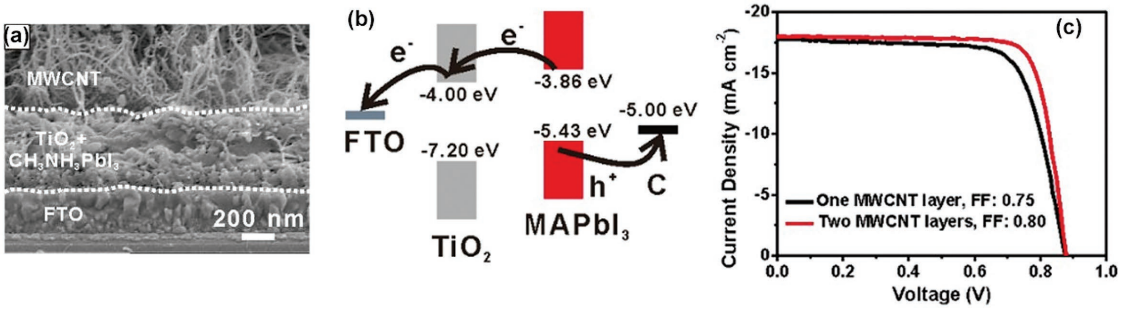

Figure 19. A common architecture of monolithic PSCs that does not include an insulating layer between ESC and back contact A). B,C) Show energy levels of (A) and J-V curves of such device showing one of the best FFs till date. Reproduced with permission.[188] Copyright 2015, The Royal Society of Chemistry.

NiO[213] and TPDI[125] and have achieved PCE 16, 15.3, 15.3 and 15.5%, respectively, however, as they do not fall under the HSC-free category, their performance is not exclusively discussed here. Nevertheless, such designs are suitable when high stability and performance in monolithic based PSCs is desired, as they do not employ a humidity sensitive spiro-OMeTAD as HTM. We refer reader to a recent review by Bakr et al.[22f] for more comprehensive understanding of various such architectures.

5.5. Low Temperature Processing of Selective Contacts on Flexible Substrates

When it comes to the market applications, four key features of any PV technology determine its market success, i.e., cost, efficiency, stability or lifetime and the added functionality.[12,214] The added functionalities such as transparency, flexibility and aesthetics become particularly important when the PVs have to be installed for indoor, portable or integrated applications such as in indoor electronics, wearables, and solar windows etc.[92] Since PSCs have shown to work in low or diffused light,[215] and have demonstrated PCE >15% in flexible devices[216] with fair indoor stability,[217] it makes them a preferred choice for indoor and portable applications, outperforming the DSCs (≈8.5%) and OPVs (≈11.5%).[92] Flexible PSCs are also important as they can be prepared on plastic and metallic substrates which are ≈30% and ≈90% cheaper than glass substrates.[218]

The flexible PSCs are mostly developed at T < 150 °C on conducting plastic substrates such as polyethylene terephthalate (PET), polyethersulfone (PES), polyethylene naphthalate (PEN) or polycarbonate (PC) and metallic substrates such as titanium, stainless steel and nickel foil.[219] For details on flexible PSCs, we refer to a comprehensive review by Di Giacomo et al.[9e] In brief, among the devices made on conducting plastic substrates, PCE ≈15.3 and 14.9% have been achieved using PET-ITO[217b] employing a TiO_2 NP ESC and PEN-ITO[109] with $ZnSnO_4$ ESC, respectively. An excellent PV performance and bending stability is also reported for f-PSCs when the PET substrates is incorporated with Ag-mesh and a transparent conducting polymer (PH1000), resulting in PCE ≈14% as shown in **Figure 20**a–h. The best performance in f-PSCs to date is reported using ZnO thin ESC in an architecture PEN/ITO/ZnO/MAPbI3/PTAA/Au (PCE ≈15.6%, Table 2).[160] However, while employing ZnO as an ESC, one must note that a low temperature processed ZnO often induces more defect sites in PSCs leading to a thermal degradation of perovskite.[220] Similarly, flexible PSCs employing a p-type organic layer has also yielded PCE over 12% (PET-ITO/PEDOT:PSS/perovskite/PCBM/Au).[217b]

On the other hand, flexible PSCs made on opaque metallic foils have shown PCE >10% using Ti foil[183,221] and much less

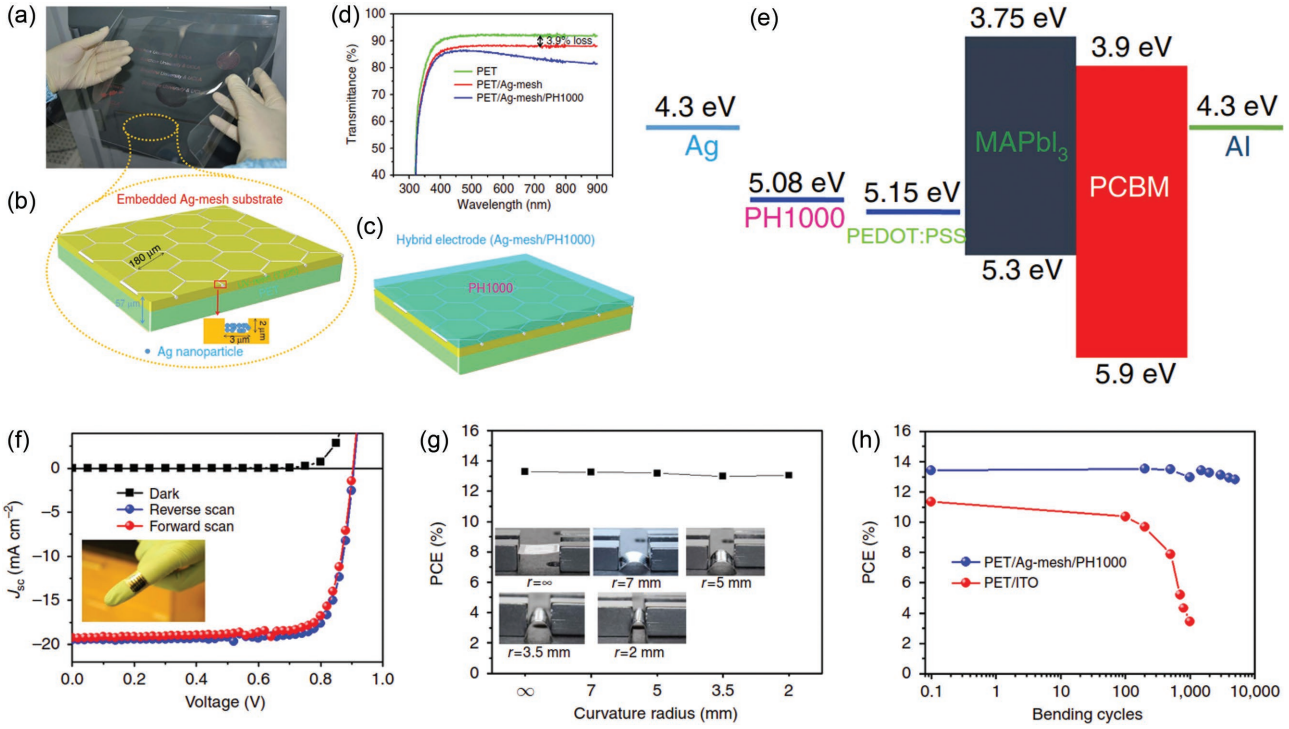

Figure 20. A modified PET electrode incorporated with a transparent conducting polymer (PH1000) and Ag mesh. a) Is a real image of such a substrate, b) and c) show the details of Ag-mesh incorporation and also deposition of PH1000 on PET to develop a hybrid PET/Ag-mesh/PH1000 electrode, d) transmission spectra of bare PET, PET/Ag-mesh, PET/Ag-mesh/PH1000-based substrates, e) corresponding energy-level diagram of the various material components employed, (f) J–V curves in reverse and forward scan of the best performing flexible PET/Ag-mesh/PH1000/PEDOT:PSS/$MAPbI_3$/PCBM/Al solar cell (Inset shows picture of a f-PSC). The device showed no hysteresis upon changing scan directions, g) bending stability of f-PSC within a specified radius of ∞, 7, 5, 3.5 and 2 mm. The inset shows the real images of the corresponding bending radii, respectively, and h) PCE of flexible PSCs as a function of bending cycles at a radius of 5 mm. Reproduced with permission.[216a] Copyright 2016, Macmillan Publishers Limited.

for a stainless steel counterpart (<4%).[193] The significantly higher performance in Ti foil is understood as a better interaction between TiO_2 ESC and also the native TiO_x layer at the substrate resulting in efficient charge extraction at the interface. However, the key issue here is the requirement of a back contact with high transparency so that maximum light can reach to the absorber layer. Therefore, the typically employed relatively thicker Au layer (≈100 nm) is replaced by a thin ITO layer mixed with CNT or Ag mesh.[221,222] Nevertheless, the highest performance (PCE ≈10.3%) in such devices has been achieved on Ti-foil with an insulating scaffold (Al_2O_3).[183]

5.5.1. Fiber Shaped or Unconventional PSCs

Inspired from the progress in fibrous DSCs and the need for integrated wearable energy generation and storage devices, fiber or wire shaped PSCs are also witnessed recently.[193,194,223] Although the performance (PEC <4%) is much lower than the predecessors, the DSCs (PCE ≈9%),[224] numerous research opportunities exist, particularly in terms of ESC-perovskite interface optimization. Such un-conventional PV designs are of particular interest as they, when incorporated as electronic textile, pave way to wearable PV technology and modern electronics. Here the advantage PSCs offered over DSCs is the absence of liquid electrolyte despite the latter's high PCE.

A first report on wire-shaped PSCs (w-PSCs) by Qiu et al.[193] in 2014 reported ≈200 µm thick device on a stainless steel wire and a PCE ≈3.3% (J_{SC} ≈10 mA cm^{-2} and V_{OC} ≈650 mV). Although the performance is much below liquid electrolyte based DSCs, it is higher than their solid-state DSCs (PCE ≈2.6%)[225] and polymer counterparts (PCE ≈2.6%).[226] In another report, He et al.[223] introduced obelisk-like vertically aligned ZnO nanorods at low temperature (<100 °C) enabled faster charge extraction (J_{SC} ≈15 mA cm^{-2}) and a PCE ≈3.8%. To further improve the performance, strategies need to be developed for a thick pin-hole free perovskite layer so as to avoid a contact between ESC and HSC. Nonetheless, the w-PSCs demonstrated the ability to be transformed into electronic-textile of size up to few cm^2, the first demonstration of a perovskite fabric. Future researches to improve performance of w-PSCs should consider improving the contact between ESC and core substrate, transparency of back contact (as w-PSCs are back illuminated due to opaque core material), control over perovskite morphology to avoid ESC-HSC shunting, physical encapsulation for humidity stability, and enhancing their resilience during twisting or bending.

6. Interfacial Modifiers to Improve PV Performance of Perovskite Solar Cells

Towards the two pre-requisites of a high performing PV device, i.e., light absorption and a complete charge collection, the $CH_3NH_3PbX_3$ offers a high absorption coefficient in the visible spectrum (≈10^5 cm^{-1}) which consequent high density of carriers. However, the charge extraction is often challenging even in films of thickness ≈300 nm. This is due to the various recombination processes within the perovskite film and especially at the device interfaces, as we have commented in Section 2.

Strategies to overcome the various recombination involve depositing perovskite over a lead iodide (PbI_2) monolayer,[227] post-treating $CH_3NH_3PbI_3$ film with di-ammonium iodide,[29b] incorporation of amino-substituted perylene diimide derivative (N-PDI) as ESC to replace the commonly used TiO_2[228] or as an interfacial modifier[229] between PCBM and metal back contact, and manipulating the perovskite crystal growth via a polymer matrix.[29a] Similarly, interface modification is also carried out at the ESC-perovskite interface, at HSC-perovskite interface, at ESC/TCO interface, and at perovskite-metal interface in order to enhance the charge transfer efficiency. **Table 4** lists the PV improvement in various such devices. The modifiers employed include thin insulating oxide layers, i.e., Al_2O_3, self-assembled layer (SAM) of fullerene derivatives, inorganic materials such as CsBr and CsCl, small molecules, thiols ligands, and polymers.

TiO_2 remains the most common selective contact material till date which is known for sub-bandgap states arising from under-coordinated surface Ti(IV) ions in its lattice and its surface defects. The TiO_2 based PSCs often demonstrate significant non-radiative recombination. A thin layer of fullerene derivatives[32c,87a,230] or PCBM[231] and PCBA[232] have shown to increase electron injection into ESC. Wojciechowski et al.[32c] demonstrated via PL decay and photothermal deflection spectroscopy that the traps states are significantly passivated when the TiO_2 layer is functionalized with a fullerene derivative SAM. Not only an efficient charge extraction is observed from the PL decay, the slope of the absorption at the band edge (corresponding to Urbach energy) also evidenced significant improvement in TiO_2 lattice disorder (**Figure 21**). Furthermore, electroluminescence spectra of samples provide a direct evidence of the 5 to 10 folds' reduction in non-radiative recombination at the interface. Another key issue is the low charge mobility of TiO_2 which often hinders electron collection leading to hysteresis in the device. This is overcome by introducing a PCBM overcoating, a material of several orders of higher electronic mobility that reduced the dark current at the interface and improved the hysteresis-free performance.[20c,233] Without the PCBM coating, the TiO_2 based devices require pre-polarization for efficient charge extractions, which would otherwise leads to large hysteresis in the PSCs made using them.[20c,234]

Similarly, improvement at HSC-perovskite interface, such as by introduction of Mo-IPA (Molybdenum iso-propoxide) assisted perovskite layer fabrication, resulted in VBM (Valence band maximum) alignment of perovskite with spiro-OMeTADand a more efficient hole extraction.[235] The interfacial layers also demonstrated stability improvement, especially under the UV-light due to interface modification.[236] In another report, a small molecule based HSC, N-atom-linked phenylcarbazole-fluorene end-capped with spirobifluorene derivatives demonstrated PCE ≈17.2% and also a long term stability.[237] Research has also been carried out to improve perovskite metal interface to obtain smoother and more compact junction and to avoid series resistance at the metal electrode side,[33] and at FTO/ESC contact by creating a negative dipole to alter the work function of the substrate which enhances the electrostatic potential across the device.[31b,238]

7. Interfaces Towards Stability of Perovskite Solar Cells

When it comes to practical deployment of the solar cell technology, the stability becomes as important as their initial PCE.[243] Although PSCs have shown exceptional PV performance in almost all of their device architectures, they are known to degrade when exposed to outdoor conditions such as humidity, temperature, UV light, light soaking and under the effect of an electric field.[22e,244] The predominant reasons for instability are intrinsic: (i) structural instability that arises from the fact that the materials constituting a perovskite crystal are chemically unstable and are subjected to a phase change under the effect of atmospheric factors,[22d,245] and (ii) change in current-voltage profile upon applying an electric bias which could either be attributed to the ferroelectric polarization of the MAX_3 or due to ion movement of halide ions (see the hysteresis section of the article for details).[66b,d,75] It is noteworthy that although moisture affects the long term performance of PSCs, a controlled moisture environment during device fabrication is crucial to obtain high photoluminescence and a high PCE.[246] The origin of this effect is attributed to a reduction in trap states due to the partial solvation of the MA ion and "self-healing" of the perovskite crystal.[247] However, over a long term exposure, water ingress into PSC decomposes perovskite crystal due to its water solubility.[248]

Numerous articles suggesting improving chemical stability or elimination of hysteresis in PSCs by chemically modifying the $CH_3NH_3PbX_3$ or by controlling the external factors such as water and oxygen ingress in a device, putting UV-filters, and device encapsulation[8b,244a,249] or incorporating the perovskite film in a polymer matrix.[250] However, there have been significant contribution to degradation from the interfacing contacts too. It is evidenced that replacement of most common HSC in n-type PSCs, i.e., spiro-OMeTAD by humidity resistant counterparts such as PTAA and inorganic counterparts or in p-type PSCs, replacement of organic HSC, i.e., PEDOT:PSS by NiO enhanced device stability significantly.[22f] Reports on the role of interfaces determining perovskite stability are also published.[146,251] As the structural stability of perovskite and also the effect of external atmospheric factors are well documented, herein we limit our discussion within the scope of this article, i.e., the case for the interfaces namely, ESC/perovskite and HSC/perovskite towards device stability. This is particularly important after the reports that interfaces are also crucial for long term stability[78,252] and a recent demonstration that a perovskite layer itself could be stable when exposed to humidity and light and it is rather the interface properties that induces degradation within the devices as the characteristics of the interface changes over time.[253] Another landmark report is the finding that the perovskite deposited on metal oxides typical leads to deterioration of film up to first few nanometers due to the catalytic nature of the MOS thereby leaving some volatile residuals at the interface.[23] This surface degradation is significantly higher for inorganic selective contacts and much lower for organic rivals. A first 10 and ≈30 nm of the perovskite layer deposited in-situ via evaporation did not show any perovskite related peaks on ITO and

Table 4. An account of various interfacial modifiers employed in perovskite solar cells.

Interface to be modified	Modifier	Device architecture	V_{OC} [V]		J_{SC} [mA cm^{-2}]		FF		PCE [%]		Ref.
			Test Cell	Ref. cell	Test Cell	Ref. cell	Test Cell	Ref. cell	Test Cell	Ref. cell	
ESC-perovskite	4-Cl-PhCOOH, PhCOOH	FTO/c-,m-TiO_2/ $FA_xMA_{1-x}PbI_{3-y}Br_y$/Spiro/Au	1.07	1.05	22.28	21.64	0.77	0.76	18.43	17.46	Zhu et al.[239]
ESC-perovskite	PCBA[*a)]	FTO/c-TiO_2/ $CH_3NH_3PbI_3$/Spiro/Ag	1.16	1.08	21.38	14.94	0.72	0.63	17.76	10.17	Dong et al.[232]
ESC-perovskite	PbO monolayer	FTO/c-TiO_2/ $CH_3NH_3PbI_{3-x}Cl_x$/Spiro/Au	1.02	0.98	21.96	20.5	0.76	–	17.03	≈12	Liang et al.[227]
ESC-perovskite	La_2O_3	FTO/c-,m-TiO_2/ $CH_3NH_3PbI_3$/Spiro/Au	1.01	0.90	20.84	18.73	0.66	0.75	15.81	11.10	Shaikh et al.[240]
ESC-perovskite	C_{60}-SAM	FTO/c-TiO_2/ $CH_3NH_3PbI_{3-x}Cl_x$/Spiro/Au	1.02	0.90	21.7	18.6	0.67	0.46	15.0	7.6	Wojciechowski et al.[32c]
ESC-perovskite	PCBM	FTO/ZnO NRs/ $CH_3NH_3PbI_3$/Spiro/Au	0.96	0.81	22.06	18.57	0.55	0.53	11.67	7.93	Xu et al.[231]
HSC-perovskite	DEA[*b)]	FTO/NiO/DEA/Perovskite/PCBM/PN4N/Ag	0.95	0.94	20.90	17.71	0.80	0.65	15.90	10.97	Bai et al.[32d]
HSC-perovskite	GeO2	ITO-PEDOT:PSS/ $CH_3NH_3PbI_{3-x}Cl_x$/PCBM/Ag	0.96	0.89	21.55	18.57	0.74	0.67	10.97	15.15	Wang et al.[241]
HSC-perovskite	Mo-IPA[*c)]	FTO/c-TiO_2/ $CH_3NH_3PbI_3$/Spiro/Au	0.90	0.91	22.06	20.86	0.57	0.59	10.8	12.0	Fu et al.[235]
Metal/perovskite-PCBM	Doped Bphen[*d)]	ITO-PEDOT:PSS/ $CH_3NH_3PbI_3$/PCBM/Ag	0.95	0.88	21.89	20.06	0.75	0.59	15.87	10.77	Jiang et al.[33]
Metal-perovskite	C_{60}-N	ITO-PEDOT:PSS/ $CH_3NH_3PbI_3$/PCBM/Ag	–	–	–	–	–	–	15.5	7.5	Liu et al.[31b]
Metal-perovskite	TPB[*e)]	FTO/c-TiO_2/ $CH_3NH_3PbI_3$/Au	0.81	0.74	13.26	11.68	0.58	0.61	6.26	5.26	Xu et al.[242]

[*a)]6,6]-phenyl-C61-butyric acid (PCBA); [*b)]Diethanolamine; [*c)]Molybdenum isopropoxide; [*d)]N,N,N′,N′-Tetraphenyl-benzidine (TPB); [*e)]4,7-diphenyl-1,10- phenanthroline (Bphen) doped with bis(2-methyldibenzo-[f,h]-quinoxaline) (Ir(MDQ)2(acac)).

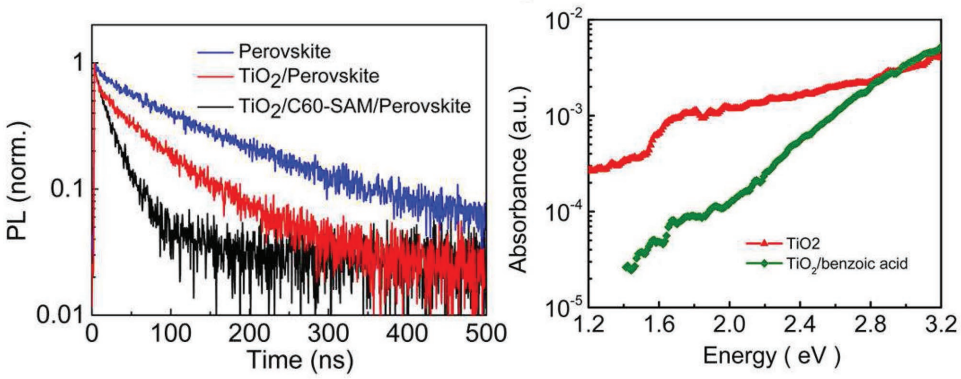

Figure 21. (Left) Normalized PL decays of perovskite films interfaced with TiO_2 only and TiO_2 functionalized with a C_{60}-SAM, and (right) photo-thermal deflection spectra of TiO_2 based films and a mimic of C_{60}-SAM (benzoic acid). Reproduced with permission.[32c] Copyright 2014, American Chemical Society.

MoO_3, respectively (**Figure 22**); whereas a only 3 nm thin layer of perovskite on PEIE and PEDOT:PSS feature of a perovskite film. This could also explain why passivation of typical MOS layers via an organic interfacial modifiers results in improved performance.

7.1. Degradation at ESC/Perovskite Interface (Mesoporous vs Planar)

So far, the most common employed MOSs in mesoporous PSCs are TiO_2 and ZnO. Whereas the former has been known

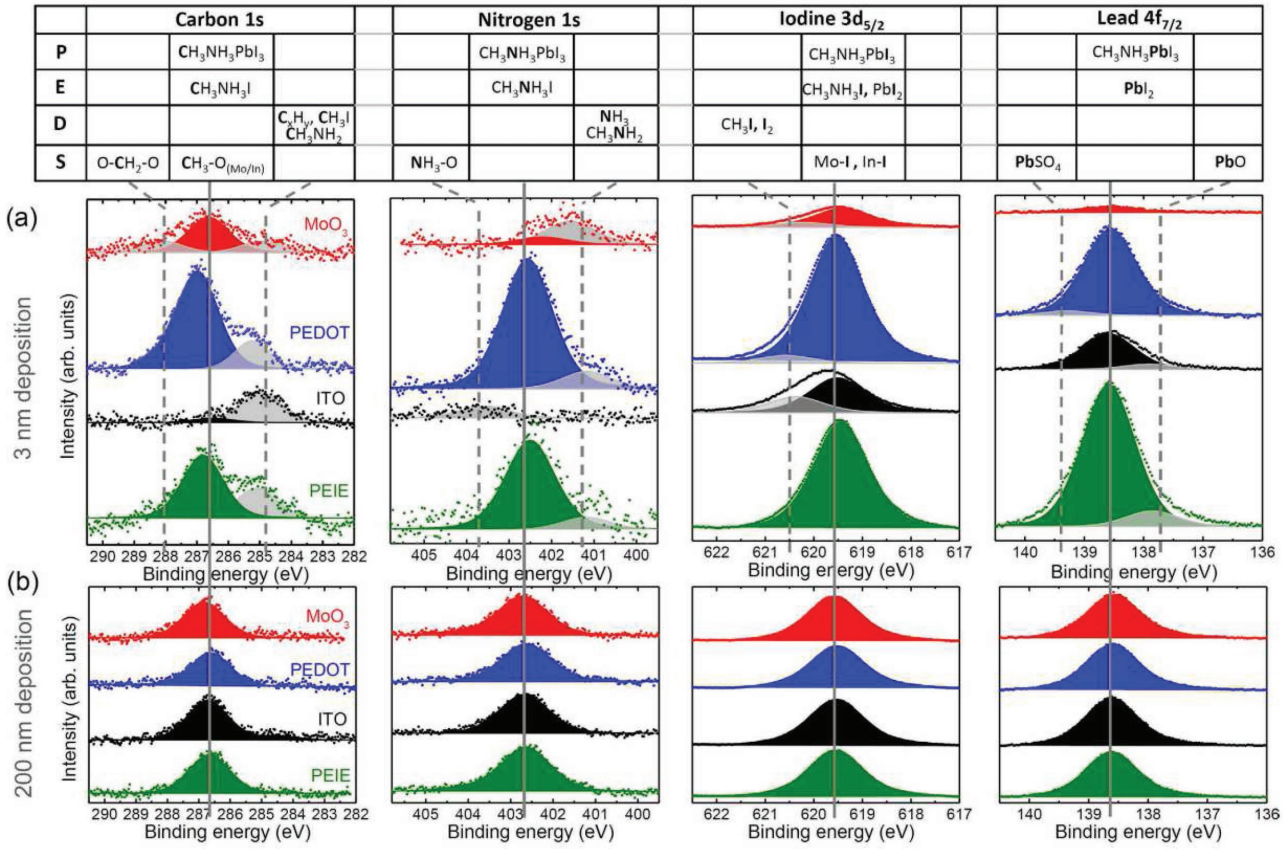

Figure 22. UV photoelectron spectra of an in-situ evaporated perovskite layer on four different selective contacts (or substrates) showing the occupied density of states. The thickness of the perovskite layer is systematically increased and probed to investigate the interfacial properties. The graphs show traces of carbon, nitrogen, iodine, and lead spectra of $MAPbI_3$. The solid vertical lines mark the expected binding energy in perovskite for each element, while the dashed lines show the positions of additional chemical environments observed at low coverage before the stoichiometrically correct perovskite is formed. The table above lists possible reaction products responsible for the additionally observed peaks, divided into products (P), educts (E), decomposition products (D), and surface bonds (S). Reproduced with permission.[23] Copyright 2017, Macmillan Publishers Limited.

to degrade when exposed to UV light and also induce surface degradation[21c,22a,b] in its NPs morphology, the latter has been known to deprotonate perovskite layer due to the presence of hydroxide groups on its surface.[96,220] Yet mesoporous architecture offers better stability than their planar rivals because the perovskite crystal decomposes upon degradation leaving discontinued film with increased grain boundaries,[251,253] and in such cases, the mesoporous layer helps maintaining stable charge transport channels. TiO_2 NPs are also known to induce instability in the device when expose to UV-radiation due to light induced adsorption of surface adsorbed oxygen.[22b] The presence of oxygen sites (Ti_3^+) on TiO_2 surface may act as traps which are activated in presence of oxygen. One could argue stable performance of the same materials in DSSCs in presence of UV light; however, it is important to note that in DSSCs, these surface traps are passivated by acetonitrile in liquid electrolyte.[254] Replacing TiO_2 with Al_2O_3 in PSCs has shown a stable performance for 1000 h when exposed to UV-light. This phenomenon also induce instability in planar PSCs, although the rate of observed degradation is relatively slower than PSCs with a mesoporousTiO_2.[22b]

Alternatively, TiO_2 nanorods (NRs) showed greater stability compared to NP based or even planar analogues, in un-encapsulated PSCs[21c] or even their sealed analogues.[22a] PSCs with three types of TiO_2 (**Figure 23**), fabricated and sealed in an inert atmosphere, showed different degradation profile at similar testing conditions. Fastest degradation is observed in planar PSCs that retained only <10% of initial PCE after 2500 h followed by a NPs based device that retained nearly 50% of original PCE. However, NRs based devices surprisingly showed slight improvement in performance as shown in Figure 23d and also in **Table 5**. It shows that besides humidity, the nature of interface to be one of the dominating factors for instability.[22e,255] As the devices were sealed in an inert atmosphere and the effect of humidity is negligible, and therefore, one would expect as similar degradation behavior for all three device types.[22a] The XRD analysis of replica of the aged devices (after 2500 h) showed that whereas, the NRs based PSCs retained >80% of initial perovskite phase fraction (calculated from the major XRD peaks of $CH_3NH_3PbI_3$ at 2θ ≈14.4 and ≈28.8°), NPs based and planar PSCs showed drastic diminishing of perovskite, probably due to the fact that the ESC films here induces surface degradation of perovskite film by reacting with it unlike NRs that seems to avoid it. This could be related to more thermodynamically stable rutile NRs than anatase NPs, and (ii) the different surface energy of NRs owing to their different size and crystallinity (NRs are single crystalline and have a larger volume ≈4.7×10^6 nm^3) than NPs (polycrystalline and significantly smaller volume ≈8.2×10^3 nm^3). However, regarding the different degradation rate of planar and mesoporous TiO_2 NPs based PSCs, is not fully understood so far.

Efforts to modify the characteristics of the ESC interface has demonstrated improvement in stability of PSCs. Ito et al.[256] modified the surface of TiO_2 by coating a thin layer of Sb_2S_3 and observed improvement in photostability of device without encapsulation. Incorporation of Sb_2S_3 between perovskite and TiO_2 avoided surface degradation of $CH_3NH_3PbI_3$ crystals. A similar report,[257] where surface passivation of TiO_2 by a thin layer of CdS suppressed interface defects and reduced charge

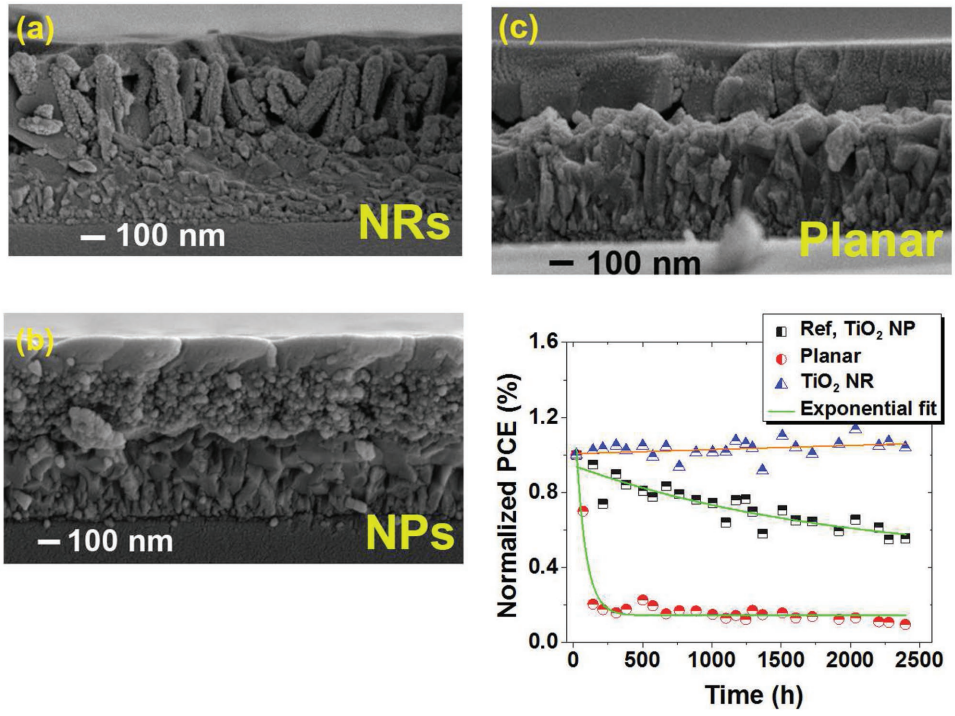

Figure 23. Cross sectional view of PSCs employing three types of interfaces: a) TiO_2 nanorods, b) TiO_2 compact layer (a planar PSC configuration), and c) TiO_2 NP layer using commercial their commercial paste. d) Normalized PV performance of the three PSCs (encapsulated) stored in dry air (Rel. H <30% at room temperature and in dark). Reproduced with permission.[22a] Copyright 2015, American Chemical Society.

Table 5. Stability tests carried out for various types of PSCs. Unless specified, otherwise the abbreviation used in device configuration column corresponds to following: c-T = compact TiO_2, m-T = mesoporous TiO_2 (NPs), $MAX_3 = CH_3NH_3PI_3$ (X = Cl, Br, I), S = Spiro, P = P3HT, C = Carbon, A = Al_2O_3, Z = ZrO_2, P:P = PEDOT:PSS, Sealed = S, Not Sealed = NS. The performance of the devices is measured at standard test conditions.

Device architecture	Interfacing material		Device fabrication conditions	Stability test conditions	Test duration and/device encapsulation?	Initial PCE [%]	Percentage of PCE change [%]	Reference
	ESC	HSC						
Mesoporous	C,m-TiO_2	Spiro	Rel. H 50%, ambient air and temperature	Rel. H 15%, dry air, room temperature	2400 h (NS)	10.2	−15%	Yin et al.[251]
	C,m-Zn_2SnO_4	Spiro	NA	Dark, dry air, room temperature	≈700 h (NS)	13.3	−26%	Bera et al.[259]
	ZnO-NRs	Spiro	NA	Ambient, room temperature	500 h (NS)	5	−14%	Bi et al.[258]
	c-TiO_2	Spiro	Inert atmosphere	Rel. H 40%, dry air, room temperature	1300 h (NS)	12.1	−95%	Fakharuddin et al.[21c]
	c-T/TiO_2 NRs	Spiro	Inert atmosphere	Rel. H 40%, dry air, room temperature	1300 h (NS)	5.8	−40%	
	c-T/TiO_2 NRs-$TiCl_4$	Spiro	Inert atmosphere	Rel. H 40%, dry air, room temperature	1300 h (NS)	12.2	+14%	
	c-T/TiO_2-NPs/CdS	Spiro	Ambient	Light soaking, ambient	12 h (NS)	9	−20%	Hwang et al.[257]
	c-T/TiO_2 NPs	Spiro	Inert atmosphere	R. H <40%, room temperature	2500 h (S)	7.9	−40%	Fakharuddin et al.[22a]
	c-T/TiO_2 NRs	Spiro	Inert atmosphere	R. H <40%, room temperature	2500 h (S)	10.5	+5%	
	c,m-TiO_2	TPDI	–	Ambient, 25–30 °C, R. H. 40–50%	720 h	13%	−5%	Zhang et al.[125]
Planar n-i-p	c-TiO_2	Spiro	Inert atmosphere	R. H <40%, room temperature	2500 h (S)	5.8	−95%	Fakharuddin et al.[22a]
	c-T/CsBr	Spiro	Inert atmosphere	UV-light (360 nm) at 523 mW cm^{-2}	20 min (NS)	16.1	−30%	Li et al.[236a]
HTM free	C,m-TiO_2/ZrO_2	HTL free	Ambient	Ambient, light soaking at AM 1.5	1008 h (NS)	10.5	+1%	Mei et al.[8b]
Inverted planar (p-i-n)	$PC_{61}BM$	PEDOT:PSS	Inert atmosphere	Ambient, 20 °C, R. H. 30%	50 m (NS)	11.7	−99%	Zhang et al[263]
	PCBM	PEDOT:PSS	Inert atmosphere	Inert atmosphere, room temperature	500 h (NS)	14	−10%	Li et al.[216a]
	PCBM	PEDOT:PSS	Inert atmosphere	Inert atmosphere, 45 °C	≈100 h (NS)	14	−31%	
	PCBM	PEDOT:PSS	Inert atmosphere	Inert atmosphere, 70 °C	≈100 h (NS)	14	−85%	
	PCBM	CPE-K[a)]	Inert atmosphere	Ambient ≈20 °C, R. H. ≈40%	120 m (NS)	12.5	−60%	Choi et al.[264]
	PCBM	PEDOT:PSS	Inert atmosphere	Ambient, ≈20 °C, R. H. ≈40%	120 m (NS)	12.5	−99%	
	ZnO	PEDOT:PSS	–	Ambient, 30 °C, R. H. 60%	≈1000 h	16.1	−20%	Chang et al.[191]
	C_{60}/BCP	CuSCN	Inert atmosphere	Ambient air, in dark	40 h (NS)	16.6	−(10–15)%	Ye et al.[20b]
	ZnO	NiO_X	Ambient	Ambient, 25 °C, R. H. 30–50%	1440 h	16.1	−5%	You et al.[88]
	$PC_{61}BM$	Cu:NiO_X	–	Ambient	240 h (NS)	≈15	−(5–8)%	Kim et al.[265]

Table 5. Continued.

Device architecture	Device configuration	Device fabrication conditions	Stability test conditions	Test duration and/device encapsulation?	Initial PCE [%]	Percentage of PCE change [%]	Reference
Flexible PSCs	PET-ITO/MAI_3/PC_6|BM/Al	Inert atmosphere	Ambient, 20 °C, R. H. 30%	50 m (NS)	9.7	–30%	Zhang et al.[263]
	PET-ITO/MAI_3/PC_6|BM/Al	Inert atmosphere	Ambient, 20 °C, R. H. 30%	300 m (NS)	9.7	–99%	
	PET-ITO/Ag-mesh/PH1000/P:P/MAI_3/PCBM/Al	Inert atmosphere	Inert atmosphere, room temperature	500 h (NS)	14	–8%	Li et al.[216a]
	PET-ITO/Ag-mesh/PH1000/P:P/MAI_3/PCBM/Al	Inert atmosphere	Inert atmosphere, 45 °C	≈100 h (NS)	14	–25%	
	PET-ITO/Ag-mesh/PH1000/P:P/MAI_3/PCBM/Al	Inert atmosphere	Inert atmosphere, 70 °C	≈100 h (NS)	14	–77%	
	PET/P:P:MAI_3/PCBM/PTCDI[b]/Cr_2O_3-Cr/Au/PU[c]	Inert atmosphere	Ambient	≈10 h (NS)	≈12	–20%	Kaltenbrunner et al.[217b]

[a]**CPE-K**: Poly[2,6-(4,4-bis-potas-siumbutanylsulfonate-4H-cyclopenta-[2,1-b;3,4-b']-dithiophene)alt-4,7-(2,1,3-benzothiadiazole)]; [b]**PTCDI**: N, N-dimethyl-3,4,9,10-tetracarboxylic perylenediimide; [c]**PU**: Polyurethane.

recombination, showed relatively stable performance during 12 h of light soaking compared to a bare TiO_2 analogue.

Similarly, replacement of TiO_2 NPs with alternatives such as ZnO NRs,[258] and Zn_2SnO_4[259] have also demonstrated improved stability thereby evidencing that the interfacing material matters in long term durable performance of PSCs (Table 5). While the TiO_2 based PSCs showed ≈50% power drop only after 10 days, Zn_2SnO_4 PSCs retained 86% of initial PCE even after 30 days of testing. The Zn_2SnO_4 favored well-crystallized perovskite morphology with significantly larger grains (≈2 µm) which avoided moisture attack on grain boundaries, a susceptible site to degradation.[166a,260] Another possible reason of stable performance could be the stronger bonding between $CH_3NH_3PbI_3$ and Zn_2SnO_4 than between $CH_3NH_3PbI_3$ and TiO_2 that improved the interface characteristics.

7.1.1. Stability of Planar PSCs

The planar PSC have showed drastic degradation not only under light soaking[261] but also during their shelf-life testing.[22a] The degradation was drastic under light soaking resulting in complete power drop in the devices. An 80–90% performance drop is observed for their unencapsulated laboratory scale devices[38] as well as their encapsulated large area modules.[21c,22a] While one could argue that the drop in the PV performance in the former could be due to the presence of humidity, the latter were sealed in a glove box and the contribution from humidity is negligible. It is therefore conceivable that the interface (c-TiO_2-perovskite) is highly reactive with perovskite crystals. Other possible reasons are the photo-degradation of c-TiO_2 due to surface adsorbed oxygen in presence of UV-light, as discussed before, and also its surface defects. A recent work by Li et al.[236a] report UV-stable performance of a planar PSC by incorporating an interface modifier, i.e., cesium bromide (CsBr) between c-TiO_2 and perovskite which not only improved the photocatalytic activity of ESC but also reduced interfacial defect sites. The report suggests a reduction in reactivity of TiO_2 upon incorporation of CsBr thereby affirming our understanding that a planar device can, in principle, degrade in absence of humidity.[22a] The fact that encapsulated planar and mesoporous-TiO_2 PSCs degraded in absence of humidity, it seems conceivable that the highly reactive TiO_2-perovskite interface plays a dominant role towards instability. This can also be understood from the fact that when a thick less reactive insulating oxide layer (ZrO_2, ≈2 µm) is employed on top of TiO_2, the PSCs showed one of the highest stability (1000 h under light soaking) till date.[8b]

7.2. Interface Effect and Stability in Flexible PSCs

Flexible PSCs are more prone to degradation as an uneven substrate surface, such as in the case of PET-ITO, may result in distortion of perovskite film morphology above it as also evidenced by Schmidt et al.[262] creating an additional degradation channel. Towards a robust and highly conductive substrate, Li et al.[216a] reported an Ag-embedded substrate modified with a polymer conductor (PH1000) to support low sheet resistance which is also mechanically robust as it employs a protective layer of PET

(≈57 µm) which retained not only at room temperature (92% of original performance, PCE≈14%), but also, more importantly at higher temperature ≈45 °C (75% of original PCE). Interestingly the stability is higher than that of a reference device made on rigid ITO (90% at room temperature and 69% on 45 °C).

7.3. Stability at ITO and Back Contact Interfaces

The degradation can also take place at ITO- or metal back contact. The PSCs with organic selective contacts, i.e., PEDOT: PSS, which is acidic, react with ITO surface that leads to corrosion. This can be avoided by modifying ITO surface. For example, HSC-free *f*-PSCs without a PEDOT:PSS layer demonstrated ≈6 times higher stable performance than a rival.[263] Similarly, the degradation due to metal contact is overcome via incorporating a Cr_2O_3/Cr interlayer between perovskite and metal contact and pre-treating the PET/ITO substrate with dimethylsulphoxide resulted in an air stable performance (**Figure 24**).[217a] It is important to note that the device is extremely thin (≈3 µm) and showed a stabile performance compared to that of a glass ITO based PSCs.

7.4. Degradation at HTM/Perovskite Interface

Since the inception of PSCs, most designs employ an organic hole transporting layer (≈300 nm), typically small molecules (spiro-OMeTAD), conducting polymers (P3HT, PTAA and PANI etc.), and inorganic HTMs (CuPc, NiO, CuO etc.), as a hole selective contact.[22f,266] Despite the fact that the most successful device till date employ inorganic HSCs these organic charge selective contacts are sensitive to moisture and oxygen and thereby induce degradation in PSCs.[267] A common example is the widely employed spiro-OMeTAD doped with Li-salt (Li-TFSI) which, owing to its extremely hygroscopic nature, tends to react with humidity.[268] Apart from extrinsic degradation routes, it has been recently reported how the chemical reaction between *spiro*-$OMeTAD^+$ and migrating I^- from the perovskite absorber progressively reduces the hole transporting material conductivity and deteriorates solar cell performance.[85] The research activities seeking stable PSCs from an HSC perspective can be classified as: (i) dopant free HSCs, (ii) inorganic or organic alternatives to the commonly used hygroscopic spiro-OMeTAD, (iii) post-modification of HSC or encapsulation to protect the device from humidity, and (iv) by adding new less reactive additives to spiro-OMeTAD.[22f] However, as the focus of the present article is on the role of interfaces only, we limit our discussion to the reports where a modification in HSC/perovskite interface increased the stability in the device. We present case studies from two type of devices here; firstly a mesoporous architecture employing an HSC (Figure 1a) and secondly a p-i-n planar architecture (Figure 1f) that employs an HSC on conducting substrates, also called an inverted planar PSC.

Despite the fact that highest efficiency PSCs employs spiro-OMeTAD as a HSC, it is known to degrade in presence of

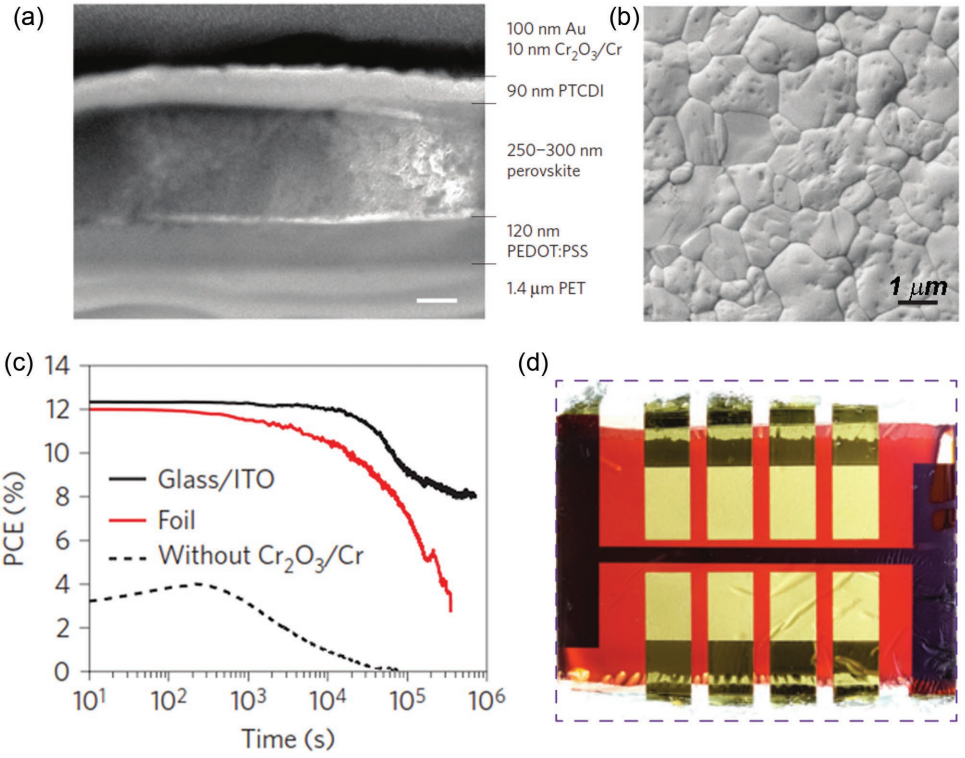

Figure 24. An ultrathin flexible PSC (≈3 µm). a) Cross-sectional view of a full f-PSC exhibiting uniform and well-separated layers of active materials. Scale bar, 100 nm, b) SEM image of perovskite morphology film on PEDOT:PSS-coated foil. Scale bar, 1 µm, c) stability testing of f-PSCs employing Cr_2O_3/Cr barrier layer and modified PET-ITO (red line) compared with pristine flexible (dashed line) and glass ITO based (black line) counterparts. The pristine flexible PSC showed drastic drop in PCE, and d) a photograph of f-PSC. Reproduced with permission.[217b] Copyright 2015, Nature Publishing Group.

moisture, primarily due to the presence of Li-salt dopant in it. Replacement of spiro-OMeTAD with alternative HTMs such as 5, 10, 15-triphenyl-5H-diindolo[3, 2-a:3′, 2′-c]carbazole(TPDI) has shown to increase the PCE from 15.1% to 15.5%.[125] In the absence of Li-TFSI as a dopant in both HTLs, the devices showed PCE ≈10.8 and ≈13.6%, respectively. It is important to note that TPDI is a HSC with two order of magnitude higher hole mobility (μ_h for TPDI 3.5×10^{-3} cm^{-2} V^{-1} s^{-1}) than spiro-OMeTAD ((μ_h for TPDI 4×10^{-5} cm^{-2} V^{-1} s^{-1}).[125] Besides the higher PCE, the PSCs employing a pristine TPDI also showed enhanced air-stability; the PCE only dropped by 5% for pristine TPDI based PSCs and ≈17% for their doped analogues. The use of an iridium complex instead of the commonly Co complex additive used to enhance the conductivity of spiro-OMeTAD also has a significant beneficial effect in the long term stability.[267a] Other alternatives to spiro-OMeTAD are inorganic NiO, and CuSCN which can be employed in mesoporous PSCs.

Inverted PSCs also called planar heterojunction PSCs suffer from significant degradation primarily arising from their organic ESC and HSC components. The design typically employs either a thin PCBM layer, an ESC which is sensitive to moisture, and PEDOT:PSS as a HSC which is acidic in nature and also known to degrade in the presence of humidity.[161] Despite the fact that incorporation of organic ESC and HSC routinely resulted in PCE as high as 15–17% (Table 3), the devices often degrade drastically even during their shelf-life testing thereby putting a question mark on their commercial deployment. Thanks to the optimization of these selective contacts, inverted planar PSCs started to show signs of stable performance recently.[88,192,269] Firstly, interface engineering at ESC via (i) replacing organic PCBM by inorganic ESC such as NiO[88,270] and NiO_x:Cu[271] and (ii) post-treatment of PCBM or anorganic-inorganic bi-layer design such as $PC_{61}BM/TiO_x$[172] and $PC_{61}BM/ZnO$[171] demonstrated significantly enhanced stability in these device (Table 5). These inorganic counterparts demonstrated stable performance in presence of humidity and also are not corrosive to the substrates underneath.

Towards the stability of HSC layer in inverted PSCs, replacing the typically employed humidity sensitive and acidic organic selective contact (PEDOT:PSS, PH ≈2)[272] with an air-stable inorganic counterpart such as NiO, CuSCN, MoO_3, and $Cu:NiO_x$ has also shown enhanced stability.[22f] It is important to note that PEDOT:PSS film itself reacts with humidity and form new complexes (water-PEDOT:PSS) which alter its energy levels and thereby hole extraction efficiency of a device. Inorganic HSCs have demonstrated significantly high stability in this class of PSCs; for example, CuSCN based PSCs showed a stable performance for 40 h.[35] Similarly, $Cu:NiO_X$ based PSCs showed stable performance and retained >90% of initial PCE after 240 h compared to a PEDOT:PSS based PSCs (PCE dropped by 70%). The details of such many alternatives is given in Table 5. One of the best stability in such devices is reported when both the inorganic selective contacts are replaced with inorganic counterparts (**Figure 25**), resulting in PCE 16.1% and also a significantly stable performance for 60 days.[88]

Another possible degradation route is the reaction between perovskite and metal back contact (Ag) which corrodes Ag. Incorporation of an intermediate layer such as ZnO and Cr_2O_3-Cr has shown to form an effective barrier to overcome such degradation. Nevertheless, one of the highest stability in inverted planar PSCs is shown in devices replacing both the organic components simultaneously. You et al.[88] reported a fully MOS based inverted planar device which retained >90% of initial

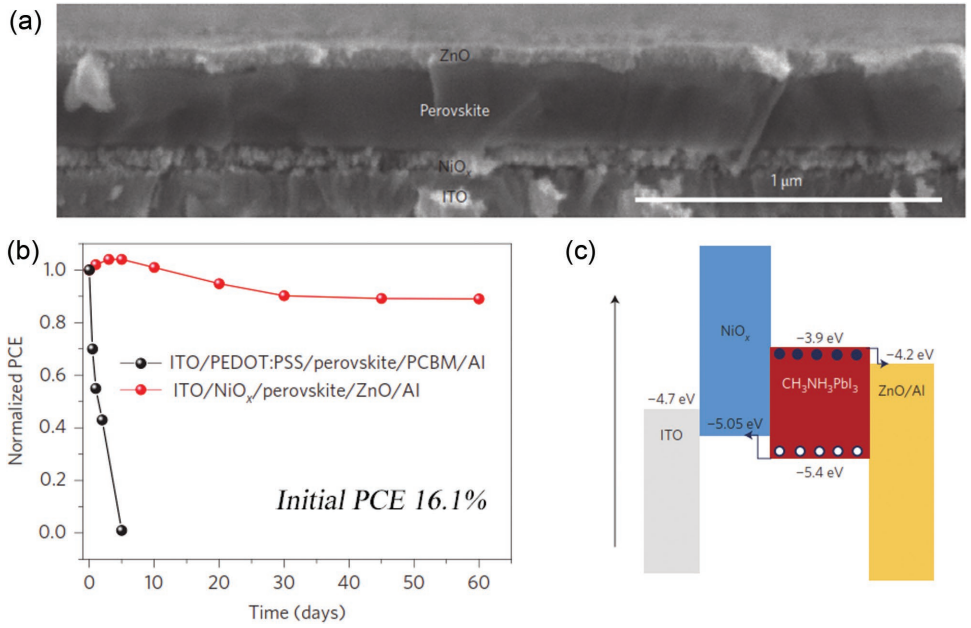

Figure 25. a) Cross-sectional image of an inverted planar PSC employing inorganic ESC and HSC (the unfinished Al electrode is not included) with the structure glass/ITO/NiOx/perovskite/ZnO, b) air stability of device and a reference PSC employing organic selective contacts, and c) schematic showing energy levels of materials components of the air-stable inverted planar PSC. Reproduced with permission. Copyright 2016, Nature Publishing Group.

PCE even after 60 days of shelf life testing and at room temperature light soaking contrary to an organic counterpart that degraded in merely 5 days. The MOS based inverted PSCs also showed a remarkable PCE ≈16.1% at standard test conditions.

As PSCs have demonstrated a photoconversion energy as high as other commercial solar devices (CdTe, CIGS, polycrystalline Si), one of the key challenges is achieving their long term stable performance when exposed to outdoor conditions. It can be seen from Table 3 and 5 that PSCs are fabricated with a wide variety of materials and design architectures, many of which are intrinsically unstable. It can also be noted that even the similar PSC architectures fabricated at different laboratories resulted in different stability, which is because the durability of these devices largely depends on the purity of starting materials, fabrication methods and conditions, and also the characteristics of the device interfaces. Unlike silicon and thin film solar cells where decades of research has brought them to deliver a stable performance over 20 years with negligible intrinsic degradation, these materials resembles OPVs where instability mostly arises from the materials components itself such as photo-oxidation, change in morphologies over time, and interfacial degradation.[273] We therefore believe that stability protocols of PSCs are more likely to follow the consensus being developed for OPVs[274] and DSCs[12,243] as the device degradation involves chemical modifications. For a detailed overview of the protocols that may be adopted while reporting stability of PSCs, we refer to the comprehensive reports highlighting various ISOS protocols to be adopted while measuring and reporting operational stability (indoor and outdoor).[12,243,274] Although so far, not many reports have followed any standard protocol while reporting stability of PSCs, we recommend that the perovskite community should follow few considerations while reporting such data. Most importantly the overestimation in PV performance of PSCs due to anomalous hysteresis and their erroneous efficiency reporting (missing IV data for reverse and forward scan, stabilized maximum power output and statistical analysis) must be carefully looked at.[275] For a reliable device characterization, we suggest a measurement protocol developed by Zimmermann et al.[276] The protocol is derived from standard *J-V* measurements, power point tracking and stabilized PV parameters as well as characteristics extracted from time resolved current density-voltage measurements. The PSCs research community needs to report stabilized PV performance for both scan directions and preferably the *J-V* curves at various scan conditions (delay time, scan rate etc.) in order to provide a clearer picture of device performance. We recommend a recently published checklist while reporting the PV performance,[275] (ii) while reporting the stability of PSCs, the protocols such as those for dark or indoor testing (ISOS-D-1, shelf-life, ISOS-D-2, high temperature storage, and ISOS-D-3, damp heat) or those for outdoor (ISOS-O-1-3)[273] must be followed so that a consensus on the stability is made and a true picture of device performance is obtained.

It is important to note that the PSCs are subjected to stress when continuously exposed to incident light. A standard light soaking protocol (humidity, temperature and power of incident light) should therefore be considered while reporting such tests. This will be a critical test in PSCs provided the fact that perovskite materials polarize when exposed to light inducing hysteresis in the device. We recommend that stability tests need to be divided in to materials' stability (ESC, HSC, perovskite, back contact, transparent electrode and interfaces) and device operation stability under various atmospheric conditions. One can also note that most of the stability tests carried out on PSCs (Table 5) are with un-encapsulated devices, a practice that should not be carried out particularly while using TiO_2 based PSCs. This is due to the fact that TiO_2 owing to its oxygen vacancies behaves differently in an environment with less or no oxygen[22b] and therefore the performance of sealed and open devices could largely differ. Also important to note that the stability of flexible PSCs, if their intended deployment is for indoor applications, will have to follow less stringent conditions as they will not be exposed to continuous light soaking.

8. Conclusions and Future Outlook

In this article we have addressed the importance of the charge selective contacts and their interfaces in perovskite solar cells (PSCs) and provided an overview of the different types of interfaces and how they determine device operation and stability. The electron selective contact (ESC) and hole selective contact (HSC) layers are deployed in PSCs in different architectures from planar to nanostructured. As can be seen in **Figure 26**, there has been tremendous progress in terms of efficiency, scalability and stability of PSCs. We see the application of perovskite in different architectures, wide variety of designs including flexible solar cells on plastic and metallic substrates, their large area modules and also different applications such as in batteries, and light emitting diodes etc.

The archetypical materials as ESCs are metal oxides, most commonly TiO_2, SnO_2, ZnO and other metal-oxides, including many doped variations and combinations of these. Additionally, we find organic ESCs in inverted solar cells using PCBM or C_{60}, however, recently use of organic molecules (and semiconductors) is also demonstrated (Ref. [17] of this article). Even ESC-free PSCs have been fabricated. The same is observed for the HSC, where the standard is the organic spiro-OMeTAD, but many other organic, inorganic, small molecules and polymers counterparts have also been successfully implemented (See Ref. [22f] of this manuscript). The reason for this large variety is manifold: Historically the PSCs started as extremely thin absorber cell, where the dye of a dye-sensitized solar cells (DSSCs) had been replaced by an inorganic thin absorber layer, the methyl ammonium lead halide perovskite. Consequently, the material of choice was mesoporous TiO_2 and spiro-OMeTAD as used in solid-state DSSCs. However, since then many different device architectures have been demonstrated, and it is clear, that the PSCs are not excitonic solar cells as dye-sensitized and organic solar cells. Therefore, it can be expected that other ESCs and HSCs optimized for excitonic solar cells will adapt better to the PSCs.

PSCs resemble in its function more thin film inorganic solar cells; however, they present some new features that have not been previously observed in other photovoltaic technologies as ion migration, accumulation capacitance or inductive loops. In contrast to organic and other hybrid solar cell, the ESC and HSC in PSCs only need to function as charge selective layers.

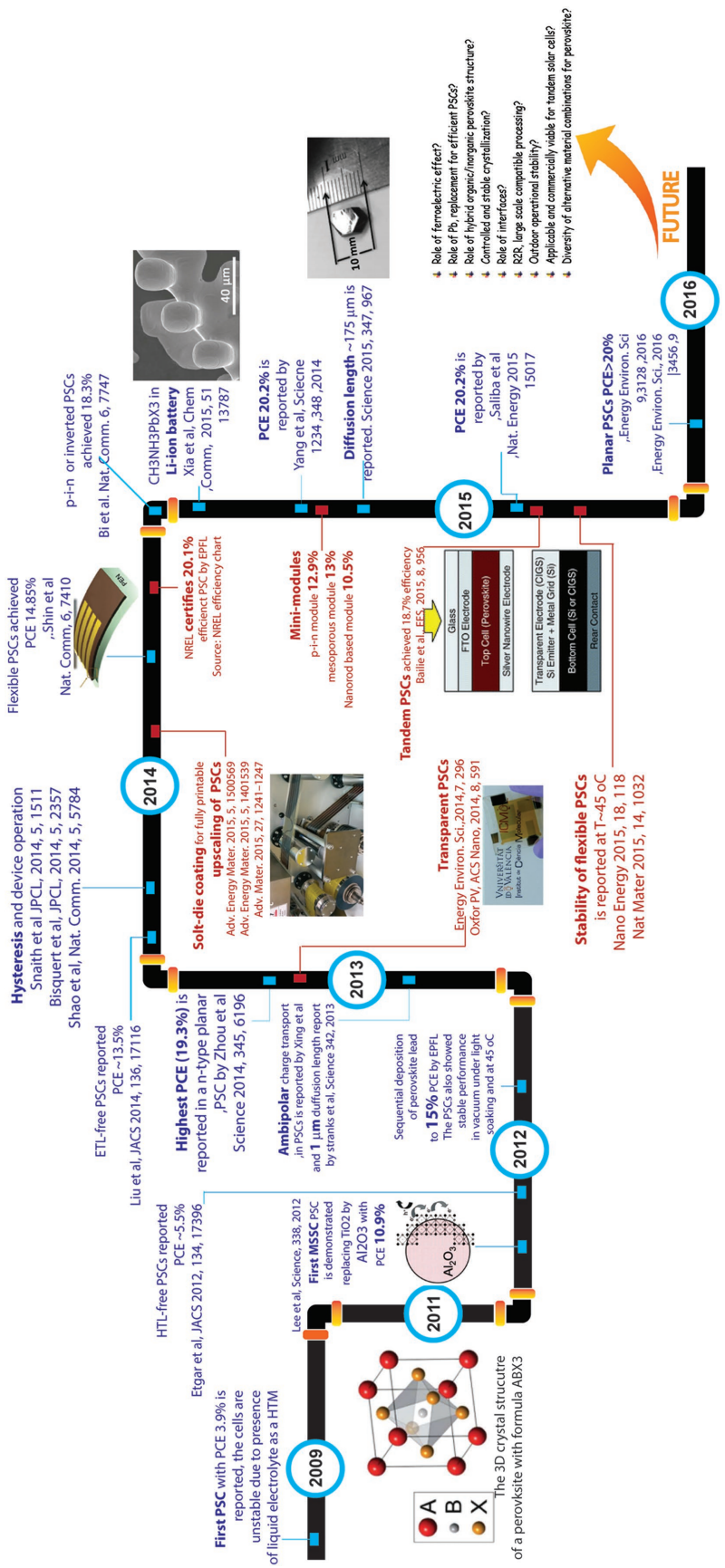

Figure 26. A timeline showing key developments in perovskite solar cells since their inception in 2009. The notes above the line (in blue text) shows developments towards efficiency and also understanding of device working mechanism whereas the notes below the line (red text) shows milestones towards scalability and stability. The text in black on the right (future) shows key questions that need to be addressed to completely understand the working of these devices for a commercially deployable device. For each Figure adapted in this timeline, a citation is added within the Figure itself. Crystal structure is reproduced with permission.[277] Copyright 2014, The Royal Society of Chemistry. Schematic of Al_2O_3 is reproduced with permission.[7] Copyright 2012, American Association for the Advancement of Science. Upscaling photo is reproduced with permission.[278] Copyright 2015, Wiley-VCH. Photo of transparent PSCs is reproduced with permission.[279] Copyright 2014, The Royal Society of Chemistry. Schematic of solar cells is adapted with permission.[280] Copyright 2015, article published under a Creative Commons CC-BY license. Schematic of tandem cells is reproduced with permission.[10] Copyright 2015, The Royal Society of Chemistry. Image of perovskite nanostructure is reproduced with permission.[281] Copyright 2015, The Royal Society of Chemistry. Image of a perovskite single crystal is reproduced with permission.[282] Copyright 2015, American Association for the Advancement of Science.

Exciton splitting at this interface is not necessary. Especially the standard HSC spiro-OMeTAD is probably not ideal, as it has a relative low charge carrier mobility forming amorphous films and only functions well when doped with additives. Furthermore, recently an irreversible chemical reaction between spiro-MeOTAD$^+$ and migrating I^- is reported at perovskite/HSC interface which leads to deterioration in device performance and instability.[85]

Currently, it is not clear, what the ideal interfacial layers to the perovskite are, however, it can be assumed that for different device architectures different materials are ideal. Even more, it can be assumed that the different perovskite preparation methods – leading to different perovskite films – also show optimized performance with different interfacial layers, which is even more the case for different chemical perovskite compositions. Currently, most PSCs are primarily optimized in terms of efficiency. However, other aspects will play a major role for industrial fabrication and commercialization. Next to solar cells stability, which strongly depend on the interfacial layers, also fabrication issues will have strong impact on the choice of interfacial layers. This is particularly important as perovskite film morphology depends on the underneath layer (scaffold, in case of Al_2O_3). Ideally, low temperature processing routes will be used, which will allow roll-to-roll fabrication on flexible substrates. The solar cells stability will also strongly depend on these layers as replacement of organic selective contacts with inorganic ones have shown significant stable performance for inverted planar architectures. Therefore, next to the optimized electronic properties the interfacial layers also need be stable and ideally serve as protection layers for the perovskite. Screening of stable selective contacts is more important after the report[23] that perovskite layer grown on some metal oxide leads to surface degradation leading to some byproducts at the interface, a phenomena which is much less pronounced for organic rivals.

The interfacial selective contacts also have a strong effect on the often observed hysteresis phenomenon. The most common selective contact, TiO_2, often demonstrate a hysteretic effect. There are a number of explanations to this hysteretic effect, such as ferroelectric behavior, ion migration, interfacial capacitive effects and trapping processes. However, the effect strongly depends on the interfacial layers, device architecture (planar or mesoporous/nanostructured), the materials, and the perovskite processing, etc. For example, in devices with PCBM or C_{60} as interfacial layer replacing or just covering the TiO_2 layer, this effect is much smaller, sometimes even negligible. This indicates that hysteresis strongly depends on the nature of the interface and its interaction with the perovskite layer. It seems that high efficiency and stable devices show less of this hysteretic effect. Therefore, it could be that hysteresis is indicating limitations of the cells and possibilities exist to avoid it by optimizing the processing parameters, device architectures and interfacial layers which in this case would also lead to high efficiency and maybe also an improved stability.

For highly efficient PSCs, the perovskite film should be employed between charge selective layers to suppress interfacial recombination. Surface traps that act as recombination centers at the interfaces must be eliminated and the physical mechanism of charge accumulation have to be completely understood. This makes a good "matching" between the materials necessary, which concerns not only the energetic levels, but also is important for structural alignment at the interface. Finally, most selective interfacial layers have a relative low charge carrier mobility. In this case, they should be as thin as possible, still leading to compact, pinhole free layers to have minimal transport resistance.

Also the ideal device architectures of the interface to the perovskite layer is not yet completely decided. Record PSC have been obtained with mesoporous TiO_2, nevertheless a very significant progress in the performance of planer solar cells has been made over the last year, and very recently, without TiO_2 (Ref. [17] of this article). Usually metal oxides such as TiO_2, SnO_2, ZnO and doped variations of them or also binary metal oxides are used, while TiO_2 is by far the most common material. However, currently it seems completely open, whether it is really the best material. Even though PSCs based on mesoporous TiO_2 films currently hold the efficiency record, it is also not clear whether this mesoporous scaffold is really needed for efficient crystallization of the perovskite film. An issue without a scaffold might be the device stability, which seems to improve in cells with nanostructured metal-oxides as these might be able to protect the perovskite layer. It has been shown very early on already that also an insulating mesoporous scaffold (Al_2O_3) can be used to replace the mesoporous TiO_2 film due to the ambipolar nature of the perovskite layer. In this case, the mesoporous layer just acts as crystallization layer and scaffold for the perovskite. High efficiency and stability achieved in PSCs using insulating scaffolds such as Al_2O_3 and ZrO_2 would open up extensive investigation. The nature of the perovskite film also allows having just one selective contact and having a metal contact directly on the perovskite on the other side. This ESC or HSC free p-n type devices do function astonishing well, but do not show the same performance and stability as p-i-n type devices, where both sides have the selective contacts. Also important to note that a hysteresis-free behavior is yet to be observed in these single interface devices, but it has been reduced with surface treatments.

Towards long term stability and commercialization, PSC technology is advancing in order to follow the standard developed by International Electrochemical Committee IEC 61646 (thin-film terrestrial PV modules–design qualification and type approval), although it seems that qualifying other standards such as IEC 61215 (crystalline silicon terrestrial PV modules–design qualification), and IEC 62108 (concentrator photovoltaic (CPV) modules and assemblies–design qualification and type approval) might take longer to be accomplished.[243] For PV technologies such as OPVs, DSCs and PSCs, the IEC 61646 seems more suitable, nonetheless, to reach a deployable stage the PSCs have to undergo outdoor exposure tests at maximum power output, UV-protection tests, thermal cycling tests (–40–85 °C, 200 cycles), damp heat (85 °C, R.H 85% for 1000 h), and light soaking (1 sun, ≈80 °C). Although initial reports on stability are encouraging, PSCs still have a long way to reach a deployable PV technology. PSCs manufacturing companies such as Oxford Photovoltaics have made important announcements towards stability and deployment in upcoming years. Nonetheless, to achieve long-term operational stability, stable selective contacts are as important as perovskite layer itself.

It remains exciting, what progress will be made, and how the understanding of different observed features increases and leads to improved device efficiency and stability. As indicated in Figure 26, there are still a number of open questions. Answering these will help us to gain deeper understanding, which will pave the way to commercialization. It is very likely that we have not yet found the "ideal" interface, promoting efficient charge extraction from the perovskite, not creating or even passivating surface traps at the interface, and improving the device stability. Maybe there is not "one" material, but different pathways which might be successful. The most exciting physics happens at the interfaces, so a better understanding of the details of the interfacial process will also give us more information on current limitations and ideas how to overcome these.

Acknowledgements

A.F. acknowledges Alexander von Humboldt Foundation for the postdoctoral research fellowship. R.J. acknowledges the Ministry of Education (KPT), Govt. of Malaysia, for the fundamental research grant (RDU140126) on perovskite solar cells. The authors from INAM-UJI acknowledge the support from Generalitat Valenciana under project PROMETEOII/2014/020 and from MINECO of Spain Government under project MAT2016-76892-C3-1-R.

Conflict of Interest

The authors declare no conflict of interest.

Keywords

renewable energy, interfacial charge transfer, interface modification, interfacial defects in perovskite solar cells, hysteresis in perovskites

Received: March 7, 2017
Revised: April 11, 2017
Published online:

[1] a) M. Era, S. Morimoto, T. Tsutsui, S. Saito, *Appl. Phys. Lett.* **1994**, *65*, 676; b) H. Oshima, K. Miyano, Y. Konishi, M. Kawasaki, Y. Tokura, *Appl. Phys. Lett.* **1999**, *75*, 1473; c) D. B. Mitzi, K. Chondroudis, C. R. Kagan, *IBM J. Res. Dev.* **2001**, *45*, 29.

[2] a) S. Mathews, R. Ramesh, T. Venkatesan, J. Benedetto, *Science* **1997**, *276*, 238; b) C. R. Kagan, D. B. Mitzi, C. D. Dimitrakopoulos, *Science* **1999**, *286*, 945; c) B. B. Van Aken, T. T. M. Palstra, A. Filippetti, N. A. Spaldin, *Nat. Mater.* **2004**, *3*, 164.

[3] A. Kojima, K. Teshima, Y. Shirai, T. Miyasaka, *J. Am. Chem. Soc.* **2009**, *131*, 6050.

[4] a) J. Wu, Z. Lan, J. Lin, M. Huang, Y. Huang, L. Fan, G. Luo, *Chem. Rev.* **2015**, *115*, 2136; b) A. Hagfeldt, G. Boschloo, L. Sun, L. Kloo, H. Pettersson, *Chem. Rev.* **2010**, *110*, 6595.

[5] J. H. Im, C. R. Lee, J. W. Lee, S. W. Park, N. G. Park, *Nanoscale* **2011**, *3*, 4088.

[6] H. S. Kim, C. R. Lee, J. H. Im, K. B. Lee, T. Moehl, A. Marchioro, S. J. Moon, R. Humphry-Baker, J. H. Yum, J. E. Moser, M. Grätzel, N. G. Park, *Sci. Rep.* **2012**, 2.

[7] a) M. M. Lee, J. Teuscher, T. Miyasaka, T. N. Murakami, H. J. Snaith, *Science* **2012**, *338*, 643; b) J. Burschka, N. Pellet, S. J. Moon, R. Humphry-Baker, P. Gao, M. K. Nazeeruddin, M. Grätzel, *Nature* **2013**, *499*, 316; c) N. J. Jeon, J. H. Noh, Y. C. Kim, W. S. Yang, S. Ryu, S. I. Seok, *Nat. Mater.* **2014**, *13*, 897; d) H. Zhou, Q. Chen, G. Li, S. Luo, T. B. Song, H. S. Duan, Z. Hong, J. You, Y. Liu, Y. Yang, *Science* **2014**, *345*, 542; e) M. Saliba, T. Matsui, K. Domanski, J.-Y. Seo, A. Ummadisingu, S. M. Zakeeruddin, J.-P. Correa-Baena, W. R. Tress, A. Abate, A. Hagfeldt, M. Grätzel, *Science* **2016**, https://doi.org/10.1126/science.aah5557; f) M. Saliba, T. Matsui, J.-Y. Seo, K. Domanski, J.-P. Correa-Baena, M. K. Nazeeruddin, S. M. Zakeeruddin, W. Tress, A. Abate, A. Hagfeldt, M. Gratzel, *Energy Environ. Sci.* **2016**, https://doi.org/10.1039/C5EE03874J.

[8] a) A. Fakharuddin, F. De Rossi, T. M. Watson, L. Schmidt-Mende, R. Jose, *APL Mater.* **2016**, *4*, 091505; b) A. Mei, X. Li, L. Liu, Z. Ku, T. Liu, Y. Rong, M. Xu, M. Hu, J. Chen, Y. Yang, M. Gratzel, H. Han, *Science* **2014**, *345*, 295; c) P. F. Ndione, W. J. Yin, K. Zhu, S. H. Wei, J. J. Berry, *J. Mater. Chem. A* **2015**, *3*, 21940.

[9] a) M. H. Kumar, N. Yantara, S. Dharani, M. Graetzel, S. Mhaisalkar, P. P. Boix, N. Mathews, *Chem. Commun.* **2013**, *49*, 11089; b) C. Roldán-Carmona, O. Malinkiewicz, A. Soriano, G. Mínguez Espallargas, A. Garcia, P. Reinecke, T. Kroyer, M. I. Dar, M. K. Nazeeruddin, H. J. Bolink, *Energy Environ. Sci.* **2014**, *7*, 994; c) Y. Yang, J. You, Z. Hong, Q. Chen, M. Cai, T. B. Song, C. C. Chen, S. Lu, Y. Liu, H. Zhou, *ACS Nano* **2014**, *8*, 1674; d) F. Di Giacomo, V. Zardetto, A. D'Epifanio, S. Pescetelli, F. Matteocci, S. Razza, A. Di Carlo, S. Licoccia, W. M. M. Kessels, M. Creatore, T. M. Brown, *Adv. Energ. Mater.* **2015**, 5; e) F. Di Giacomo, A. Fakharuddin, R. Jose, T. M. Brown, *Energy Environ. Sci.* **2016**, *9*, 3007; f) D. Liu, T. L. Kelly, *Nat. Photonics* **2014**, *8*, 133.

[10] a) G. Y. Margulis, M. G. Christoforo, D. Lam, Z. M. Beiley, A. R. Bowring, C. D. Bailie, A. Salleo, M. D. McGehee, *Adv. Energy Mater.* **2013**, *3*, 1657; b) C. D. Bailie, M. G. Christoforo, J. P. Mailoa, A. R. Bowring, E. L. Unger, W. H. Nguyen, J. Burschka, N. Pellet, J. Z. Lee, M. Grätzel, R. Noufi, T. Buonassisi, A. Salleo, M. D. McGehee, *Energy Environ. Sci.* **2015**, *8*, 956.

[11] a) I. Grinberg, D. V. West, M. Torres, G. Gou, D. M. Stein, L. Wu, G. Chen, E. M. Gallo, A. R. Akbashev, P. K. Davies, J. E. Spanier, A. M. Rappe, *Nature* **2013**, *503*, 509; b) Q. Wang, Y. Xie, F. Soltani-Kordshuli, M. Eslamian, *Renewable Sustainable Energy Rev.* **2016**, *56*, 347; c) C.-Y. Chen, J.-H. Chang, K.-M. Chiang, H.-L. Lin, S.-Y. Hsiao, H.-W. Lin, *Adv. Funct. Mater.* **2015**, https://doi.org/10.1002/adfm.201503448n/a.

[12] A. Fakharuddin, R. Jose, T. M. Brown, F. Fabregat-Santiago, J. Bisquert, *Energy Environ. Sci.* **2014**, *7*, 3952.

[13] a) V. D'Innocenzo, G. Grancini, M. J. P. Alcocer, A. R. S. Kandada, S. D. Stranks, M. M. Lee, G. Lanzani, H. J. Snaith, A. Petrozza, *Nat. Commun.* **2014**, 5; b) N. Marinova, S. Valero, J. L. Delgado, *J. Colloid Interface Sci.* **2017**, *488*, 373.

[14] a) W. S. Yang, J. H. Noh, N. J. Jeon, Y. C. Kim, S. Ryu, J. Seo, S. I. Seok, *Science* **2015**, *348*, 1234; b) M. Saliba, S. Orlandi, T. Matsui, S. Aghazada, M. Cavazzini, J.-P. Correa-Baena, P. Gao, R. Scopelliti, E. Mosconi, K.-H. Dahmen, F. De Angelis, A. Abate, A. Hagfeldt, G. Pozzi, M. Graetzel, M. K. Nazeeruddin, *Nat. Energy* **2016**, https://doi.org/10.1038/nenergy.2015.17, http://www.nature.com/articles/nenergy201517#supplementary-information15017; c) D. Bi, W. Tress, M. I. Dar, P. Gao, J. Luo, C. Renevier, K. Schenk, A. Abate, F. Giordano, J.-P. Correa Baena, J.-D. Decoppet, S. M. Zakeeruddin, M. K. Nazeeruddin, M. Grätzel, A. Hagfeldt, *Science Adv.* **2016**, 2.

[15] K. Wojciechowski, M. Saliba, T. Leijtens, A. Abate, H. J. Snaith, *Energy Environ. Sci.* **2014**, *7*, 1142.

[16] J. M. Ball, M. M. Lee, A. Hey, H. J. Snaith, *Energy Environ. Sci.* **2013**, *6*, 1739.

[17] C. Momblona, L. Gil-Escrig, E. Bandiello, E. M. Hutter, M. Sessolo, K. Lederer, J. Blochwitz-Nimoth, H. J. Bolink, *Energy Environ. Sci.* **2016**, *9*, 3456.
[18] D. Liu, J. Yang, T. L. Kelly, *J. Am. Chem. Soc.* **2014**, *136*, 17116.
[19] E. Edri, S. Kirmayer, A. Henning, S. Mukhopadhyay, K. Gartsman, Y. Rosenwaks, G. Hodes, D. Cahen, *Nano Lett.* **2014**, *14*, 1000.
[20] a) J. H. Heo, H. J. Han, D. Kim, T. K. Ahn, S. H. Im, *Energy Environ. Sci.* **2015**, *8*, 1602; b) S. Ye, W. Sun, Y. Li, W. Yan, H. Peng, Z. Bian, Z. Liu, C. Huang, *Nano Lett.* **2015**, *15*, 3723; c) C. Tao, S. Neutzner, L. Colella, S. Marras, A. R. Srimath Kandada, M. Gandini, M. D. Bastiani, G. Pace, L. Manna, M. Caironi, C. Bertarelli, A. Petrozza, *Energy Environ. Sci.* **2015**, *8*, 2365.
[21] a) T. Salim, S. Sun, Y. Abe, A. Krishna, A. C. Grimsdale, Y. M. Lam, *J. Mater. Chem. A* **2015**, *3*, 8943; b) Y. Wu, W. Chen, Y. Yue, J. Liu, E. Bi, X. Yang, A. Islam, L. Han, *ACS Appl. Mater. Interfaces* **2015**, *7*, 20707; c) A. Fakharuddin, F. Di Giacomo, I. Ahmed, Q. Wali, T. M. Brown, R. Jose, *J. Power Sources* **2015**, *283*, 61.
[22] a) A. Fakharuddin, F. Di Giacomo, A. L. Palma, F. Matteocci, I. Ahmed, S. Razza, A. D'Epifanio, S. Licoccia, J. Ismail, A. Di Carlo, T. M. Brown, R. Jose, *ACS Nano* **2015**, *9*, 8420; b) T. Leijtens, G. E. Eperon, S. Pathak, A. Abate, M. M. Lee, H. J. Snaith, *Nat. Commun.* **2013**, *4*, 2885; c) J. Xu, A. Buin, A. H. Ip, W. Li, O. Voznyy, R. Comin, M. Yuan, S. Jeon, Z. Ning, J. J. McDowell, P. Kanjanaboos, J. P. Sun, X. Lan, L. N. Quan, D. H. Kim, I. G. Hill, P. Maksymovych, E. H. Sargent, *Nat. Commun.* **2015**, 6; d) T. Leijtens, G. E. Eperon, N. K. Noel, S. N. Habisreutinger, A. Petrozza, H. J. Snaith, *Adv. Energy Mater.* **2015**, *5*, 1500963; e) Y. Rong, L. Liu, A. Mei, X. Li, H. Han, *Adv. Energy Mater.* **2015**, *5*, 1501066; f) Z. H. Bakr, Q. Wali, A. Fakharuddin, L. Schmidt-Mende, T. M. Brown, R. Jose, *Nano Energy* **2017**, http://dx.doi.org/10.1016/j.nanoen.2017.02.025.
[23] S. Olthof, K. Meerholz, *Sci. Rep.* **2017**, *7*, 40267.
[24] a) Q. Wali, A. Fakharuddin, I. Ahmed, M. H. Ab Rahim, J. Ismail, R. Jose, *J. Mater. Chem. A* **2014**, *2*, 17427; b) Q. Wali, A. Fakharuddin, R. Jose, *J. Power Sources* **2015**, *293*, 1039.
[25] a) W. Ke, G. Fang, Q. Liu, L. Xiong, P. Qin, H. Tao, J. Wang, H. Lei, B. Li, J. Wan, G. Yang, Y. Yan, *J. Am. Chem. Soc.* **2015**, *137*, 6730; b) E. H. Anaraki, A. Kermanpur, L. Steier, K. Domanski, T. Matsui, W. Tress, M. Saliba, A. Abate, M. Gratzel, A. Hagfeldt, J.-P. Correa-Baena, *Energy Environ. Sci.* **2016**, *9*, 3128.
[26] J. Bisquert, D. Cahen, G. Hodes, S. Rühle, A. Zaban, *J. Phys. Chem. B* **2004**, *108*, 8106.
[27] C. Wehrenfennig, G. E. Eperon, M. B. Johnston, H. J. Snaith, L. M. Herz, *Adv. Mater.* **2014**, *26*, 1584.
[28] E. Guillén, F. J. Ramos, J. A. Anta, S. Ahmad, *J. Phys. Chem. C* **2014**, *118*, 22913.
[29] a) D. Bi, C. Yi, J. Luo, J.-D. Décoppet, F. Zhang, S. M. Zakeeruddin, X. Li, A. Hagfeldt, M. Grätzel, *Nat. Energy* **2016**, *1*, 16142; b) T. Zhao, C.-C. Chueh, Q. Chen, A. Rajagopal, A. K. Y. Jen, *ACS Energ. Lett.* **2016**, *1*, 757.
[30] a) C. S. Ponseca, T. J. Savenije, M. Abdellah, K. Zheng, A. Yartsev, T. Pascher, T. Harlang, P. Chabera, T. Pullerits, A. Stepanov, J. P. Wolf, V. Sundström, *J. Am. Chem. Soc.* **2014**, *136*, 5189; b) K. Wang, C. Liu, P. Du, J. Zheng, X. Gong, *Energy Environ. Sc.* **2015**, *8*, 1245.
[31] a) J. Shi, X. Xu, D. Li, Q. Meng, *Small* **2015**, *11*, 2472; b) Y. Liu, M. Bag, L. A. Renna, Z. A. Page, P. Kim, T. Emrick, D. Venkataraman, T. P. Russell, *Adv. Energ. Mater.* **2016**, *6*, 1600664.
[32] a) W. Li, J. Li, L. Wang, G. Niu, R. Gao, Y. Qiu, *J. Mater. Chem. A* **2013**, *1*, 11735; b) F. Wang, Y. Chen, G. Han, Q. Zhang, Q. Ma, *Curr. Appl. Phys* **2016**, *16*, 1353; c) K. Wojciechowski, S. D. Stranks, A. Abate, G. Sadoughi, A. Sadhanala, N. Kopidakis, G. Rumbles, C. Z. Li, R. H. Friend, A. K. Y. Jen, H. J. Snaith, *ACS Nano* **2014**, *8*, 12701; d) Y. Bai, H. Chen, S. Xiao, Q. Xue, T. Zhang, Z. Zhu, Q. Li, C. Hu, Y. Yang, Z. Hu, F. Huang, K. S. Wong, H. L. Yip, S. Yang, *Adv. Funct. Mater.* **2016**, *26*, 2950.
[33] L. L. Jiang, S. Cong, Y. H. Lou, Q. H. Yi, J. T. Zhu, H. Ma, G. F. Zou, *J. Mater. Chem. A* **2015**, *4*, 217.
[34] a) A. Dualeh, T. Moehl, N. Tétreault, J. Teuscher, P. Gao, M. K. Nazeeruddin, M. Grätzel, *ACS Nano* **2014**, *8*, 362; b) A. Pockett, G. E. Eperon, T. Peltola, H. J. Snaith, A. Walker, L. M. Peter, P. J. Cameron, *J. Phys. Chem. C* **2015**, *119*, 3456; c) A. R. Pascoe, N. W. Duffy, A. D. Scully, F. Huang, Y. B. Cheng, *J. Phys. Chem. C* **2015**, *119*, 4444; d) H. S. Kim, I. Mora-Sero, V. Gonzalez-Pedro, F. Fabregat-Santiago, E. J. Juarez-Perez, N. G. Park, J. Bisquert, *Nat. Commun.* **2013**, *4*, 2242.
[35] E. J. Juarez-Perez, M. Wuβler, F. Fabregat-Santiago, K. Lakus-Wollny, E. Mankel, T. Mayer, W. Jaegermann, I. Mora-Sero, M. Wußler, *J. Phys. Chem. Lett.* **2014**, *5*, 680.
[36] A. Guerrero, G. Garcia-Belmonte, I. Mora-Sero, J. Bisquert, Y. S. Kang, T. J. Jacobsson, J.-P. Correa-Baena, A. Hagfeldt, *J. Phys. Chem. C* **2016**, *120*, 8023.
[37] F. Fabregat-Santiago, G. Garcia-Belmonte, I. Mora-Seró, J. Bisquert, *PCCP* **2011**, *13*, 9083.
[38] M. Anaya, W. Zhang, B. C. Hames, Y. Li, F. Fabregat-Santiago, M. E. Calvo, H. J. Snaith, H. Miguez, I. Mora-Sero, *J. Mater. Chem. C* **2017**, *5*, 634.
[39] J. Bisquert, G. Garcia-Belmonte, Á. Pitarch, H. J. Bolink, *Chem. Phys. Lett.* **2006**, *422*, 184.
[40] a) I. Zarazua, J. Bisquert, G. Garcia-Belmonte, *J. Phys. Chem. Lett.* **2016**, *7*, 525; b) I. Zarazua, G. Han, P. P. Boix, S. Mhaisalkar, F. Fabregat-Santiago, I. Mora-Seró, J. Bisquert, G. Garcia-Belmonte, *J. Phys. Chem. Lett.* **2016**, *7*, 5105.
[41] L. Contreras, J. Idigoras, A. Todinova, M. Salado, S. Kazim, S. Ahmad, J. A. Anta, *PCCP* **2016**, *18*, 31033.
[42] V. W. Bergmann, Y. Guo, H. Tanaka, I. M. Hermes, D. Li, A. Klasen, S. A. Bretschneider, E. Nakamura, R. Berger, S. A. L. Weber, *ACS Appl. Mater. Interfaces* **2016**, *8*, 19402.
[43] Y. F. Chen, Y. T. Tsai, D. M. Bassani, R. Clerc, D. Forgacs, H. J. Bolink, M. Wussler, W. Jaegermann, G. Wantz, L. Hirsch, *J. Mater. Chem. A* **2016**, *4*, 17529.
[44] E. J. Juarez-Perez, R. S. Sanchez, L. Badia, G. Garcia-Belmonte, Y. S. Kang, I. Mora-Sero, J. Bisquert, *J. Phys. Chem. Lett.* **2014**, *5*, 2390.
[45] R. Gottesman, P. Lopez-Varo, L. Gouda, J. A. Jimenez-Tejada, J. Hu, S. Tirosh, A. Zaban, J. Bisquert, *Chem*, **2014**, *1*, 776.
[46] D. W. deQuilettes, W. Zhang, V. M. Burlakov, D. J. Graham, T. Leijtens, A. Osherov, V. Bulović, H. J. Snaith, D. S. Ginger, S. I. D. Stranks, *Nat. Comm.* **2016**, *7*, 11683.
[47] A. Marchioro, J. Teuscher, D. Friedrich, M. Kunst, R. van de Krol, T. Moehl, M. Gratzel, J.-E. Moser, *Nat. Photonics* **2014**, *8*, 250.
[48] W. Tress, N. Marinova, O. Inganäs, M. K. Nazeeruddin, S. M. Zakeeruddin, M. Graetzel, *Adv. Energy Mater.* **2015**, *5*, 1400812.
[49] D. W. DeQuilettes, S. M. Vorpahl, S. D. Stranks, H. Nagaoka, G. E. Eperon, M. E. Ziffer, H. J. Snaith, D. S. Ginger, *Science* **2015**, *348*, 683.
[50] E. Climent-Pascual, B. C. Hames, J. S. Moreno-Ramirez, A. L. Alvarez, E. J. Juarez-Perez, E. Mas-Marza, I. Mora-Sero, A. de Andres, C. Coya, *J. Mater. Chem. A* **2016**, *4*, 18153.
[51] M. A. Green, K. Emery, Y. Hishikawa, W. Warta, E. D. Dunlop, *PROG Photovoltaics Res. App.* **2016**, *24*, 3.
[52] J. H. Heo, D. H. Song, S. H. Im, *Adv. Mater.* **2014**, *26*, 8179.
[53] a) Y. Shao, Y. Yuan, J. Huang, *Nat. Energy* **2016**, *1*, 15001; b) W. Tress, in *Organic-Inorganic Halide Perovskite Photovoltaics: From Fundamentals to Device Architectures*, https://doi.org/10.1007/978-3-319-35114-8_3 (Eds: N.-G. Park, M. Grätzel, T. Miyasaka), Springer International Publishing, Cham **2016**, p. 53.

[54] B. Cai, Y. Xing, Z. Yang, W.-H. H. Zhang, J. Qiu, *Energy Environ. Sci.* **2013**, *6*, 1480.
[55] Y. Zou, D. Gendron, R. Badrou-Aïch, A. Najari, Y. Tao, M. Leclerc, *Macromolecules* **2009**, *42*, 2891.
[56] E. Edri, S. Kirmayer, M. Kulbak, G. Hodes, D. Cahen, *J. Phys. Chem. Lett.* **2014**, *5*, 429.
[57] S. Chen, Y. Hou, H. Chen, M. Richter, F. Guo, S. Kahmann, X. Tang, T. Stubhan, H. Zhang, N. Li, N. Gasparini, C. O. R. Quiroz, L. S. Khanzada, G. J. Matt, A. Osvet, C. J. Brabec, *Adv. Energy Mater.* **2016**, *6*, 1600132.
[58] Y. Hou, W. Chen, D. Baran, T. Stubhan, N. A. Luechinger, B. Hartmeier, M. Richter, J. Min, S. Chen, C. O. R. Quiroz, N. Li, H. Zhang, T. Heumueller, G. J. Matt, A. Osvet, K. Forberich, Z.-G. Zhang, Y. Li, B. Winter, P. Schweizer, E. Spiecker, C. J. Brabec, *Adv. Mater.* **2016**, *28*, 5112.
[59] W. Tress, *Adv. Energy Mater.* **2017**, *7*, 1602358.
[60] P. Tiwana, P. Docampo, M. B. Johnston, H. J. Snaith, L. M. Herz, *ACS Nano* **2011**, *5*, 5158.
[61] W. H. Nguyen, C. D. Bailie, E. L. Unger, M. D. McGehee, *J. Am. Chem. Soc.* **2014**, *136*, 10996.
[62] E. Edri, S. Kirmayer, D. Cahen, G. Hodes, *J. Phys. Chem. Lett.* **2013**, *4*, 897.
[63] S. Ryu, J. H. Noh, N. J. Jeon, Y. Chan Kim, W. S. Yang, J. Seo, S. I. Seok, *Energy Environ. Sci.* **2014**, *7*, 2614.
[64] M. Kröger, S. Hamwi, J. Meyer, T. Riedl, W. Kowalsky, A. Kahn, *Org. Electronics* **2009**, *10*, 932.
[65] C. G. Wu, C. H. Chiang, S. H. Chang, *Nanoscale* **2016**, *8*, 4077.
[66] a) Z. Xiao, Y. Yuan, Y. Shao, Q. Wang, Q. Dong, C. Bi, P. Sharma, A. Gruverman, J. Huang, *Nat. Mater.* **2015**, *14*, 193; b) H. J. Snaith, A. Abate, J. M. Ball, G. E. Eperon, T. Leijtens, N. K. Noel, S. D. Stranks, J. T. W. Wang, K. Wojciechowski, W. Zhang, *J. Phys. Chem. Lett.* **2014**, *5*, 1511; c) R. S. Sanchez, V. Gonzalez-Pedro, J. W. Lee, N. G. Park, Y. S. Kang, I. Mora-Sero, J. Bisquert, *J. Phys. Chem. Lett.* **2014**, *5*, 2357; d) E. L. Unger, E. T. Hoke, C. D. Bailie, W. H. Nguyen, A. R. Bowring, T. Heumüller, M. G. Christoforo, M. D. McGehee, *Energy Environ. Sci.* **2014**, *7*, 3690.
[67] a) J. M. Frost, K. T. Butler, A. Walsh, *APL Mater.* **2014**, 2; b) J. Wei, Y. Zhao, H. Li, G. Li, J. Pan, D. Xu, Q. Zhao, D. Yu, *J. Phys. Chem. Lett.* **2014**, *5*, 3937; c) H. W. Chen, N. Sakai, M. Ikegami, T. Miyasaka, *J. Phys. Chem. Lett.* **2015**, *6*, 164.
[68] Y. Shao, Z. Xiao, C. Bi, Y. Yuan, J. Huang, *Nat. Commun.* **2014**, *5*, 5784.
[69] Y. Yang, J. Xiao, H. Wei, L. Zhu, D. Li, Y. Luo, H. Wu, Q. Meng, *RSC Adv.* **2014**, *4*, 52825.
[70] a) O. Almora, I. Zarazua, E. Mas-Marza, I. Mora-Sero, J. Bisquert, G. Garcia-Belmonte, *J. Phys. Chem. Lett.* **2015**, *6*, 1645; b) B. Chen, M. Yang, X. Zheng, C. Wu, W. Li, Y. Yan, J. Bisquert, G. Garcia-Belmonte, K. Zhu, S. Priya, *J. Phys. Chem. Lett.* **2015**, *6*, 4693.
[71] Y. Deng, Z. Xiao, J. Huang, *Adv. Energy Mater.* **2015**, *5*, 1500721.
[72] a) Y. Zou, R. J. Holmes, *Adv. Energy Mater.* **2016**, *6*, 1501994; b) C. Zhang, D. Sun, X. Liu, C.-X. Sheng, Z. V. Vardeny, *J. Phys. Chem. Lett.* **2017**, *8*, 1429.
[73] a) T. Y. Yang, G. Gregori, N. Pellet, M. Grätzel, J. Maier, *Angew. Chem.– Int. Ed.* **2015**, *54*, 7905; b) R. Gottesman, E. Haltzi, L. Gouda, S. Tirosh, Y. Bouhadana, A. Zaban, E. Mosconi, F. De Angelis, *J. Phys. Chem. Lett.* **2014**, *5*, 2662.
[74] J. A. Christians, J. S. Manser, P. V. Kamat, *J. Phys. Chem. Lett.* **2015**, *6*, 852.
[75] W. Tress, N. Marinova, T. Moehl, S. M. Zakeeruddin, M. K. Nazeeruddin, M. Grätzel, *Energy Environ. Sci.* **2015**, *8*, 995.
[76] H. S. Kim, N. G. Park, *J. Phys. Chem. Lett.* **2014**, *5*, 2927.
[77] a) J. Xiong, B. Yang, R. Wu, C. Cao, Y. Huang, C. Liu, Z. Hu, H. Huang, Y. Gao, J. Yang, *Org. Electron.* **2015**, *24*, 106; b) A. H. Ip, L. H. Quan, M. M. Adachi, J. J. McDowell, J. Xu, D. H. Kim, E. H. Sargent, *Appl. Phys. Lett.* **2015**, *106*, 143902.
[78] J. H. Heo, M. S. You, M. Hyuk Chang, W. J. Yin, T. K. Ahn, S.-J. Lee, S.-J. Sung, D. Hwan Kim, S. Hyuk Im, *Nano Energy* **2015**, *15*, 530.
[79] H. Nagaoka, F. Ma, D. W. Dequilettes, S. M. Vorpahl, M. S. Glaz, A. E. Colbert, M. E. Ziffer, D. S. Ginger, *J. Phys. Chem. Lett.* **2015**, *6*, 669.
[80] J. Seo, S. Park, Y. Chan Kim, N. J. Jeon, J. H. Noh, S. C. Yoon, S. I. Seok, *Energy Environ. Sci.* **2014**, *7*, 2642.
[81] D. Bryant, S. Wheeler, B. C. O'Regan, T. Watson, P. R. F. Barnes, D. Worsley, J. Durrant, *J. Phys. Chem. Lett.* **2015**, *6*, 3190.
[82] I. Jeong, H. Jin Kim, B. S. Lee, H. Jung Son, J. Young Kim, D. K. Lee, D. E. Kim, J. Lee, M. J. Ko, *Nano Energy* **2015**, *17*, 131.
[83] O. Almora, C. Aranda, I. Zarazua, A. Guerrero, G. Garcia-Belmonte, *ACS Energy Lett.* **2016**, https://doi.org/10.1021/acsenergylett.6b00116209.
[84] G. Garcia-Belmonte, J. Bisquert, *ACS Energy Lett.* **2016**, *1*, 683.
[85] J. Carrillo, A. Guerrero, S. Rahimnejad, O. Almora, I. Zarazua, E. Mas-Marza, J. Bisquert, G. Garcia-Belmonte, *Adv. Energy Mater.* **2016**, *6*, 1502246.
[86] W. Tress, J. P. Correa Baena, M. Saliba, A. Abate, M. Graetzel, *Adv. Energy Mater.* **2016**, *6*, 1600396.
[87] a) M. Valles-Pelarda, B. C. Hames, I. García-Benito, O. Almora, A. Molina-Ontoria, R. S. Sánchez, G. Garcia-Belmonte, N. Martín, I. Mora-Sero, *J. Phys. Chem. Lett.* **2016**, *7*, 4622; b) J. B. Patel, J. Wong-Leung, S. Van Reenen, N. Sakai, J. T. W. Wang, E. S. Parrott, M. Liu, H. J. Snaith, L. M. Herz, M. B. Johnston, *Adv. Elect. Mater.* **2017**, *3*, 1600470.
[88] J. You, L. Meng, T. B. Song, T. F. Guo, W. H. Chang, Z. Hong, H. Chen, H. Zhou, Q. Chen, Y. Liu, N. De Marco, Y. Yang, *Nat. Nanotech.* **2016**, *11*, 75.
[89] W. Li, W. Zhang, S. Van Reenen, R. J. Sutton, J. Fan, A. A. Haghighirad, M. B. Johnston, L. Wang, H. J. Snaith, *Energy Environ. Sci.* **2016**, *9*, 490.
[90] a) F. Hao, C. C. Stoumpos, D. H. Cao, R. P. H. Chang, M. G. Kanatzidis, *Nat. Photonics* **2014**, *8*, 489; b) M. H. Kumar, S. Dharani, W. L. Leong, P. P. Boix, R. R. Prabhakar, T. Baikie, C. Shi, H. Ding, R. Ramesh, M. Asta, M. Graetzel, S. G. Mhaisalkar, N. Mathews, *Adv. Mater.* **2014**, *26*, 7122; c) N. K. Noel, S. D. Stranks, A. Abate, C. Wehrenfennig, S. Guarnera, A.-A. Haghighirad, A. Sadhanala, G. E. Eperon, S. K. Pathak, M. B. Johnston, A. Petrozza, L. M. Herz, H. J. Snaith, *Energy Environ. Sci.* **2014**, *7*, 3061.
[91] T. Dittrich, E. A. Lebedev, J. Weidmann, *Phys. Status Solidi A* **1998**, *165*, R5.
[92] T. M. Brown, F. De Rossi, F. Di Giacomo, G. Mincuzzi, V. Zardetto, A. Reale, A. Di Carlo, *J. Mater. Chem. A* **2014**, *2*, 10788.
[93] Q. Wali, A. Fakharuddin, A. Yasin, M. H. Ab Rahim, J. Ismail, R. Jose, *J. Alloys Compd* **2015**, *646*, 32.
[94] a) L. Schmidt-Mende, J. L. MacManus-Driscoll, *Mater. Today* **2007**, *10*, 40; b) K. Mahmood, B. S. Swain, A. Amassian, *Adv. Energy Mater.* **2015**, *5*, 1500568; c) Z. Liang, Q. Zhang, L. Jiang, G. Cao, *Energy Environ. Sci.* **2015**, *8*, 3442.
[95] a) K. Mahmood, B. S. Swain, A. Amassian, *Nanoscale* **2014**, *6*, 14674; b) S. Zhang, X. Li, X. Gao, L. Lei, X. Ding, Q. Gao, *Chem. Lett.* **2015**, *44*, 1022.
[96] Y. Cheng, Q. D. Yang, J. Xiao, Q. Xue, H. W. Li, Z. Guan, H. L. Yip, S. W. Tsang, *ACS Appl. Mater. Interfaces* **2015**, *7*, 19986.
[97] A. Nicolaev, T. L. Mitran, S. Iftimie, G. A. Nemnes, *Sol. Energy Mater. Sol. Cells* **2015**, https://doi.org/10.1016/j.solmat.2015.10.023.
[98] J. Xiao, Y. Yang, X. Xu, J. Shi, L. Zhu, S. Lv, H. Wu, Y. Luo, D. Li, Q. Meng, *J. Mater. Chem. A* **2015**, *3*, 5289.

[99] S. Bai, Z. Wu, X. Wu, Y. Jin, N. Zhao, Z. Chen, Q. Mei, X. Wang, Z. Ye, T. Song, R. Liu, S. T. Lee, B. Sun, *Nano Res.* **2014**, *7*, 1749.
[100] a) D. Y. Son, J. H. Im, H. S. Kim, N. G. Park, *J. Phys. Chem. C* **2014**, *118*, 16567; b) J. Zhang, P. Barboux, T. Pauporté, *Adv. Energy Mater.* **2014**, *4*, 1400932.
[101] D. Y. Son, K. H. Bae, H. S. Kim, N. G. Park, *J. Phys. Chem. C* **2015**, *119*, 10321.
[102] O. Malinkiewicz, A. Yella, Y. H. Lee, G. M. Espallargas, M. Graetzel, M. K. Nazeeruddin, H. J. Bolink, *Nat. Photonics* **2013**, *8*, 128.
[103] Z. G. Zhu, Y. Bai, X. Liu, C.-C. Chueh, S. Yang, A. K. Y. Jen, *Adv. Mater.* **2016**, *28*, 6478.
[104] J. Liu, C. Gao, L. Luo, Q. Ye, X. He, L. Ouyang, X. Guo, D. Zhuang, C. Liao, J. Mei, W. Lau, *J. Mater. Chem. A* **2015**, *3*, 11750.
[105] A. Kogo, Y. Numata, M. Ikegami, T. Miyasaka, *Chem. Lett.* **2015**, *44*, 829.
[106] a) A. Bera, K. Wu, A. Sheikh, E. Alarousu, O. F. Mohammed, T. Wu, *J. Phys. Chem. C* **2014**, *118*, 28494; b) W. Li, J. Fan, J. Li, Y. Mai, L. Wang, *J. Am. Chem. Soc.* **2015**, *137*, 10399.
[107] L. Zhu, Z. Shao, J. Ye, X. Zhang, X. Pan, S. Dai, *Chem. Comm.* **2016**, *52*, 970.
[108] T. J. Coutts, D. L. Young, X. Li, W. P. Mulligan, X. Wu, *J. Vac. Sci. Technol., A* **2000**, *18*, 2646.
[109] S. S. Shin, W. S. Yang, J. H. Noh, J. H. Suk, N. J. Jeon, J. H. Park, J. S. Kim, W. M. Seong, S. I. Seok, *Nat. Commun.* **2015**, 6, https://doi.org/10.1038/ncomms8410.
[110] B. Roose, S. Pathak, U. Steiner, *Chem. Soc. Rev.* **2015**, *44*, 8326.
[111] a) R. Jose, V. Thavasi, S. Ramakrishna, *J. Am. Ceram. Soc.* **2009**, *92*, 289; b) Q. Zhang, G. Cao, *Nano Today* **2011**, *6*, 91.
[112] a) K. Manseki, T. Ikeya, A. Tamura, T. Ban, T. Sugiura, T. Yoshida, *RSC Adv.* **2014**, *4*, 9652; b) M. Yang, R. Guo, K. Kadel, Y. Liu, K. O'Shea, R. Bone, X. Wang, J. He, W. Li, *J. Mater. Chem. A* **2014**, *2*, 19616; c) X. Zhang, Z. Bao, X. Tao, H. Sun, W. Chen, X. Zhou, *RSC Adv.* **2014**, *4*, 64001; d) D. H. Kim, G. S. Han, W. M. Seong, J. W. Lee, B. J. Kim, N. G. Park, K. S. Hong, S. Lee, H. S. Jung, *ChemSusChem* **2015**, *8*, 2392; e) R. Long, O. V. Prezhdo, *ACS Nano* **2015**, *9*, 11143; f) X. Yin, Y. Guo, Z. Xue, P. Xu, M. He, B. Liu, *Nano Res.* **2015**, https://doi.org/10.1007/s12274-015-0711-4.
[113] a) G. Westin, M. Leideborg, K. Lashgari, V. A. Coleman, K. Jansson, A. Pohl, *Int. J. Nanotechnol.* **2009**, *6*, 828; b) K. Mahmood, B. S. Swain, H. S. Jung, *Nanoscale* **2014**, https://doi.org/10.1039/c4nr02065k9127; c) J. Wang, M. Qin, H. Tao, W. Ke, Z. Chen, J. Wan, P. Qin, L. Xiong, H. Lei, H. Yu, G. Fang, *Appl. Phys. Lett.* **2015**, *106*, 121104; d) J. Dong, Y. Zhao, J. Shi, H. Wei, J. Xiao, X. Xu, J. Luo, J. Xu, D. Li, Y. Luo, Q. Meng, *Chem. Commun.* **2014**, *50*, 13381.
[114] P. Qin, A. L. Domanski, A. K. Chandiran, R. Berger, H. J. Butt, M. I. Dar, T. Moehl, N. Tetreault, P. Gao, S. Ahmad, M. K. Nazeeruddin, M. Grätzel, *Nanoscale* **2014**, *6*, 1508.
[115] a) A. K. Chandiran, F. Sauvage, M. Casas-Cabanas, P. Comte, S. M. Zakeeruddin, M. Graetzel, *J. Phys. Chem. C* **2010**, *114*, 15849; b) A. K. Chandiran, F. Sauvage, L. Etgar, M. Graetzel, *J. Phys. Chem. C* **2011**, *115*, 9232; c) Z. S. Wang, M. Yanagida, K. Sayama, H. Sugihara, *Chem. Mater.* **2006**, *18*, 2912.
[116] a) Y. Diamant, S. Chappel, S. G. Chen, O. Melamed, A. Zaban, *Coord. Chem. Rev.* **2004**, *248*, 1271; b) F. Fabregat-Santiago, J. García-Cañadas, E. Palomares, J. N. Clifford, S. A. Haque, J. R. Durrant, G. Garcia-Belmonte, J. Bisquert, *J. Appl. Phys.* **2004**, *96*, 6903; c) L. Schmidt-Mende, S. M. Zakeeruddin, M. Grätzel, *Appl. Phys. Lett.* **2005**, *86*, 013504.
[117] G. S. Han, H. S. Chung, B. J. Kim, D. H. Kim, J. W. Lee, B. S. Swain, K. Mahmood, J. S. Yoo, N. G. Park, J. H. Lee, H. S. Jung, *J. Mater. Chem. A* **2015**, *3*, 9160.
[118] K. Mahmood, B. S. Swain, A. Amassian, *Nanoscale* **2015**, *7*, 12812.
[119] K. Mahmood, B. S. Swain, A. R. Kirmani, A. Amassian, *J. Mater. Chem. A* **2015**, *3*, 9051.
[120] V. Gonzalez-Pedro, E. J. Juarez-Perez, W. S. Arsyad, E. M. Barea, F. Fabregat-Santiago, I. Mora-Sero, J. Bisquert, *Nano Lett.* **2014**, *14*, 888.
[121] S. D. Stranks, G. E. Eperon, G. Grancini, C. Menelaou, M. J. P. Alcocer, T. Leijtens, L. M. Herz, A. Petrozza, H. J. Snaith, *Science* **2013**, *342*, 341.
[122] W. Tian, C. Zhao, J. Leng, R. Cui, S. Jin, *J. Am. Chem. Soc.* **2015**, *137*, 12458.
[123] a) J. D. Park, B. H. Son, J. K. Park, S. Y. Kim, J.-Y. Park, S. Lee, Y. H. Ahn, *AIP Adv.* **2014**, *4*, 067106; b) W. H. Leng, P. R. F. Barnes, M. Juozapavicius, B. C. O'Regan, J. R. Durrant, *J. Phys. Chem. Lett.* **2010**, *1*, 967.
[124] E. Hendry, M. Koeberg, B. O'Regan, M. Bonn, *Nano Lett.* **2006**, *6*, 755.
[125] F. Zhang, X. Yang, M. Cheng, J. Li, W. Wang, H. Wang, L. Sun, *J. Mater. Chem. A* **2015**, *3*, 24272.
[126] C. Tanase, E. J. Meijer, P. W. M. Blom, D. M. de Leeuw, *Phys. Rev. Lett.* **2003**, *91*, 216601.
[127] H. S. Kim, J. W. Lee, N. Yantara, P. P. Boix, S. A. Kulkarni, S. Mhaisalkar, M. Grätzel, N. G. Park, *Nano Lett.* **2013**, *13*, 2412.
[128] S. S. Mali, C. S. Shim, H. K. Park, J. Heo, P. S. Patil, C. K. Hong, *Chem. Mater.* **2015**, *27*, 1541.
[129] L. Liang, Z. Huang, L. Cai, W. Chen, B. Wang, K. Chen, H. Bai, Q. Tian, B. Fan, *ACS Appl. Mater. Interfaces* **2014**, *6*, 20585.
[130] B. Cai, D. Zhong, Z. Yang, B. Huang, S. Miao, W. H. Zhang, J. Qiu, C. Li, *J. Mater. Chem. C* **2015**, *3*, 729.
[131] D. Zhong, B. Cai, X. Wang, Z. Yang, Y. Xing, S. Miao, W. H. Zhang, C. Li, *Nano Energy* **2015**, *11*, 409.
[132] G. Peng, J. Wu, S. Wu, X. Xu, J. E. Ellis, G. Xu, A. Star, D. Gao, *J. Mater. Chem. A* **2016**, *4*, 1520.
[133] S. H. Lee, X.-G. Zhang, B. Smith, S. S. A. Seo, Z. W. Bell, J. Xu, *Appl. Phys. Lett.* **2010**, *96*, 193116.
[134] W. Q. Wu, F. Huang, D. Chen, Y. B. Cheng, R. A. Caruso, *Adv. Func. Mater.* **2015**, *25*, 3264.
[135] J. Qiu, Y. Qiu, K. Yan, M. Zhong, C. Mu, H. Yan, S. Yang, *Nanoscale* **2013**, *5*, 3245.
[136] H. Tao, W. Ke, J. Wang, Q. Liu, J. Wan, G. Yang, G. Fang, *J. Power Sources* **2015**, *290*, 144.
[137] a) X. Gao, J. Li, J. Baker, Y. Hou, D. Guan, J. Chen, C. Yuan, *Chem. Commun.* **2014**, *50*, 6368; b) R. Salazar, M. Altomare, K. Lee, J. Tripathy, R. Kirchgeorg, N. T. Nguyen, M. Mokhtar, A. Alshehri, S. A. Al-Thabaiti, P. Schmuki, *ChemElectroChem* **2015**, *2*, 824; c) J. Zhang, T. Pauporté, *ChemPhysChem* **2015**, *16*, 2836; d) P. Qin, M. Paulose, M. I. Dar, T. Moehl, N. Arora, P. Gao, O. K. Varghese, M. Grätzel, M. K. Nazeeruddin, *Small* **2015**, *11*, 5533.
[138] C. Liu, Z. Qiu, W. Meng, J. Chen, J. Qi, C. Dong, M. Wang, *Nano Energy* **2015**, *12*, 59.
[139] G. S. Han, H. S. Chung, D. H. Kim, B. J. Kim, J. W. Lee, N. G. Park, I. S. Cho, J. K. Lee, S. Lee, H. S. Jung, *Nanoscale* **2015**, *7*, 15284.
[140] a) S. H. Lin, Y. H. Su, H. W. Cho, P. Y. Kung, W. P. Liao, J. J. Wu, *J. Mater. Chem. A* **2016**, *4*, 1119; b) W. Huang, F. Huang, E. Gann, Y. B. Cheng, C. R. McNeill, *Adv. Funct. Mater.* **2015**, *25*, 5529.
[141] Y. Yu, J. Li, D. Geng, J. Wang, L. Zhang, T. L. Andrew, M. S. Arnold, X. Wang, *ACS Nano* **2015**, *9*, 564.
[142] X. Chen, S. Yang, Y. C. Zheng, Y. Chen, Y. Hou, X. H. Yang, H. G. Yang, *Adv. Sci.* **2015**, *2*, 1500105.
[143] X. Xu, H. Zhang, J. Shi, J. Dong, Y. Luo, D. Li, Q. Meng, *J. Mater. Chem. A* **2015**, *3*, 19288.
[144] W. Qiu, M. Buffière, G. Brammertz, U. W. Paetzold, L. Froyen, P. Heremans, D. Cheyns, *Org. Electronics: Physics, Materials, Applications* **2015**, *26*, 30.
[145] a) L. Etgar, *MRS Bulletin* **2015**, *40*, 674; b) Y. Liu, S. Ji, S. Li, W. He, K. Wang, H. Hu, C. Ye, *J. Mater. Chem. A* **2015**, *3*, 14902.
[146] S. K. Pathak, A. Abate, P. Ruckdeschel, B. Roose, K. C. Gödel, Y. Vaynzof, A. Santhala, S. I. Watanabe, D. J. Hollman, N. Noel,

A. Sepe, U. Wiesner, R. Friend, H. J. Snaith, U. Steiner, *Adv. Funct. Mater.* **2014**, *24*, 6046.
[147] H. J. Snaith, N. C. Greenham, R. H. Friend, *Adv. Mater.* **2004**, *16*, 1640.
[148] S. Hong, A. Han, E. C. Lee, K. W. Ko, J. H. Park, H. J. Song, M. H. Han, C. H. Han, *Curr. Appl. Physics* **2015**, *15*, 574.
[149] X. Wang, Y. Fang, L. He, Q. Wang, T. Wu, *Mater. Sci. Semicond. Process.* **2014**, *27*, 569.
[150] G. E. Eperon, V. M. Burlakov, P. Docampo, A. Goriely, H. J. Snaith, *Adv. Funct. Mater.* **2014**, *24*, 151.
[151] M. Liu, M. B. Johnston, H. J. Snaith, *Nature* **2013**, *501*, 395.
[152] Q. Chen, H. Zhou, Z. Hong, S. Luo, H. S. Duan, H. H. Wang, Y. Liu, G. Li, Y. Yang, *J. Am. Chem. Soc.* **2014**, *136*, 622.
[153] S. Shi, Y. Li, X. Li, H. Wang, *Mater. Horizons* **2015**, *2*, 378.
[154] a) L. K. Ono, S. R. Raga, S. Wang, Y. Kato, Y. Qi, *J. Mater. Chem. A* **2015**, *3*, 9074; b) B. Wu, K. Fu, N. Yantara, G. Xing, S. Sun, T. C. Sum, N. Mathews, *Adv. Energy Mater.* **2015**, *5*, 1500829.
[155] W. J. Yin, T. Shi, Y. Yan, *Adv. Mater.* **2014**, *26*, 4653.
[156] J. P. Correa Baena, L. Steier, W. Tress, M. Saliba, S. Neutzner, T. Matsui, F. Giordano, T. J. Jacobsson, A. R. Srimath Kandada, S. M. Zakeeruddin, A. Petrozza, A. Abate, M. K. Nazeeruddin, M. Gratzel, A. Hagfeldt, *Energy Environ. Sci.* **2015**, *8*, 2928.
[157] J. Song, E. Zheng, X. F. Wang, W. Tian, T. Miyasaka, *Sol. Energy Mater. Sol. Cell.* **2016**, *144*, 623.
[158] Z.-L. Tseng, C.-H. Chiang, C.-G. Wu, *Sci. Rep.* **2015**, *5*, 13211.
[159] W. Qiu, U. W. Paetzold, R. Gehlhaar, V. Smirnov, H.-G. Boyen, J. G. Tait, B. Conings, W. Zhang, C. Nielsen, I. McCulloch, L. Froyen, P. Heremans, D. Cheyns, *J. Mater. Chem. A* **2015**, *3*, 22824.
[160] J. H. Heo, M. H. Lee, H. J. Han, B. R. Patil, J. S. Yu, S. H. Im, *J. Mater. Chem. A* **2016**, *4*, 1572.
[161] L. Meng, J. You, T. F. Guo, Y. Yang, *Acc. Chem. Res.* **2016**, *49*, 155.
[162] S. Sun, T. Salim, N. Mathews, M. Duchamp, C. Boothroyd, G. Xing, T. C. Sum, Y. M. Lam, *Energy Environ. Sci.* **2014**, *7*, 399.
[163] G. Xing, N. Mathews, S. Sun, S. S. Lim, Y. M. Lam, M. Graẗzel, S. Mhaisalkar, T. C. Sum, *Science* **2013**, *342*, 344.
[164] a) W. A. Laban, L. Etgar, *Energy Environ. Sci.* **2013**, *6*, 3249; b) M. Hu, L. Liu, A. Mei, Y. Yang, T. Liu, H. Han, *J. Mater. Chem. A* **2014**, *2*, 17115; c) J. Shi, J. Dong, S. Lv, Y. Xu, L. Zhu, J. Xiao, X. Xu, H. Wu, D. Li, Y. Luo, Q. Meng, *Appl. Phys. Lett.* **2014**, *104*, 063901.
[165] J. Y. Jeng, Y. F. Chiang, M. H. Lee, S. R. Peng, T. F. Guo, P. Chen, T. C. Wen, *Adv. Mater.* **2013**, *25*, 3727.
[166] a) W. Nie, H. Tsai, R. Asadpour, J. C. Blancon, A. J. Neukirch, G. Gupta, J. J. Crochet, M. Chhowalla, S. Tretiak, M. A. Alam, H. L. Wang, A. D. Mohite, *Science* **2015**, *347*, 522; b) C. Bi, Q. Wang, Y. Shao, Y. Yuan, Z. Xiao, J. Huang, *Nat. Commun.* **2015**, *6*, 7747.
[167] a) H. Zhang, J. Cheng, F. Lin, H. He, J. Mao, K. S. Wong, A. K. Y. Jen, W. C. H. Choy, *ACS Nano* **2016**, *10*, 1503; b) J. H. Park, J. Seo, S. Park, S. S. Shin, Y. C. Kim, N. J. Jeon, H.-W. Shin, T. K. Ahn, J. H. Noh, S. C. Yoon, C. S. Hwang, S. I. Seok, *Adv. Mater.* **2015**, *27*, 4013.
[168] J. You, Z. Hong, T. B. Song, L. Meng, Y. Liu, C. Jiang, H. Zhou, W. H. Chang, G. Li, Y. Yang, *Appl. Phys. Lett.* **2014**, *105*, 183902.
[169] F. Hou, Z. Su, F. Jin, X. Yan, L. Wang, H. Zhao, J. Zhu, B. Chu, W. Li, *Nanoscale* **2015**, *7*, 9427.
[170] P. W. Liang, C. C. Chueh, S. T. Williams, A. K. Y. Jen, *Adv. Energy Mater.* **2015**, *5*, 1402321.
[171] L. Q. Zhang, X. W. Zhang, Z. G. Yin, Q. Jiang, X. Liu, J. H. Meng, Y. J. Zhao, H. L. Wang, *J. Mater. Chem. A* **2015**, *3*, 12133.
[172] P. Docampo, J. M. Ball, M. Darwich, G. E. Eperon, H. J. Snaith, *Nat. Commun.* **2013**, *4*, 2761.
[173] N. Ahn, D. Y. Son, I. H. Jang, S. M. Kang, M. Choi, N. G. Park, *J. Am. Chem. Soc.* **2015**, *137*, 8696.
[174] K. Aitola, K. Sveinbjornsson, J.-P. Correa-Baena, A. Kaskela, A. Abate, Y. Tian, E. M. J. Johansson, M. Gratzel, E. I. Kauppinen, A. Hagfeldt, G. Boschloo, *Energy Environ. Sci.* **2016**, *9*, 461.
[175] W. Q. Wu, F. Huang, D. Chen, Y. B. Cheng, R. A. Caruso, *Adv. Energ. Mater.* **2016**, *6*, 1502027.
[176] J. F. Li, Z. L. Zhang, H. P. Gao, Y. Zhang, Y. L. Mao, *J. Mater. Chem. A* **2015**, *3*, 19476.
[177] D. Y. Son, K. H. Bae, H. S. Kim, N. G. Park, *J. Phys. Chem. C* **2015**, *119*, 10321.
[178] L. S. Oh, D. H. Kim, J. A. Lee, S. S. Shin, J. W. Lee, I. J. Park, M. J. Ko, N. G. Park, S. G. Pyo, K. S. Hong, J. Y. Kim, *J. Phys. Chem. C* **2014**, *118*, 22991.
[179] S. S. Mali, C. S. Shim, C. K. Hong, *Sci. Rep.* **2015**, *5*, 11424.
[180] J. Song, E. Zheng, J. Bian, X.-F. Wang, W. Tian, Y. Sanehira, T. Miyasaka, *J. Mater. Chem. A* **2015**, *3*, 10837.
[181] Y. Dkhissi, F. Huang, S. Rubanov, M. Xiao, U. Bach, L. Spiccia, R. A. Caruso, Y.-B. Cheng, *J. Power Sources* **2015**, *278*, 325.
[182] M. M. Tavakoli, Q. Lin, S. F. Leung, G. C. Lui, H. Lu, L. Li, B. Xiang, Z. Fan, *Nanoscale* **2016**, *8*, 4276.
[183] J. Troughton, D. Bryant, K. Wojciechowski, M. J. Carnie, H. Snaith, D. A. Worsley, T. M. Watson, *J. Mater. Chem. A* **2015**, *3*, 9141.
[184] Q. Hu, J. Wu, C. Jiang, T. Liu, X. Que, R. Zhu, Q. Gong, *ACS Nano* **2014**, *8*, 10161.
[185] J. T.-W. Wang, J. M. Ball, E. M. Barea, A. Abate, J. a. Alexander-Webber, J. Huang, M. Saliba, I. Mora-Sero, J. Bisquert, H. J. Snaith, R. J. Nicholas, *Nano Lett.* **2014**, *14*, 724.
[186] D. Bi, S.-J. Moon, L. Haggman, G. Boschloo, L. Yang, E. M. J. Johansson, M. K. Nazeeruddin, M. Gratzel, A. Hagfeldt, *RSC Adv.* **2013**, *3*, 18762.
[187] H. Zhou, Y. Shi, K. Wang, Q. Dong, X. Bai, Y. Xing, Y. Du, T. Ma, *J. Phys. Chem. C* **2015**, *119*, 4600.
[188] Z. Wei, H. Chen, K. Yan, X. Zheng, S. Yang, *J. Mater. Chem. A* **2015**, *3*, 24226.
[189] K. Yan, Z. Wei, J. Li, H. Chen, Y. Yi, X. Zheng, X. Long, Z. Wang, J. Wang, J. Xu, S. Yang, *Small* **2015**, *11*, 2269.
[190] Y. Yang, K. Ri, A. Mei, L. Liu, M. Hu, T. Liu, X. Li, H. Han, *J. Mater. Chem. A* **2015**, *3*, 9103.
[191] C. Y. Chang, K. T. Lee, W. K. Huang, H. Y. Siao, Y. C. Chang, *Chem. Mater.* **2015**, *27*, 5122.
[192] L. Zheng, D. Zhang, Y. Ma, Z. Lu, Z. Chen, S. Wang, L. Xiao, Q. Gong, *Dalton Trans.* **2015**, *44*, 10582.
[193] L. Qiu, J. Deng, X. Lu, Z. Yang, H. Peng, *Angew. Chem. Int. Ed.* **2014**, *53*, 10425.
[194] M. Lee, Y. Ko, Y. Jun, *J. Mater. Chem. A* **2015**, *3*, 19310.
[195] Y. Zhong, P. Chen, B. Yang, X. Zuo, L. Zhou, X. Yang, G. Li, *Appl. Phys. Lett.* **2015**, *106*, 263903.
[196] E. M. Hutter, G. E. Eperon, S. D. Stranks, T. J. Savenije, *J. Phys. Chem. Lett.* **2015**, *6*, 3082.
[197] a) T. Leijtens, S. D. Stranks, G. E. Eperon, R. Lindblad, E. M. J. Johansson, I. J. McPherson, H. Rensmo, J. M. Ball, M. M. Lee, H. J. Snaith, *ACS Nano* **2014**, *8*, 7147; b) Y. Zhang, M. Liu, G. E. Eperon, T. Leijtens, D. P. McMeekin, M. Saliba, W. Zhang, M. De Bastiani, A. Petrozza, L. M. Herz, M. B. Johnston, H. Lin, H. Snaith, *Mater. Horiz.* **2015**, *2*, 315.
[198] Q. Lin, A. Armin, R. C. R. Nagiri, P. L. Burn, P. Meredith, *Nat. Photonics* **2015**, *9*, 106.
[199] E. Edri, S. Kirmayer, S. Mukhopadhyay, K. Gartsman, G. Hodes, D. Cahen, *Nat. Comm.* **2014**, *5*, 3461.
[200] S. Ryu, J. Seo, S. S. Shin, Y. C. Kim, N. J. Jeon, J. H. Noh, S. I. Seok, *J. Mater. Chem. A* **2015**, *3*, 3271.
[201] Y. Zhou, C. Fuentes-Hernandez, J. Shim, J. Meyer, A. J. Giordano, H. Li, P. Winget, T. Papadopoulos, H. Cheun, J. Kim, M. Fenoll, A. Dindar, W. Haske, E. Najafabadi, T. M. Khan, H. Sojoudi,

S. Barlow, S. Graham, J.-L. Brédas, S. R. Marder, A. Kahn, B. Kippelen, *Science* **2012**, *336*, 327.
[202] Merck-Spiro, Spiro price, http://www.merck-performance-materials.com/en/solar_and_energy/photovoltaics/dssc/dssc.html, accessed: January, 2017.
[203] Z. M. Beiley, M. D. McGehee, *Energy Environ. Sci.* **2012**, *5*, 9173.
[204] A. Kay, M. Grätzel, *Sol. Energy Mater. Sol. Cells* **1996**, *44*, 99.
[205] Z. Ku, Y. Rong, M. Xu, T. Liu, H. Han, *Sci. Rep.* **2013**, 3, https://doi.org/10.1038/srep03132.
[206] Z. Li, S. A. Kulkarni, P. P. Boix, E. Shi, A. Cao, K. Fu, S. K. Batabyal, J. Zhang, Q. Xiong, L. H. Wong, N. Mathews, S. G. Mhaisalkar, *ACS Nano* **2014**, *8*, 6797.
[207] H. Wei, J. Xiao, Y. Yang, S. Lv, J. Shi, X. Xu, J. Dong, Y. Luo, D. Li, Q. Meng, *Carbon* **2015**, *93*, 861.
[208] Y. Chen, J. Peng, D. Su, X. Chen, Z. Liang, *ACS Appl. Mater. Interfaces* **2015**, *7*, 4471.
[209] F. Zhang, X. Yang, H. Wang, M. Cheng, J. Zhao, L. Sun, *ACS Appl. Mater. Interfaces* **2014**, *6*, 16140.
[210] S. Gamliel, A. Dymshits, S. Aharon, E. Terkieltaub, L. Etgar, *J. Phys. Chem. C* **2015**, *119*, 19722.
[211] F. Zhang, X. Yang, M. Cheng, W. Wang, L. Sun, *Nano Energy* **2016**, *20*, 108.
[212] S. N. Habisreutinger, T. Leijtens, G. E. Eperon, S. D. Stranks, R. J. Nicholas, H. J. Snaith, *Nano Lett.* **2014**, *14*, 5561.
[213] K. Cao, Z. Zuo, J. Cui, Y. Shen, T. Moehl, S. M. Zakeeruddin, M. Grätzel, M. Wang, *Nano Energy* **2015**, *17*, 171.
[214] A. Fakharuddin, P. S. Archana, Z. Kalidin, M. M. Yusoff, R. Jose, *RSC Adv.* **2013**, *3*, 2683.
[215] C. W. Chen, H. W. Kang, S. Y. Hsiao, P. F. Yang, K. M. Chiang, H. W. Lin, *Adv. Mater.* **2014**, https://doi.org/10.1002/adma.201402461.
[216] a) Y. Li, L. Meng, Y. Yang, G. Xu, Z. Hong, Q. Chen, J. You, G. Li, Y. Yang, Y. Li, *Nat Commun.* **2016**, *7*; b) D. Yang, R. Yang, J. Zhang, Z. Yang, S. Liu, C. Li, *Energy Environ. Sci.* **2015**, *8*, 3208.
[217] a) H. C. Weerasinghe, Y. Dkhissi, A. D. Scully, R. A. Caruso, Y.-B. Cheng, *Nano Energy* **2015**, *18*, 118; b) M. Kaltenbrunner, G. Adam, E. D. Glowacki, M. Drack, R. Schwodiauer, L. Leonat, D. H. Apaydin, H. Groiss, M. C. Scharber, M. S. White, N. S. Sariciftci, S. Bauer, *Nat. Mater.* **2015**, *14*, 1032.
[218] G. Hashmi, K. Miettunen, T. Peltola, J. Halme, I. Asghar, K. Aitola, M. Toivola, P. Lund, *Renew. Sustainable Energy Rev.* **2011**, *15*, 3717.
[219] a) V. Zardetto, T. M. Brown, A. Reale, A. Di Carlo, *J. Polymer Sci. Part B: Polymer Physics* **2011**, *49*, 638; b) B. Susrutha, L. Giribabu, S. P. Singh, *Chem. Commun.* **2015**, *51*, 14696.
[220] J. Yang, B. D. Siempelkamp, E. Mosconi, F. De Angelis, T. L. Kelly, *Chem. Mater.* **2015**, *27*, 4229.
[221] M. Lee, Y. Jo, D. S. Kim, H. Y. Jeong, Y. Jun, *J. Mater. Chem. A* **2015**, *3*, 14592.
[222] J. Deng, L. Qiu, X. Lu, Z. Yang, G. Guan, Z. Zhang, H. Peng, *J. Mater. Chem. A* **2015**, *3*, 21070.
[223] S. He, L. Qiu, X. Fang, G. Guan, P. Chen, Z. Zhang, H. Peng, *J. Mater. Chem. A* **2015**, *3*, 9406.
[224] M. Peng, D. Zou, *J. Mater. Chem. A* **2015**, *3*, 20435.
[225] H. Sun, H. Li, X. You, Z. Yang, J. Deng, L. Qiu, H. Peng, *J. Mater. Chem. A* **2014**, *2*, 345.
[226] D. Liu, M. Zhao, Y. Li, Z. Bian, L. Zhang, Y. Shang, X. Xia, S. Zhang, D. Yun, Z. Liu, A. Cao, C. Huang, *ACS Nano* **2012**, *6*, 11027.
[227] X. Liang, W. Li, J. Li, G. Niu, L. Wang, *J. Mater. Chem. A* **2016**, *4*, 16913.
[228] H. Zhang, L. Xue, J. Han, Y. Q. Fu, Y. Shen, Z. Zhang, Y. Li, M. Wang, *J. Mater. Chem. A* **2016**, *4*, 8724.
[229] J. Min, Z. G. Zhang, Y. Hou, C. O. R. Quiroz, T. Przybilla, C. Bronnbauer, F. Guo, K. Forberich, H. Azimi, T. Ameri, E. Spiecker, Y. Li, C. J. Brabec, *Chem. Mater.* **2015**, *27*, 227.
[230] Y. Li, Y. Zhao, Q. Chen, Y. Yang, Y. Liu, Z. Hong, Z. Liu, Y. T. Hsieh, L. Meng, Y. Li, Y. Yang, *J. Am. Chem. Soc.* **2015**, *137*, 15540.
[231] Y. Xu, Y. Wang, J. Yu, B. Feng, H. Zhou, J. Zhang, J. Duan, X. Fan, P. A. Van Aken, P. D. Lund, H. Wang, *IEEE J. Photovoltaics* **2016**.
[232] Y. Dong, W. Li, X. Zhang, Q. Xu, Q. Liu, C. Li, Z. Bo, *Small* **2016**, *12*, 1098.
[233] a) G. Yang, H. Tao, P. Qin, W. Ke, G. Fang, *J. Mater. Chem. A* **2016**, *4*, 3970; b) H.-S. Kim, I.-H. Jang, N. Ahn, M. Choi, A. Guerrero, J. Bisquert, N.-G. Park, *J. Phys. Chem. Lett.* **2015**, *6*, 4633.
[234] J. M. Azpiroz, E. Mosconi, J. Bisquert, F. De Angelis, *Energy Environ. Sci.* **2015**, *8*, 2118.
[235] Q. Fu, X. Tang, L. Tan, Y. Zhang, Y. Liu, L. Chen, Y. Chen, *J. Phys. Chem. C* **2016**, *120*, 15089.
[236] a) W. Li, W. Zhang, S. Van Reenen, R. J. Sutton, J. Fan, A. A. Haghighirad, M. B. Johnston, L. Wang, H. J. Snaith, *Energy Environ. Sci.* **2016**, *9*, 490; b) J. Cao, J. Yin, S. Yuan, Y. Zhao, J. Li, N. Zheng, *Nanoscale* **2015**, *7*, 9443.
[237] S. S. Reddy, K. Gunasekar, J. H. Heo, S. H. Im, C. S. Kim, D. H. Kim, J. H. Moon, J. Y. Lee, M. Song, S. H. Jin, *Adv. Mater.* **2016**, *28*, 686.
[238] H. P. Dong, Y. Li, S. F. Wang, W. Z. Li, N. Li, X. D. Guo, L. D. Wang, *J. Mater. Chem. A* **2015**, *3*, 9999.
[239] L. F. Zhu, Y. Z. Xu, J. J. Shi, H. Y. Zhang, X. Xu, Y. H. Zhao, Y. H. Luo, Q. B. Meng, D. M. Li, *RSC Adv.* **2016**, *6*, 82282.
[240] S. F. Shaikh, H. C. Kwon, W. Yang, H. Hwang, H. Lee, E. Lee, S. Ma, J. Moon, *J. Mater. Chem. A* **2016**, *4*, 15478.
[241] Z. K. Wang, M. Li, D. X. Yuan, X. B. Shi, H. Ma, L. S. Liao, *ACS Appl. Mater. Interfaces* **2015**, *7*, 9645.
[242] Y. Xu, J. Shi, S. Lv, L. Zhu, J. Dong, H. Wu, Y. Xiao, Y. Luo, S. Wang, D. Li, X. Li, Q. Meng, *ACS Appl. Mater. Interfaces* **2014**, *6*, 5651.
[243] R. Roesch, T. Faber, E. Von Hauff, T. M. Brown, M. Lira-Cantu, H. Hoppe, *Adv. Energy Mater.* **2015**, *5*, 1501407.
[244] a) T. A. Berhe, W. N. Su, C. H. Chen, C. J. Pan, J. H. Cheng, H. M. Chen, M. C. Tsai, L. Y. Chen, A. A. Dubale, B. J. Hwang, *Energy Environ. Sci.* **2016**, *9*, 323; b) M. Shahbazi, H. Wang, *Sol. Energy* **2016**, *123*, 74; c) D. Wang, M. Wright, N. K. Elumalai, A. Uddin, *Sol. Energy Mater. Sol. Cells* **2016**, *147*, 255.
[245] Y. H. Lee, J. Luo, R. Humphry-Baker, P. Gao, M. Grätzel, M. K. Nazeeruddin, *Adv. Funct. Mater.* **2015**, *25*, 3925.
[246] M. K. Gangishetty, R. W. J. Scott, T. L. Kelly, *Nanoscale* **2016**, https://doi.org/10.1039/C5NR04179A.
[247] G. E. Eperon, S. N. Habisreutinger, T. Leijtens, B. J. Bruijnaers, J. J. Van Franeker, D. W. Dequilettes, S. Pathak, R. J. Sutton, G. Grancini, D. S. Ginger, R. A. J. Janssen, A. Petrozza, H. J. Snaith, *ACS Nano* **2015**, *9*, 9380.
[248] a) J. Yang, B. D. Siempelkamp, D. Liu, T. L. Kelly, *ACS Nano* **2015**, *9*, 1955; b) J. M. Frost, K. T. Butler, F. Brivio, C. H. Hendon, M. Van Schilfgaarde, A. Walsh, *Nano Lett.* **2014**, *14*, 2584.
[249] a) L. Zheng, Y. H. Chung, Y. Ma, L. Zhang, L. Xiao, Z. Chen, S. Wang, B. Qu, Q. Gong, *Chem. Commun.* **2014**, *50*, 11196; b) B. Conings, J. Drijkoningen, N. Gauquelin, A. Babayigit, J. D'Haen, L. D'Olieslaeger, A. Ethirajan, J. Verbeeck, J. Manca, E. Mosconi, F. D. Angelis, H.-G. Boyen, *Adv. Energy Mater.* **2015**, *5*, 1500477; c) K. Leo, *Nat. Nanotechnol.* **2015**, *10*, 574.
[250] N. A. Manshor, Q. Wali, K. K. Wong, S. K. Muzakir, A. Fakharuddin, L. Schmidt-Mende, R. Jose, *PCCP* **2016**, *18*, 21629.
[251] J. Yin, J. Cao, X. He, S. Yuan, S. Sun, J. Li, N. Zheng, L. Lin, *J. Mater. Chem. A* **2015**, *3*, 16860.

[252] J. Xiong, B. Yang, C. Cao, R. Wu, Y. Huang, J. Sun, J. Zhang, C. Liu, S. Tao, Y. Gao, J. Yang, *Org. Electronics: Physics, Materials, Applications* **2016**, *30*, 30.
[253] F. Matsumoto, S. M. Vorpahl, J. Q. Banks, E. Sengupta, D. S. Ginger, *J. Phys. Chem. C* **2015**, *119*, 20810.
[254] K. Schwanitz, U. Weiler, R. Hunger, T. Mayer, W. Jaegermann, *J. Phys. Chem. C* **2007**, *111*, 849.
[255] a) G. Niu, X. Guo, L. Wang, *J. Mater. Chem. A* **2015**, *3*, 8970; b) Y. Rong, Z. Ku, A. Mei, T. Liu, M. Xu, S. Ko, X. Li, H. Han, *J. Phys. Chem. Lett.* **2014**, *5*, 2160.
[256] S. Ito, S. Tanaka, K. Manabe, H. Nishino, *J. Phys. Chem. C* **2014**, *118*, 16995.
[257] I. Hwang, M. Baek, K. Yong, *ACS Appl. Mater. Interfaces* **2015**, *7*, 27863.
[258] D. Bi, G. Boschloo, S. Schwarzmüller, L. Yang, E. M. J. Johansson, A. Hagfeldt, *Nanoscale* **2013**, *5*, 11686.
[259] A. Bera, A. D. Sheikh, M. A. Haque, R. Bose, E. Alarousu, O. F. Mohammed, T. Wu, *ACS Appl. Mater. Interfaces* **2015**, *7*, 12404.
[260] J. S. Yun, A. Ho-Baillie, S. Huang, S. H. Woo, Y. Heo, J. Seidel, F. Huang, Y. B. Cheng, M. A. Green, *J. Phys. Chem. Lett.* **2015**, *6*, 875.
[261] C. Law, L. Miseikis, S. Dimitrov, P. Shakya-Tuladhar, X. Li, P. R. F. Barnes, J. Durrant, B. C. O'Regan, *Adv. Mater.* **2014**, *26*, 6268.
[262] T. M. Schmidt, T. T. Larsen-Olsen, J. E. Carlé, D. Angmo, F. C. Krebs, *Adv. Energy Mater.* **2015**, *5*, 1500569.
[263] Y. Zhang, X. Hu, L. Chen, Z. Huang, Q. Fu, Y. Liu, L. Zhang, Y. Chen, *Org. Electronics* **2016**, *30*, 281.
[264] H. Choi, C. K. Mai, H. B. Kim, J. Jeong, S. Song, G. C. Bazan, J. Y. Kim, A. J. Heeger, *Nat. Commun.* **2015**, *6*, 7348.
[265] J. H. Kim, P. W. Liang, S. T. Williams, N. Cho, C. C. Chueh, M. S. Glaz, D. S. Ginger, A. K. Y. Jen, *Adv. Mater.* **2015**, *27*, 695.
[266] Z. Yu, L. Sun, *Adv. Energy Mater.* **2015**, *5*, 1500213.
[267] a) L. Badia, E. Mas-Marzá, R. S. Sánchez, E. M. Barea, J. Bisquert, I. Mora-Seró, *APL Mater.* **2014**, *2*, 081507; b) X. Dong, X. Fang, M. Lv, B. Lin, S. Zhang, J. Ding, N. Yuan, *J. Mater. Chem. A* **2015**, *3*, 5360; c) S. Guarnera, A. Abate, W. Zhang, J. M. Foster, G. Richardson, A. Petrozza, H. J. Snaith, *J. Phys. Chem. Lett.* **2015**, *6*, 432; d) I. C. Smith, E. T. Hoke, D. Solis-Ibarra, M. D. McGehee, H. I. Karunadasa, *Angew. Chem.– Int. Ed.* **2014**, *53*, 11232; e) I. Hwang, I. Jeong, J. Lee, M. J. Ko, K. Yong, *ACS Appl. Mater. Interfaces* **2015**, *7*, 17330.
[268] a) S. Kazim, F. J. Ramos, P. Gao, M. K. Nazeeruddin, M. Grätzel, S. Ahmad, *Energy Environ. Sci.* **2015**, *8*, 1816; b) W. Chen, X. Bao, Q. Zhu, D. Zhu, M. Qiu, M. Sun, R. Yang, *J. Mater. Chem. C* **2015**, *3*, 10070; c) J. Liu, Y. Wu, C. Qin, X. Yang, T. Yasuda, A. Islam, K. Zhang, W. Peng, W. Chen, L. Han, *Energy Environ. Sci.* **2014**, *7*, 2963; d) M. Franckevičius, A. Mishra, F. Kreuzer, J. Luo, S. M. Zakeeruddin, M. Grätzel, *Mater. Horizons* **2015**, *2*, 613; e) Y. Liu, Q. Chen, H. S. Duan, H. Zhou, Y. Yang, H. Chen, S. Luo, T. B. Song, L. Dou, Z. Hong, Y. Yang, *J. Mater. Chem. A* **2015**, *3*, 11940; f) Q. Luo, Y. Zhang, C. Liu, J. Li, N. Wang, H. Lin, *J. Mater. Chem. A* **2015**, *3*, 15996; g) C. Steck, M. Franckevičius, S. M. Zakeeruddin, A. Mishra, P. Bäuerle, M. Grätzel, *J. Mater. Chem. A* **2015**, *3*, 17738.
[269] a) X. Bao, Y. Wang, Q. Zhu, N. Wang, D. Zhu, J. Wang, A. Yang, R. Yang, *J. Power Sources* **2015**, *297*, 53; b) A. Guerrero, J. You, C. Aranda, Y. S. Kang, G. Garcia-Belmonte, H. Zhou, J. Bisquert, Y. Yang, *ACS Nano* **2016**, *10*, 218.
[270] J. Y. Jeng, K. C. Chen, T. Y. Chiang, P. Y. Lin, T. D. Tsai, Y. C. Chang, T. F. Guo, P. Chen, T. C. Wen, Y. J. Hsu, *Adv. Mater.* **2014**, *26*, 4107.
[271] J. H. Kim, S. T. Williams, N. Cho, C. C. Chueh, A. K. Y. Jen, *Adv. Energy Mater.* **2015**, *5*, 1401229.
[272] M. P. de Jong, L. J. v. IJzendoorn, M. J. A. de Voigt, *Appl. Phys. Lett.* **2000**, *77*, 2255.
[273] M. O. Reese, S. A. Gevorgyan, M. Jørgensen, E. Bundgaard, S. R. Kurtz, D. S. Ginley, D. C. Olson, M. T. Lloyd, P. Morvillo, E. A. Katz, A. Elschner, O. Haillant, T. R. Currier, V. Shrotriya, M. Hermenau, M. Riede, K. R. Kirov, G. Trimmel, T. Rath, O. Inganäs, F. Zhang, M. Andersson, K. Tvingstedt, M. Lira-Cantu, D. Laird, C. McGuiness, S. Gowrisanker, M. Pannone, M. Xiao, J. Hauch, R. Steim, D. M. DeLongchamp, R. Rösch, H. Hoppe, N. Espinosa, A. Urbina, G. Yaman-Uzunoglu, J.-B. Bonekamp, A. J. J. M. van Breemen, C. Girotto, E. Voroshazi, F. C. Krebs, *Sol. Energy Mater. Sol. Cell.* **2011**, *95*, 1253.
[274] M. Jørgensen, K. Norrman, S. A. Gevorgyan, T. Tromholt, B. Andreasen, F. C. Krebs, *Adv. Mater.* **2012**, *24*, 580.
[275] *Nat. Mater.* **2015**, *14*, 1073.
[276] E. Zimmermann, K. K. Wong, M. Müller, H. Hu, P. Ehrenreich, M. Kohlstädt, U. Würfel, S. Mastroianni, G. Mathiazhagan, A. Hinsch, T. P. Gujar, M. Thelakkat, T. Pfadler, L. Schmidt-Mende, *APL Mater.* **2016**, *4*, 091901.
[277] G. E. Eperon, S. D. Stranks, C. Menelaou, M. B. Johnston, L. M. Herz, H. J. Snaith, *Energy Environ. Sci.* **2014**, *7*, 982.
[278] K. Hwang, Y.-S. Jung, Y.-J. Heo, F. H. Scholes, S. E. Watkins, J. Subbiah, D. J. Jones, D.-Y. Kim, D. Vak, *Adv. Mater.* **2015**, *27*, 1241.
[279] C. Roldán-Carmona, O. Malinkiewicz, R. Betancur, G. Longo, C. Momblona, F. Jaramillo, L. Camacho, H. J. Bolink, *Energy Environ. Sci.* **2014**, *7*, 2968.
[280] S. S. Shin, W. S. Yang, J. H. Noh, J. H. Suk, N. J. Jeon, J. H. Park, J. S. Kim, W. M. Seong, S. I. Seok, *Nat. Commun.* **2015**, *6*, 7410.
[281] H.-R. Xia, W.-T. Sun, L.-M. Peng, *Chem. Comm.* **2015**, *51*, 13787.
[282] Q. Dong, Y. Fang, Y. Shao, P. Mulligan, J. Qiu, L. Cao, J. Huang, *Science* **2015**, *347*, 967.